A COMPARISON OF OBSERVED PERMANENT TILTS AND STRAINS DUE TO EARTHQUAKES WITH THOSE CALCULATED FROM DISPLACEMENT DISLOCATIONS IN ELASTIC EARTH MODELS

Thesis by

John Robert McGinley, Jr.

In Partial Fulfillment of the Requirements

For the Degree of

Doctor of Philosophy

California Institute of Technology

Pasadena, California

1969

(Submitted July 22, 1968)

ACKNOWLEDGMENTS

The author gratefully acknowledges advice and encouragement during this study from Prof.'s S. W. Smith and C. B. Archambeau. Many useful discussions were held with staff members of the Seismological Laboratory at the California Institute of Technology particularly Prof.'s D. L. Anderson and J. N. Brune.

The author worked with Prof. Ari Ben-Menahem on the results presented in Chapter 3. While writing Chapter 3 a preprint of an article by Ben-Menahem and Singh (1968) came to the author's attention. This article gives a more general mathematical treatment of eigenvector expansions for Green's functions than is given here and includes a rederivation of the Green's function for the static deformation of a homogeneous elastic sphere. The work of Prof. Ben-Menahem and the author which is the subject of Chapter 3 is referenced in the preprint.

Mrs. Barbara Sloan typed the manuscript and Mr. Laszlo Lenches drafted most of the figures.

The author held a National Science Foundation Graduate Fellowship during most of the time when the work presented here was carried out. This research was supported by the Air Force Office of Scientific Research, Office of Aerospace Research, United States Air Force, under AFOSR contract AF-49(638)-1337. A portion of the research was also supported by NASA Research Grant NGR 05-002-069.

The author gratefully acknowledges the help from these sources.

ABSTRACT

Theoretical solutions are derived for a model of faulting in elastic media and for the effect of lateral inhomogeneities on the earth's free oscillations. The solutions are used in a study of permanent tilts and strains observed a few hundred kilometers from earthquakes.

It is shown that the static deformational field due to a suitably chosen dislocation fault model is the same as that due to introduction of a stress free surface into a prestressed medium. Formal mathematical solutions are derived for the static deformational fields due to dislocation fault models in a homogeneous elastic sphere and a layered elastic half-space. For the layered half-space explicit solutions are given in terms of integral transforms for the surface displacements, tilts, and strains due to a slip fault and a dilatational source. A perturbation procedure is developed for calculating the effects of lateral changes in elastic constants on the earth's free oscillations. The procedure is applied to obtain expressions for the effect of some simple inhomogeneity geometries on the torsional free oscillations.

Numerical evaluation of the static, elastic, dislocation solutions shows that the observed tilts and strains are large compared with theoretical predictions and sometimes show the opposite sign. The hypothesis that a weak layer in the lower crust or upper mantle can explain the observations is investigated. It is found that a very weak layer, approaching a liquid-like behavior, does help to

explain the observations. The compatibility of a very weak layer with observed surface wave dispersion is tested using the results of the perturbation calculations for the torsional free oscillations. A very weak layer is determined as compatible with observed surface wave dispersion only if very thin and with some frequency dependence in its elastic properties. It is concluded that although a regional weak layer in the lower crust or upper mantle can help to explain the observed tilts and strains, other regional or local structural effects or source complications must also be important.

TABLE OF CONTENTS

Page

Page

Page

Page

Chapter 1

INTRODUCTION

Observations of what appear to be permanent deformations of the earth's surface at large distances from earthquakes have been reported by a number of investigators. Press (1965) reviews the observations and theoretical models up to 1965. Wideman and Major (1967) recently published 25 observations of "strain steps" from earthquakes at distances of 47 to 13,650 km. Their observations as well as many of the previous observations are unusually large when compared to predictions based on existing theoretical models of faulting in elastic media. Most of the published observations which are anomalously large are subject to question either because of the nature of the instrumentation or the temporal relationship of the observation and the earthquake.

Two earthquakes in 1966 and one in 1968 resulted in an unusually good set of observations of permanent tilt and strain at the Isabella, California recording station of the California Institute of Technology. The Parkfield earthquake[1] was very extensively studied resulting in

---

[1]Origin time 04 hrs, 26 min, 13.4 sec, GMT on June 28, 1966; epicenter at 35° 57.3' North Latitude, 120° 29.9' West Longitude, focal depth 4 km, magnitude 5.5. This is the main shock in a sequence of earthquakes in the Parkfield-Cholame area of California and will here be referred to as "the Parkfield earthquake" for convenience.

much better information about the nature of the source than is usual. Two tiltmeters at Isabella recorded permanent changes in the tilt - on one the full change was visible while the other went off scale giving a lower bound on the tilt. The Baja earthquake[2] resulted in permanent changes in tilt and strain on two tiltmeters and two strain meters at Isabella. To the author's knowledge this is the only earthquake for which four independent measurements of the surface deformational field were clearly recorded at one recording site at large distance. Offset on two strainmeters resulted from the Borrego Mountain earthquake[3] while the tiltmeters shows no perceptible offset. The source-station geometry for this earthquake is very similar to that for the Baja earthquake allowing comparison of two sets of data where many of the parameters in the models are nearly the same.

Comparison of these observations with models given in Press (1965) indicated that the observations were very large compared with the theoretical predictions based on fault dimensions and slip which were believed appropriate. In the case of the Baja earthquake the sign of one critical observation was reversed from that predicted

---

[2]Origin time 17 hr, 36 min, 26.7 sec GCT, on August 7, 1966; epicenter at 31° 48.0' North Latitude, 114° 30.0' West Longitude, focal depth 33 km, magnitude 6.3.

[3]Origin time 02 hrs, 28 min, 58.9 sec GCT on April 9, 1968; epicenter 33° 08.8' North Latitude, 116° 07.5' West Longitude, focal depth 20 km, magnitude 6.5. The epicenter and focal depth were tentatively assigned by the Seismological Laboratory at Pasadena.

by half-space models. There are a number of possible reasons for the discrepancies:

a. the mathematical model of the earthquake is inadequate either because the mechanism of the earthquake is substantially different than assumed or the mathematical representation of the mechanism is not sufficiently accurate;

b. assuming faulting is the mechanism, which is done here, the fault dimensions and slip are much larger than the field evidence has indicated; or

c. the models of earth structure used are inadequate either because

    1. the regional structure has properties which are significantly different than assumed, or

    2. local structure at the recording site is dominating the observations so that they cannot be directly related to the earthquake mechanism and regional structure.

The instrumentation is such that it is considered unlikely that the recorded permanent tilts and strains are merely a defect in the recordation. However, as implied in c.2. above, adjustments along fractures at the recording site can give local effects that result in real tilt and strain offsets but which are not useful in understanding earth structure or earthquake source mechanism. It should be noted that the "permanent" tilt or strain offsets referred to

here are offsets where there is no recovery evident on a time scale of several hours. It is not possible to specify behavior on a longer time scale because of secular changes.

In this study the emphasis is upon possible effects due to regional structure, particularly the possibility that a weak or decoupling zone in the lower crust or upper mantle is involved. A weak layer in the upper mantle has been hypothesized for reasons independent of earthquake-caused static observations (e.g. Hales, 1961). The presence of the low velocity zone suggests partial melting and concomitant weakening. Prof. D. L. Anderson and the author carried out a pilot investigation of the absorption of seismic waves which suggests substantial regional differences in absorption (see Appendix 1). There are regional variations in surface wave dispersion (e.g. Toksoz and Anderson (1966) and Brune (1968)). In the most general sense there is almost certainly regional weakening in the upper mantle. The degree of weakening and the time scale on which it occurs are important considerations in the construction of tectonic models. The work which follows compares observed static fields with theoretically calculated fields under the hypothesis of a weak layer in the lower crust or upper mantle. The effect of sphericity on the static field and the effect of a very weak layer of limited lateral extent on surface wave dispersion are also treated.

A consideration of the effect of a weak layer, or more generally of structure, is not independent of the source representation. Following Archambeau (1967) an earthquake is taken to be caused by

faulting due to shear rupture. The use of a dislocation model for predicting the static field due to faulting is evaluated and accepted for the purposes of this study. Other possibilities covered in a., b., and c. above are discussed in view of the results from the theoretical models.

The topics covered are outlined here in the order of presentation. Chapter 2 reviews the Green's function representation of the field due to a dislocation source in a layered elastic medium. The formal relationship between a displacement dislocation source and certain stress relaxation problems is naturally treated along with the Green's function representation. In Chapter 3 the Green's dyadic for an elastic sphere is derived. Application of this result when combined with published numerical solutions for structured, spherical earth models leads to the conclusion that for shallow sources at distances greater than about 20° an adequate theoretical treatment requires a spherical, structured, gravitating earth model. In Chapter 4 the theory of Chapter 2 is applied to a layered elastic half-space. Integral representations are derived for surface deformational fields due to a strike-slip source, a dip-slip source, and a dilatational source. The mathematical source which is used to model faulting is discussed in the first part of Chapter 5. In the latter part of Chapter 5 the asymptotic forms of the layered half-space solution fields and numerical solutions are used to illustrate the properties of the deformational fields due to various sources. In Chapter 6 a perturbation procedure is developed and used to calculate the

effect of lateral inhomogeneities on the earth's free oscillations. The results are used in evaluating the effect of a very thin, weak region of limited lateral extent on surface wave dispersion. It is concluded that an exceedingly weak layer can be consistent with observed surface wave dispersion if it is very thin and its properties show some frequency dependence. The observations of static tilts and strains from the earthquakes given above are listed in Chapter 7. A source model is chosen for each of the earthquakes and theoretical tilt and strain fields for half-space models and for weak layer models are compared with the observations. The effects on the predicted fields caused by varying the source parameters are considered.

A weak layer model improves the ability to fit the data, but the improvement is significant only when the weakening is so severe that it approximates a liquid layer. For either a half-space or a weak layer model the source strengths required to match the size of theoretical and observed tilts and strains are large compared to that deduced from other observations. Half-space models generally require a larger source strength than weak layer models. Some properties of the observed tilt and strain fields are not matched well by any of the models considered. The possibility that local effects at or very near the recording site are dominating the recordings remains open. The determination of the variability in size and spatial distribution of tilt and strain fields from a single earthquake is critical for a definitive interpretation of

the cause. If very local effects dominate, the recorded offsets are only useful for studying very local structure. If the seismic source or regional structure dominate the observations, then the models considered here show that the source or structure are quite different than usually assumed.

The basic conclusion is that a weak layer improves the ability of the theory to fit the observations, but the source dimensions of the earthquake and complicated regional or local effects must also be important.

Chapter 2

CONSTRUCTION OF THE GREEN'S FUNCTION FOR CERTAIN PROBLEMS IN STATIC ELASTICITY

Representation of the Displacement Field due to a Dislocation Source

Basic to all the solutions derived here is the construction of the solution to the equation governing static elasticity by use of a Green's function. Physically the Green's function is most readily thought of as the response to a "point source" where the term "source" has a physical interpretation determined by the problem. Later, as an aid in exposition, the notion of response to a point source will be used interchangeably with the term Green's function. Before giving its method of construction, the Green's function is assumed known and a representation of the displacement field due to a dislocation source is derived in dyadic notation. The result is sufficiently general for the cases to be considered. More complete treatments are given in Bergman and Schiffer (1953) and Burridge and Knopoff (1964).

The equation for the static deformation of a homogeneous, isotropic elastic medium is

$$(\lambda + 2\mu)\nabla(\nabla\cdot\vec{u}) - \mu\nabla \times (\nabla\times\vec{u}) = -\vec{F} \qquad (2\text{-}1)$$

where $\vec{u}$ is the displacement, $\vec{F}$ a body force, and λ and μ Lame's parameters. The vector operator L is defined by writing equation (2-1) as $L\vec{u} = -\vec{F}$.

Using

$$(\lambda + 2\mu)\nabla(\nabla\cdot\vec{v}) - \mu\nabla \times (\nabla \times \vec{v}) = -\vec{E} \qquad (2\text{-}2)$$

and the vector Green's theorems

$$\iiint \left[\vec{u} \cdot \{\nabla(\nabla\cdot\vec{v})\} - \vec{v}\cdot\{\nabla(\nabla\cdot\vec{u})\} \right] d\tau =$$

$$\oiint \left[(\nabla\cdot\vec{v})\vec{u} - (\nabla\cdot\vec{u})\vec{v} \right] \cdot \vec{n}\, dA \qquad (2\text{-}3)$$

and

$$\iiint \left[\vec{u}\cdot\nabla \times (\nabla \times \vec{v}) - \vec{v}\cdot\nabla \times (\nabla \times \vec{u}) \right] d\tau =$$

$$-\oiint \left[(\vec{n} \times \vec{u})\cdot(\nabla \times \vec{v}) + (\vec{n} \times \{\nabla \times \vec{u}\}) \cdot v \right] dA \qquad (2\text{-}4)\ ,$$

equation (2-5) can be obtained by subtracting μ times equation (2-4) from $(\lambda + 2\mu)$ times equation (2-3).

$$\iiint \left[\vec{u}\cdot L\vec{v} - \vec{v}\cdot L\vec{u} \right] d\tau =$$

$$(\lambda + 2\mu) \oiint \left[(\nabla\cdot\vec{v})\vec{u} - (\nabla\cdot\vec{u})\vec{v} \right] \cdot \vec{n}\, dA$$

$$+ \mu \oiint \left[(\vec{n} \times \vec{u})\cdot(\nabla \times \vec{v}) + (\vec{n} \times \{\nabla \times \vec{u}\})\cdot\vec{v} \right] dA \qquad (2\text{-}5).$$

The stress across a surface with normal $\vec{n}$ is

$$\vec{n}\cdot\underline{T}(\vec{u}) = \lambda(\nabla\cdot\vec{u})\vec{n} + 2\mu\ (\vec{n}\cdot\nabla)\vec{u} + \mu\vec{n}\times(\nabla\times\vec{u}) = \underline{T}(\vec{u})\cdot\vec{n} \qquad (2\text{-}6).$$

Using equation (2-6), the identities

$$\nabla\vec{A} = \frac{1}{2}\left[\nabla\vec{A} + \vec{A}\,\nabla - \underline{I}\times(\nabla\times\vec{A})\right]$$

and

$$\nabla\times(\vec{A}\times\vec{B}) = \vec{B}\cdot(\nabla\vec{A}) - \vec{A}\cdot(\nabla\vec{B}) + \vec{A}\,(\nabla\cdot\vec{B}) - \vec{B}\,(\nabla\cdot\vec{A}) \quad ,$$

and the divergence theorem, equation (2-5) can be written

$$\iiint\left[\vec{u}\cdot L\vec{v} - \vec{v}\cdot L\vec{u}\right]d\tau = \oiint\left\{\left[\underline{T}(\vec{v})\cdot\vec{n}\right]\cdot\vec{u} - \vec{v}\cdot\left[\underline{T}(\vec{u})\cdot\vec{n}\right]\right\}dA \qquad (2\text{-}7).$$

The Green's function for the static elastic equation is the solution of

$$L\,\underline{G}\,(\vec{r}\,|\,\vec{r}_o) = -\,\underline{I}\,\delta(\vec{r} - \vec{r}_o) \qquad (2\text{-}8)$$

where $\underline{G}$ is the Green's dyadic and $\underline{I}$ is the idemfactor. For an infinite medium it is required that $\underline{G} \to 0$ as $\vec{r} \to \infty$. $\vec{r}$ is the observational coordinate system; $\vec{r}_o$ is the source coordinate system. For vector separable coordinate systems (Morse and Feshbach, 1953, Chapter 13) each vector component of $\underline{G}$ is a solution, one in the $\vec{r}$ system and one in the $\vec{r}_o$ system, so $G(\vec{r}_o\,|\,\vec{r})$ can be substituted for $\vec{v}$ in equation (2-7) to give

$$\vec{u}(\vec{r}) = \iiint \underline{G}\cdot\vec{F}\,d\tau_o + \iint \underline{G}\cdot\left[\underline{T}_o(\vec{u})\cdot\vec{n}\right]dA_o$$

$$- \iint\left[\underline{T}_o\,(\underline{G})\cdot\vec{n}\right]\cdot\vec{u}\,dA_o \qquad (2\text{-}9).$$

With reference to Figure 2-1, choose $\vec{n}$ equal to $\vec{n}_-$ thus defining the positive sense of $\Delta\vec{u}$ by

$$\Delta\vec{u} = \vec{u}_+ - \vec{u}_- \tag{2-10}$$

where $\Delta\vec{u}$ is to be the discontinuity in the displacement field across the dislocation surface Σ. For simplicity $\vec{F}$ is now set to zero. $\vec{F}$ not equal to zero simply retains the term $\iiint \underline{G}\cdot\vec{F}\, d\tau_o$.

Apply equation (2-9) to Σ_+ and Σ_- to obtain

$$\vec{u}(\vec{r}) = \iint_{\Sigma_+} \left\{ \underline{G}\cdot \left[\underline{T}_o(\vec{u}_+)\cdot\vec{n}_+ \right] - \left[\underline{T}_o(\underline{G})\cdot\vec{n}_+ \right] \cdot\vec{u}_+ \right\} dA_o$$

$$+ \iint_{\Sigma_-} \left\{ \underline{G}\cdot \left[\underline{T}_o(\vec{u}_-)\cdot\vec{n}_- \right] - \left[\underline{T}_o(\underline{G})\cdot\vec{n}_- \right] \cdot\vec{u}_- \right\} dA_o \tag{2-11}.$$

Σ_+ and Σ_- are brought together to form the single surface Σ with normal $\vec{n}$. Continuity of stress is required which gives

$$\underline{T}\,(\vec{u}_+)\cdot\vec{n}_+ + \underline{T}\,(\vec{u}_-)\cdot\vec{n}_- = 0$$

and then by use of equation (2-10)

$$\vec{u}(\vec{r}) = \iint_{\Sigma} \left[\underline{T}_o\,(\underline{G})\cdot\vec{n} \right] \cdot \Delta\vec{u}\, dA_o \tag{2-12}.$$

Equation (2-12) is a representation of the displacement field due to a displacement dislocation. The term displacement dislocation is used to describe the above defined singularity or source which, by construction, is characterized by an element of surface across which there is a discontinuity in the displacement field, but the stress field is continuous. For convenience the term "dislocation" will be used here to refer to a displacement dislocation as defined above. The specification of a dislocation surface requires the unit vector normal to the dislocation surface, $\vec{n}$, and the value of the discontinuity in displacement, $\Delta\vec{u}$, at each point of the dislocation surface.

If there had been no surfaces present in the medium, but body forces had been applied then equation (2-9) would have become

$$\vec{u}(\vec{r}) = \iiint \underline{G}\cdot\vec{F}\, d\tau_o \qquad (2\text{-}13).$$

Burridge and Knopoff (1964) show that equation (2-12) can be written in the same form as equation (2-13). This leads to the notion of "body force equivalents" for displacement dislocation sources. The subject is thoroughly treated in their article.

In the later parts of this chapter the Green's function, $\underline{G}$, in the foregoing will be understood to be the particular solution to equation (2-8) with the medium infinite in extent. The Green's function for this case is denoted $\underline{G}_\infty$. If there is a boundary surface S in the medium, a sufficient amount of the homogeneous solution to equation (2-8) is added to $\underline{G}_\infty$ to satisfy the boundary conditions.

The additional homogeneous solution is denoted $\underline{G}_H$ so that for the complete problem including the boundary surface

$$\underline{G} = \underline{G}_\infty + \underline{G}_H \quad .$$

Relation between the Static Deformational Field of a Dislocation Source and that due to Stress Relaxation

Chapters 3 and 4 are devoted to the construction of the explicit forms of $\underline{G}$ or $\underline{T}_o(\underline{G})\cdot\vec{n}$ for use in calculating the displacement fields due to certain dislocation sources which can be interpreted as models of faulting. Although the argument for the model of faulting adopted will not be presented until Chapter 5, the relationship between the fault model adopted and a dislocation source is conveniently carried out here.

Equation (2-9) can be written

$$\vec{u}_{ini}(\vec{r}) = \iiint G\cdot\vec{F}\, d\tau_o + \iint \left\{ \underline{G}\cdot \left[\underline{T}_o(\vec{u})\cdot\vec{n} \right] - \left[\underline{T}_o(\underline{G})\cdot\vec{n} \right]\cdot\vec{u} \right\} dA_o \qquad (2\text{-}14).$$

$\vec{u}_{ini}(\vec{r})$ is interpreted here as an initial displacement field due to body forces $\vec{F}$ and surface tractions or displacements across surfaces S in the medium. $\underline{G}$ is the Green's function for the appropriate

boundary conditions. In the earth, for example, the solution is regular at the origin and the stress equals zero at the surface. The development here assumes that a fault develops on a surface Σ by the stress relaxing to zero on Σ. The surface Σ will be taken to enclose no volume. The notation Σ_+ and Σ_- is retained as in the previous section to distinguish the two "sides" of Σ, and the procedure of imagining Σ_+ and Σ_- to coalesce to form Σ is used. The stress field $\underline{T}(\vec{u}_{ini})$ associated with $\vec{u}_{ini}$ is called the prestress field. In particular there are tractions $\underline{T}(\vec{u}_{ini})\cdot\vec{n}\pm$ across the surfaces $\Sigma\pm$ for which the notations

$$\vec{\tau}_+ = \underline{T}(\vec{u}_{ini})\cdot\vec{n}_+ \quad \text{on} \quad \Sigma_+ \tag{2-15a}$$

$$\vec{\tau}_- = \underline{T}(\vec{u}_{ini})\cdot\vec{n}_- \quad \text{on} \quad \Sigma_- \tag{2-15b}$$

are used.

Let $\underline{G}'$ be the Green's function for the same conditions as equation (2-14) except that Σ is a stress free boundary. If, as Σ_+ and Σ_- coalesce, the limit of τ_+ and τ_- in equations (2-15) is zero everywhere on Σ, then redefine Σ so this is not the case. This is necessary since stress relaxation cannot occur if Σ is not prestressed. Applying equation (2-9) to the problem for which $\underline{G}'$ is the Green's function, there results

$$\vec{u}_{\Sigma}(\vec{r}) = \iiint G' \cdot \vec{F}\, d\tau_o + \oiint_S \left\{ G' \cdot \left[\underline{T}_o(\vec{u}) \cdot \vec{n} \right] - \left[\underline{T}_o(\underline{G}') \cdot \vec{n} \right] \cdot \vec{u} \right\} dA_o \tag{2-16}$$

where $\vec{F}$ and S are the same as in equation (2-14). Assume that

$$\Delta\vec{u} = \vec{u}_{\Sigma+} - \vec{u}_{\Sigma-} \tag{2-17}$$

is not zero everywhere on Σ. The assumption will be justified later.

Now using equation (2-12) a discontinuity in displacement on Σ in the amount $\Delta\vec{u}$, as determined from equation (2-16), is added to the displacement field of equation (2-14) giving

$$\vec{u}_{tot} = \vec{u}_{ini} + \iint_{\Sigma} \left[\underline{T}_o(\underline{G}) \cdot \vec{n} \right] \cdot \Delta\vec{u}\, dA_o \tag{2-18}.$$

Note that $\underline{G}$ is appropriate to the boundary conditions of the problem for equation (2-14), not to that for equation (2-16).

If the surface Σ is interpreted as a cut thus insuring the single-valuedness of $\vec{u}_{tot}$, then the boundary conditions specified in equation (2-18) uniquely determine the solution with the possible exception of an additive constant corresponding to a rigid body displacement. Similarly the solution determined by equation (2-16) is unique with the same possible exception. If such a constant appears, it can be chosen the same in both cases and will not be considered further. In equation (2-18) the boundary conditions on Σ are specification of the discontinuity in displacement, $\Delta\vec{u}$, and continuity of stress across Σ. The condition that the stress be zero on Σ in the solution given by equation (2-16) also requires that the stress is

continuous across Σ, and, since $\Delta\vec{u}$ on Σ is the same in each case, the solution to equation (2-16) satisfies the same boundary conditions as the solution to equation (2-18). The uniqueness of each solution requires that they be identical. This also justifies the assumption made in equation (2-17) that $\Delta\vec{u}$ is not zero everywhere on Σ. If it were, then $\vec{u}_\Sigma$ would be identical with $\vec{u}_{ini}$ by the above argument, but this would contradict the condition that τ_+ and τ_- are not zero everywhere on Σ.

The development above assumes that the body forces and boundary conditions which determined the prestress field remain unchanged during the process where Σ becomes a stress free surface. The exclusion of some of the prestressing body forces and boundary conditions gave rise to the conclusion of Steketee (1958) that a dislocation model of a fault necessarily resulted in an increase in stored strain energy. That this need not be the case is shown in Appendix 2.

In summary it has been shown that there is a dislocation distribution $\Delta\vec{u}(\vec{r}_o)$ on Σ which gives a displacement field which equals the change in displacement field caused by the introduction of a stress free surface,Σ, into a prestressed medium. The choice of $\Delta\vec{u}$ depends on the prestress field as is physically obvious that it must. Although a knowledge of the prestress field is the logical way to pose a problem involving prestress, it does not allow a direct calculation of $\vec{u}(\vec{r})$ by equation (2-12). Either $\Delta\vec{u}$ must be known a priori, which in effect means determing $\underline{G}'$ in equation (2-16), or equation (2-12) must be interpreted as an integral equation in

which $\Delta\vec{u}$ is to be determined by requiring that

$$\underline{T}(\vec{u}_{\pm})\cdot\vec{n}_{\pm} - \underline{T}(\vec{u}_{ini})\cdot\vec{n}_{\pm} = 0 \qquad \text{on } \Sigma.$$

It is also possible to choose $\Delta\vec{u}$'s arbitrarily or from physical considerations and use equation (2-12) to determine what prestress field must be relaxed to give that $\Delta\vec{u}$. The results of interest here are to be applied to observations far from the source region and it will be shown in Chapter 5 what is critical in the choice of the distribution in $\Delta\vec{u}$ over Σ for this problem.

Construction of the Green's Dyadic in Vector Separable Coordinates

In Chapters 3 and 4 the explicit form of the Green's function is determined for certain problems in two coordinate systems. The notation used in this section is strictly appropriate to spherical coordinates. The construction in circular cylindrical coordinates is so similar that this section will be used as a theoretical framework for that case also. Specific differences will be pointed out in Chapters 3 and 4 where each solution is given in detail.

The method of constructing the Green's dyadic $\underline{G}$ is treated here in three parts. First the construction of the homogeneous solution to equation (2-1) in a coordinate system which is natural to the problem. Then the representation of the delta function in the same coordinate system. This allows a representation of the

Green's function for an infinite medium. For these two parts to give results which are in a form where it is convenient to meet the boundary conditions the coordinate system must be "vector separable". Vector separability is discussed in Morse and Feshbach (1953, Chapter 13) where it is shown that circular cylindrical coordinates and spherical coordinates are vector separable for the static elastic problem. Finally, a sufficient amount of the homogeneous solution is added to the Green's function for an infinite medium to meet the boundary conditions for the problem at hand. For layered media the Thomson-Haskell matrix formalism is used in this last part (see, for example, Gilbert and MacDonald, 1960; or Harkrider, 1964). The development here is limited to layered media where the solution function is known explicitly in each layer. The method can be generalized to cases where the solution function is determined numerically (e.g. Gilbert and Backus, 1966).

The homogeneous solution to equation (2-1) is

$$\vec{u} = \vec{B} - \frac{1}{4(1-\sigma)} \nabla(\vec{r}\cdot\vec{B} + B_o) \qquad (2\text{-}19)$$

where $\vec{B}$ and B_o are an harmonic vector and an harmonic scalar, respectively (e.g. Lur'e, 1964). The harmonic scalar need not be retained. Solutions of the vector harmonic equation are given in Morse and Feshbach (1953, Chapter 13) in forms convenient for spherical coordinates and circular cylindrical coordinates. The solutions are denoted by

$$\vec{M}^1_{m,\ell} \quad , \quad \vec{M}^2_{m,\ell}$$

$$\vec{N}^1_{m,\ell} \quad , \quad \vec{N}^2_{m,\ell}$$

$$\vec{G}^1_{m,\ell} \quad , \quad \vec{G}^2_{m,\ell} \qquad (2\text{-}20).$$

m and ℓ are the ϕ and θ separation indices, respectively, and the superscripts 1 and 2 signify the solutions which are regular at the origin and regular at infinity, respectively. The explicit expressions are given in Chapters 3 and 4. The homogeneous form of equation (2-1) can be written

$$\frac{1}{(1-2\sigma)} \nabla(\nabla\cdot\vec{u}) + \nabla^2\vec{u} = 0 \qquad (2\text{-}21).$$

Since the $\vec{M}$ and $\vec{N}$ solutions in (2-20) have zero divergence, they are already solutions of equation (2-21). The third solution used here is obtained by substituting a constant times the $\vec{G}$ solutions into equation (2-19). The resultant set of solutions are denoted

$$\vec{M}^1_{m,\ell} \quad , \quad \vec{M}^2_{m,\ell}$$

$$\vec{N}^1_{m,\ell} \quad , \quad \vec{N}^2_{m,\ell}$$

$$\vec{E}^1_{m,\ell} \quad , \quad \vec{E}^2_{m,\ell} \qquad (2\text{-}22).$$

The notation used above and subsequently is closely patterned after that in Morse and Feshbach (1953, Chapter 13). There are differences, however, so that each form is defined explicitly at an appropriate place in the text.

The solution for

$$(\lambda + 2\mu)\nabla(\nabla\cdot\vec{u}) - \mu\nabla \times (\nabla \times \vec{u}) = - F\, \delta(\vec{r}-\vec{r}_o)\vec{n} \qquad (2\text{-}23)$$

is now constructed. Consider the problem in an infinite homogeneous medium and require that the solution be regular at the origin and at infinity. The discontinuity implied by equation (2-23) is called a "point force of magnitude F in the $\vec{n}$ direction". This is the same problem which Love (1944, Chapter VIII) calls "a force operative at a point". If the solution is constructed for any $\vec{n}$, then the solution to

$$(\lambda + 2\mu)\nabla(\nabla\cdot\underline{G}) - \mu\nabla \times (\nabla \times \underline{G}) = - \underline{I}\, \delta(\vec{r}-\vec{r}_o)$$

can be constructed where $\underline{G}$ is the Green's dyadic for equation (2-8).

In Chapter 3 the Green's dyadic is constructed explicitly for a homogeneous sphere. In Chapter 4 only certain special cases are explicitly worked out. To illustrate the method of construction of the solution to equation (2-23) consider the case when $\vec{n} = \hat{r}$ in spherical coordinates. Equation (2-23) becomes

$$(\lambda + 2\mu)\nabla(\nabla\cdot\vec{u}) - \mu\nabla \times (\nabla \times \vec{u}) = - F \frac{\delta(r-r_o)\ \delta(\theta-\theta_o)\ \delta(\phi-\phi_o)}{r^2\sin^2\theta}\ \hat{r}$$

(2-24).

Assume a solution

$$\vec{u} = \sum_m \sum_\ell p_{m\ell}(r)\ \vec{P}_{m\ell}(\theta,\phi) + b_{m\ell}(r)\ \vec{B}_{m\ell}(\theta,\phi) + c_{m\ell}(r)\ \vec{C}_{m\ell}(\theta,\phi)$$

(2-25).

$\vec{P}_{m\ell}$, $\vec{B}_{m\ell}$, and $\vec{C}_{m\ell}$ are vector spherical harmonics. Their definitions and their appearance in $\vec{E}$, $\vec{N}$, and $\vec{M}$ are detailed in Chapter 3. Substituting equation (2-25) into equation (2-24) gives

$$\begin{aligned}
&\sum_{m,\ell} (\lambda + 2\mu) \left[\frac{1}{r^2} \frac{\partial}{\partial r} \left(r^2 \frac{\partial p_{m\ell}}{\partial r} \right) - 2 \frac{p_{m\ell}}{r^2} - \frac{\mu}{(\lambda+2\mu)}\ \ell(\ell+1)\ \frac{p_{m\ell}}{r^2} \right] \vec{P}_{m\ell} \\
&\quad + \left[(\lambda + \mu)\ \frac{1}{r^2} \frac{\partial}{\partial r} (r\ p_{m\ell}) + (\lambda+3\mu)\ \frac{p_{m\ell}}{r^2} \right] \sqrt{\ell(\ell+1)}\ \vec{B}_{m\ell} \\
&\quad + \mu \left[\frac{1}{r^2} \frac{\partial}{\partial r} \left(r^2 \frac{\partial b_{m\ell}}{\partial r} \right) - \frac{(\lambda+2\mu)}{\mu}\ \ell(\ell+1)\ \frac{b_{m\ell}}{r^2} \right] \vec{B}_{m\ell} \\
&\quad + \left[- (\lambda+\mu)\ \frac{1}{r^2} \frac{\partial}{\partial r} (r\ b_{m\ell}) + (\lambda+2\mu)\ 2\ \frac{b_{m\ell}}{r^2} \right] \sqrt{\ell(\ell+1)}\ \vec{P}_{m\ell} \\
&\quad + \left[\frac{1}{r^2} \frac{\partial}{\partial r} \left(r^2\ \frac{\partial c_{m\ell}}{\partial r} \right) - \ell(\ell+1)\ \frac{c_{m\ell}}{r^2} \right] \vec{C}_{m\ell} \\
&= - F\ \frac{\delta(r-r_o)\ \delta(\theta-\theta_o)\ \delta(\phi-\phi_o)}{r^2\sin\theta}\ \hat{r}
\end{aligned}$$

(2-26).

By taking the vector dot product of $\vec{P}^*_{\mu\nu}$ into equation (2-26), multiplying by $\sin\theta\, d\theta\, d\phi$, integrating over θ and ϕ, and setting $\mu = m$, $\nu = \ell$ one obtains

$$(\lambda+2\mu)\left[\frac{1}{r^2}\frac{\partial}{\partial r}\left(r^2\frac{\partial p_{m\ell}}{\partial r}\right) - 2\frac{p_{m\ell}}{r^2} - \frac{\mu}{(\lambda+2\mu)}\ell(\ell+1)\frac{p_{m\ell}}{r^2}\right] n_{m\ell}$$

$$+\left[-(\lambda+\mu)\frac{1}{r^2}\frac{\partial}{\partial r}(r\, b_{m\ell}) + (\lambda+2\mu)\, 2\frac{b_{m\ell}}{r^2}\right]\sqrt{\ell(\ell+1)}\, n_{m\ell}$$

$$= -F\frac{\delta(r-r_o)}{r^2}\left[\hat{r}\cdot\vec{P}^*_{m\ell}(\theta_o, \phi_o)\right] \qquad (2\text{-}27)$$

where

$$n_{m\ell} = \frac{4\pi}{(2\ell+1)}\,\frac{(\ell+m)!}{(\ell-m)!}\,.$$

Multiplication by r^2dr and integration of equation (2-27) from $r_o - \varepsilon$ to $r_o + \varepsilon$, while requiring continuity of $p_{m\ell}(r)$ and $b_{m\ell}(r)$, and letting $\varepsilon \to o$ gives

$$(\lambda + 2\mu)\left(\left.\frac{\partial p_{m\ell}}{\partial r}\right|_{r_o^+} - \left.\frac{\partial p_{m\ell}}{\partial r}\right|_{r_o^-}\right) = -\frac{F}{r_o^2}\frac{1}{n_{m\ell}}\,\hat{r}\cdot\vec{P}^*_{m\ell}(\theta_o, \phi_o)$$

(2-28).

Substituting the solution from equation (2-25) into equation (2-6) with $\vec{n} = \hat{r}$ gives the stress across a surface of constant r

$$\hat{r}\cdot\underline{T}(\vec{u}) = \sum_{m,\ell}\left[(\lambda+2\mu)\frac{\partial p_{m\ell}}{\partial r} + 2\lambda\frac{p_{m\ell}}{r} - \lambda\sqrt{\ell(\ell+1)}\ \frac{b_{m\ell}}{r}\right]\vec{P}_{m\ell}$$

$$+ \mu\left[\frac{\partial b_{m\ell}}{\partial r} - \frac{b_{m\ell}}{r} + \sqrt{\ell(\ell+1)}\,\frac{p_{m\ell}}{r}\right]\vec{B}_{m\ell}$$

$$+ \mu\left[\frac{\partial c_{m\ell}}{\partial r} - \frac{c_{m\ell}}{r}\right]\vec{C}_{m\ell} \qquad (2\text{-}29).$$

From comparison of equation (2-28) and (2-29) it is seen that for each m and ℓ the traction across $r = r_o$ parallel to $\vec{P}_{m\ell}$ has a discontinuity of

$$-\frac{F}{r_o^2}\ \frac{1}{n_{m\ell}}\qquad \hat{r}\cdot\vec{P}^*_{m\ell}(\theta_o, \phi_o) \quad .$$

The cases $\vec{n} = \hat{\theta}$ and $\vec{n} = \hat{\phi}$ are treated similarly except that for these cases there is a discontinuity in both $\vec{B}_{m\ell}$ and $\vec{C}_{m\ell}$.

With the discontinuity in stress or displacement determined by the procedure outlined above, the construction is completed by adding a sufficient amount of the homogeneous solution to satisfy the boundary conditions. For a layered medium this can be accomplished with the Thomson-Haskell matrix technique.

In the jth layer of a layered medium the homogeneous solution of equation (2-1) is given by (2-22) where the elastic constants are those appropriate to the jth layer. The layer index j is suppressed

for now. The $\vec{M}$ solutions and the stresses derived from them contain only the vector $\vec{C}_{m\ell}$ so the $\vec{M}$ solutions (zero frequency limit of toroidal motion) can be treated separately. The $\vec{N}$ and $\vec{E}$ solutions (zero frequency analog of spheroidal motion) and the stresses derived from them are in terms of the vectors $\vec{P}_{m\ell}$ and $\vec{B}_{m\ell}$. In the jth layer the spheroidal-like part of the displacement can be written

$$\vec{U}_{PB}(r;\ \ell,\ m) = A_1\ \vec{E}^1_{m,\ell} + A_2\vec{N}^1_{m,\ell} + A_3\ \vec{E}^2_{m,\ell} + A_4\ \vec{N}^2_{m,\ell} \qquad (2\text{-}30).$$

The stress across a face with normal $\hat{r}$ is

$$\vec{T}_{PB}(r;\ \ell,\ m) = A_1\ \hat{r}\cdot\underline{T}\ (\vec{E}^1_{m,\ell}) + A_2\ \hat{r}\cdot\underline{T}\ (\vec{N}^1_{m,\ell})$$

$$+ A_3\ \hat{r}\cdot\underline{T}\ (\vec{E}^2_{m,\ell}) + A_4\ \hat{r}\cdot\underline{T}\ (\vec{N}^2_{m,\ell}) \qquad (2\text{-}31).$$

and from equation (2-29) the stress can also be written in terms of the vectors $\vec{P}_{m\ell}$ and $\vec{B}_{m\ell}$. Equations (2-30) and (2-31) can be rewritten

$$\vec{U}_{PB}(r;\ \ell,\ m) = U_P(r;\ \ell,\ m)\ \vec{P}_{m\ell} + U_B(r;\ \ell,\ m)\ \vec{B}_{m\ell}\ \sqrt{\ell(\ell+1)} \qquad (2\text{-}32).$$

and

$$\vec{T}_{PB}(r;\ \ell,\ m) = T_P(r;\ \ell,\ m)\ (2\vec{P}_{m\ell}) + T_B(r;\ \ell,\ m)\left(2\vec{B}_{m\ell}\ \sqrt{\ell(\ell+1)}\right)$$

(2-33).

By comparing equations (2-30) and (2-31), and (2-32) and (2-33) the following matrix equation is obtained

$$\begin{bmatrix} U_P \\ U_B \\ T_P \\ T_B \end{bmatrix} = \varepsilon(r;\, \ell,\, m) \begin{bmatrix} A_1 \\ A_2 \\ A_3 \\ A_4 \end{bmatrix} \qquad (2\text{-}34).$$

The 4 x 4 matrix $\varepsilon(r;\, \ell,\, m)$ is the solution matrix.

Its elements are given explicitly for the problems treated in Chapters 3 and 4. The layer index j is now included explicitly and equation (2-34) is written

$$U_j(r) = \varepsilon_j(r)\, A_j \qquad (2\text{-}35)$$

where the column vectors U_j and A_j are defined by equation (2-34).

The A_j are now determined for a source at depth $r = r_o$ and the following boundary conditions

a) stress equal to zero at $r = a$,

b) continuity of displacement and stress at each interface $r = r_i$, $i \neq 0$,

c) displacement regular at $r = 0$.

The interfaces are labeled as in Figure 2-2 except that r_o is replaced by $r = a$. Other boundary conditions can be treated in a similar fashion. Condition (b) gives for each interior interface

$$U_j(r_{j-1}) = U_{j-1}(r_{j-1}) \tag{2-36}$$

Apply equation (2-35) at $r = r_{j-1}$ and multiply from the left by $\varepsilon_j^{-1}(r_{j-1})$ yielding

$$A_j = \varepsilon_j^{-1}(r_{j-1})\ U_j(r_{j-1})$$

Substituting this expression into equation (2-35) at $r = r_j$ gives

$$U_j(r_j) = a_j\ U_j(r_{j-1}) \tag{2-37}$$

where

$$a_j = \varepsilon_j(r_j)\ \varepsilon_j^{-1}(r_{j-1}) \tag{2-38}.$$

The matrix a_j propagates the solution from $r = r_{j-1}$ to $r = r_j$ and is called the propagator matrix.

Let the source be at $r = r_o$ in the sth layer. Then with the definitions

$$a^{s+1} \equiv \varepsilon_s(r_s)\ \varepsilon_s^{-1}(r_o)$$

$$D^{s+1} \equiv a_{n-1}\ a_{n-2} \cdots a^{s+1}$$

$$D \equiv a_{n-1}\ a_{n-2} \cdots a_1$$

repeated use of equation (2-37) gives

$$U_n(r_{n-1}) = D\ U_1(a) + D^{s+1}\ \Delta U \tag{2-39}$$

where ΔU is the discontinuity in U due to the source.

Condition (c) requires that $A_3 = A_4 = 0$ for equation (2-30) in the nth layer (i.e. the bottommost layer) so that in the equation

$$U_n(r_{n-1}) = \varepsilon_n(r_{n-1})\, A_n \tag{2-40}$$

A_n has the form

$$A_n = \begin{bmatrix} A_{1,n} \\ A_{2,n} \\ 0 \\ 0 \end{bmatrix} \tag{2-41}$$

Note that if $A_{3,n}$ and $A_{4,n}$ were associated with the solution regular at $r = 0$, A_n would have the zero and non-zero constants in a different position but the basic procedure given here would remain unchanged. $A_{3,n}$ and $A_{4,n}$ are the non-zero constants in the solutions given in Chapter 4.

The boundary condition at $r = a$ requires

$$U_1(a) = \begin{bmatrix} U_P(a) \\ U_B(a) \\ 0 \\ 0 \end{bmatrix} \tag{2-42}.$$

Using the last three equations (2-40, 41, 42), equation (2-39) becomes with the first two terms in expanded notation (and the subscripts "PB" added to the last term)

$$\begin{bmatrix} \varepsilon_{11}(r_{n-1})\ A_{1,n} + \varepsilon_{12}(r_{n-1})\ A_{2,n} \\ \varepsilon_{21}(r_{n-1})\ A_{1,n} + \varepsilon_{22}(r_{n-1})\ A_{2,n} \\ \varepsilon_{31}(r_{n-1})\ A_{1,n} + \varepsilon_{32}(r_{n-1})\ A_{2,n} \\ \varepsilon_{41}(r_{n-1})A_{1,n} + \varepsilon_{42}(r_{n-1})\ A_{2,n} \end{bmatrix}$$

$$= \begin{bmatrix} D_{11}\ U_P(a) + D_{12}\ U_B(a) \\ D_{21}\ U_P(a) + D_{22}\ U_B(a) \\ D_{31}\ U_P(a) + D_{23}\ U_B(a) \\ D_{41}\ U_P(a) + D_{24}\ U_B(a) \end{bmatrix} + D_{PB}^{s+1}\ \Delta U_{PB}$$

(2-43).

Transposing the first term on the right to the left this is rewritten

$$X_{PB}\ Y_{PB} = -\ D_{PB}^{s+1}\ \Delta U_{PB} \qquad (2\text{-}44)$$

where

$$X_{PB} \equiv \begin{bmatrix} D_{11} & D_{12} & \varepsilon_{11}(r_{n-1}) & \varepsilon_{12}(r_{n-1}) \\ D_{21} & D_{22} & \varepsilon_{21}(r_{n-1}) & \varepsilon_{22}(r_{n-1}) \\ D_{31} & D_{32} & \varepsilon_{31}(r_{n-1}) & \varepsilon_{32}(r_{n-1}) \\ D_{41} & D_{42} & \varepsilon_{41}(r_{n-1}) & \varepsilon_{42}(r_{n-1}) \end{bmatrix}$$

and

$$Y_{PB} \equiv \begin{bmatrix} U_p(a) \\ U_B(a) \\ -A_{1,n} \\ -A_{2,n} \end{bmatrix}$$

The solution for Y_{PB} is

$$Y_{PB} = - X_{PB}^{-1} D_{PB}^{s+1} \Delta U_{PB}$$

which includes the displacements at r = a (i.e. the coefficient of $\vec{P}_{m\ell}$ or $\vec{B}_{m\ell}$ $\sqrt{\ell(\ell+1)}$ in equation (2-32)). The solution at depth can be obtained by using equations (2-37) and (2-35) although these are not explicitly calculated for the layered models considered here. The calculations for the toroidal-like case are precisely analogous except that a 2 x 2 matrix system results instead of a 4 x 4 system.

Chapter 3

THE GREEN'S DYADIC FOR THE ELASTIC DISTORTION OF A HOMOGENEOUS SPHERE AND THE SURFACE DISPLACEMENT DUE TO A BURIED DISLOCATION

The Green's dyadic is derived for a homogeneous sphere with the boundary condition of zero stress at the surface. Using the body force equivalents, expressions for the surface displacements due to two types of buried dislocations are derived. For one component of displacement the series representation was partially summed to obtain a rapidly converging form. The result is compared to the same problem in a half-space to show the effect of sphericity on the static deformational field due to seismic sources. Reference will be made to the pertinent formulas in Chapter 2 in order to relate the results given here to the theory presented there.

Derivation of the Green's Dyadic for a Homogeneous Sphere

Vector spherical harmonics are given in Morse and Feshbach (1953, pp 1799-1800) as

$$\vec{M}^1_{m,\ell} = r^{\ell}\ \vec{C}_{m\ell}\ \sqrt{\ell(\ell+1)}$$

$$\vec{M}^2_{m,\ell} = r^{-\ell-1}\ \vec{C}_{m\ell}\ \sqrt{\ell(\ell+1)}$$

$$\vec{N}^1_{m,\ell-1} = r^{\ell-1}\left[\ \ell\ \vec{P}_{m\ell} + \vec{B}_{m\ell}\ \sqrt{\ell(\ell+1)}\ \right]$$

$$\vec{N}^2_{m,\ell+1} = r^{-\ell-2}\left[-(\ell+1)\ \vec{P}_{m\ell} + \vec{B}_{m\ell}\ \sqrt{\ell(\ell+1)}\ \right] \qquad (3\text{-}1)$$

$$\vec{G}^1_{m,\ell+1} = r^{\ell+1}\left[\ \vec{B}_{m,\ell}\sqrt{\ell(\ell+1)} - (\ell+1)\ \vec{P}_{m,\ell}\ \right]$$

$$\vec{G}^2_{m,\ell-1} = R^{-\ell-1}\left[\ \vec{B}_{m,\ell}\ \sqrt{\ell(\ell+1)} + \ell\ \vec{P}_{m,\ell}\ \right] .$$

These are the functions of expression (2-20). The $\vec{P}$, $\vec{B}$, and $\vec{C}$ functions are defined by

$$\vec{P}_{m,\ell} = \hat{r}\ e^{im\phi}\ P^m_{\ell}(\cos\ \theta)$$

$$\vec{B}_{m,\ell} = \frac{r}{\sqrt{\ell(\ell+1)}}\ \nabla\left[\ e^{im\phi}\ P^m_{\ell}(\cos\ \theta)\ \right]$$

$$\vec{C}_{m,\ell} = \frac{r}{\sqrt{\ell(\ell+1)}}\ \nabla\ x\left[\ \hat{r}\ e^{im\phi}\ P^m_{\ell}(\cos\ \theta)\ \right] .$$

The coordinate system is shown in Figure 3-1.

In order to avoid an even more highly super-and subscripted notation, the convention is adopted above and throughout the text that the index m associated with the ϕ function may range from $-\ell$ to $+\ell$ while the index m associated with the θ function is always to be interpreted as $|m|$.

Define

$$\kappa = 2(1-\sigma)$$

and choose $\vec{B}$ in equation (2-19) as $2\kappa\vec{G}$. Then the solutions are

$$\vec{E}^1_{m,\ell+1} = r^{\ell+1}\left[(\ell+1)\, L_1\, \vec{P}_{m,\ell} + L_3\, \vec{B}_{m,\ell}\, \sqrt{\ell(\ell+1)} \right]$$

$$\vec{E}^2_{m,\ell-1} = r^{-\ell}\left[\ell\, L_2\, \vec{P}_{m,\ell} - L_4\, \vec{B}_{m,\ell}\, \sqrt{\ell(\ell+1)} \right] \qquad (3\text{-}2)$$

with

$$L_1 = (\ell+2) - 2\kappa$$

$$L_2 = (\ell-1) + 2\kappa$$

$$L_3 = (\ell+1) + 2\kappa$$

$$L_4 = \ell - 2\kappa \quad .$$

The stress across a face r = constant will be needed and follows from equation (2-29) together with the identities given in Appendix 3.

The results are

$$\hat{r}\cdot\underline{T}\left(\vec{M}^1_{m,\ell}\right) = \mu\ (\ell-1)\ r^{-1}\ \vec{M}^1_{m,\ell}$$

$$\hat{r}\cdot\underline{T}\left(\vec{M}^2_{m,\ell}\right) = -\mu\ (\ell+2)\ r^{-1}\ \vec{M}^2_{m,\ell}$$

$$\hat{r}\cdot\underline{T}\left(\vec{N}^1_{m,\ell-1}\right) = 2\mu\ (\ell-1)\ r^{-1}\ \vec{N}^1_{m,\ell-1} \qquad (3\text{-}3)$$

$$\hat{r}\cdot\underline{T}\left(\vec{N}^2_{m,\ell+1}\right) = -2\mu\ (\ell+2)\ r^{-1}\ \vec{N}^2_{m,\ell+1}$$

$$\hat{r}\cdot\underline{T}\left(\vec{E}^1_{m,\ell+1}\right) = 2\mu\ r^{\ell}\left[\ (\ell+1)\ L_5\ \vec{P}_{m\ell} + L_7\ \vec{B}_{m\ell}\ \sqrt{\ell(\ell+1)}\ \right]$$

$$\hat{r}\cdot\underline{T}\left(\vec{E}^2_{m,\ell-1}\right) = 2\mu\ r^{-\ell-1}\left[\ -\ell\ L_6\ \vec{P}_{m\ell} + L_8\ \vec{B}_{m\ell}\ \sqrt{\ell(\ell+1)}\ \right]$$

where

$$L_5 = \ell(\ell-1) - 4 + \kappa$$

$$L_6 = (\ell+1)(\ell+2) - 4 + \kappa$$

$$L_7 = (\ell+1)^2 - \kappa$$

$$L_8 = \ell^2 - \kappa$$

In order to expand the solution in equation (2-26) it is convenient to expand

$$\frac{\delta(\theta-\theta_o)\ \delta(\phi-\phi_o)\quad \hat{n}}{\sin\theta}$$

in terms of the functions $\vec{P}_{m\ell}$, $\vec{B}_{m\ell}$, and $\vec{C}_{m\ell}$. Then the discontinuity in the radial function is determined from equation (2-28). These results are given in Appendix 4.

For the solution matrix $\varepsilon(r;\ \ell,\ m)$ the components of the left hand side of equation (2-34) are defined by

$$\vec{u} = \sum_{m,\ell} \quad U_p \vec{P}_{m\ell} + U_B \vec{B}_{m\ell} \sqrt{\ell(\ell+1)} + U_c \vec{C}_{m\ell} \sqrt{\ell(\ell+1)} \tag{3-4a}$$

and

$$\vec{t} = \sum_{m,\ell} \quad T_p 2\vec{P}_{m\ell} + T_B 2\vec{B}_{m\ell} \sqrt{\ell(\ell+1)} + T_c \vec{C}_{m\ell} \sqrt{\ell(\ell+1)} \tag{3-4b}$$

Then the components of $\varepsilon(r)$ associated with the vectors $\vec{P}_{m\ell}$ and $\vec{B}_{m\ell}$ are defined by reference to equations (3-1), (3-2), and (3-3).

$$\varepsilon_R(r) = \begin{bmatrix} (\ell+1)\, L_1\, r^{\ell+1} & \ell r^{\ell-1} & \ell L_2 r^{-\ell} & -(\ell+1)\, r^{-\ell-2} \\ L_3\, r^{\ell+1} & r^{\ell-1} & -L_4\, r^{-\ell} & r^{-\ell-2} \\ \mu(\ell+1)\, L_5\, r^{\ell} & \mu\ell(\ell-1)\, r^{\ell-2} & -\mu\ell\ L_6\, r^{-\ell-1} & \mu(\ell+1)(\ell+2)\, r^{-\ell-3} \\ \mu\, L_7\, r^{\ell} & \mu(\ell-1)\, r^{\ell-2} & \mu\, L_8\, r^{-\ell-1} & -\mu\ (\ell+2)\, r^{-\ell-3} \end{bmatrix}$$

(3-5).

$$\varepsilon_R^{-1}(r) = \begin{bmatrix} -\mathcal{B}\ (\ell+2)\ r^{-\ell-1} & \mathcal{B}\ell(\ell+2)\ r^{-\ell-1} & -\mathcal{B}\ \frac{r^{-\ell}}{\mu} & \mathcal{B}\ell\ \frac{r^{-\ell}}{\mu} \\ C\ L_6\ r^{-\ell+1} & -C\ (\ell+1)\ L_8\ r^{-\ell+1} & C\ L_2\ \frac{r^{-\ell+2}}{\mu} & -C\ (\ell+1)\ L_4 \frac{r^{-\ell+2}}{\mu} \\ C(\ell-1)\ r^{\ell} & C(\ell+1)(\ell-1)\ r^{\ell+1} & -C\ \frac{r^{\ell+1}}{\mu} & -C\ (\ell+1)\ \frac{r^{\ell+1}}{\mu} \\ \mathcal{B}\ L_5\ r^{\ell+2} & \mathcal{B}\ell\ L_7\ r^{\ell+2} & -\mathcal{B}\ L_1\ \frac{r^{\ell+3}}{\mu} & -\mathcal{B}\ell\ L_3\ \frac{r^{\ell+3}}{\mu} \end{bmatrix}$$

(3-6).

where

$$\mathcal{B} = \frac{1}{(2\ell+3)(2\ell+1)} \qquad C = \frac{1}{(2\ell-1)(2\ell+1)} \quad .$$

For the $\varepsilon(r)$ associated with $\vec{C}_{m\ell}$

$$\varepsilon_L(r) = \begin{bmatrix} r^{\ell} & r^{-\ell-1} \\ \mu(\ell-1)\, r^{\ell-1} & -\mu\,(\ell+2)\, r^{-\ell-2} \end{bmatrix} \tag{3-7}.$$

$$\varepsilon_L^{-1}(r) = \begin{bmatrix} \frac{(\ell+2)}{(2\ell+1)}\, r^{-\ell} & \frac{1}{(2\ell+1)}\, \frac{r^{-\ell+1}}{\mu} \\ \frac{(\ell-1)}{(2\ell+1)}\, r^{\ell+1} & -\frac{1}{(2\ell+1)}\, \frac{r^{\ell+2}}{\mu} \end{bmatrix} \tag{3-8}.$$

The elements of the propagator matrix, equation (2-38), are given in Appendix 5.

To derive $\underline{G}_{\infty}$ we require that the solution be regular at r = 0 and r = ∞ with a point force source at $\vec{r}_o = (r_o, \theta_o, \phi_o)$.

In this case equation (2-43) becomes

$$
\begin{bmatrix}
\varepsilon_{11}(r_o)\, A_1 + \varepsilon_{12}(r_o)\, A_2 \\
\varepsilon_{21}(r_o)\, A_1 + \varepsilon_{22}(r_o)\, A_2 \\
\varepsilon_{31}(r_o)\, A_1 + \varepsilon_{32}(r_o)\, A_2 \\
\varepsilon_{41}(r_o)\, A_1 + \varepsilon_{42}(r_o)\, A_2
\end{bmatrix}
=
\begin{bmatrix}
\varepsilon_{13}(r_o)\, A_3 + \varepsilon_{14}(r_o)\, A_4 \\
\varepsilon_{23}(r_o)\, A_3 + \varepsilon_{24}(r_o)\, A_4 \\
\varepsilon_{33}(r_o)\, A_3 + \varepsilon_{34}(r_o)\, A_4 \\
\varepsilon_{43}(r_o)\, A_3 + \varepsilon_{44}(r_o)\, A_4
\end{bmatrix}
+
\begin{bmatrix}
0 \\
0 \\
\Delta T_P \\
\Delta T_B
\end{bmatrix}
$$

for the spheroidal-like part and

$$\begin{bmatrix} \varepsilon_{11}(r_o)\ B_1 \\ \varepsilon_{21}(r_o)\ B_1 \end{bmatrix} = \begin{bmatrix} \varepsilon_{12}(r_o)\ B_2 \\ \varepsilon_{12}(r_o)\ B_2 \end{bmatrix} + \begin{bmatrix} 0 \\ \Delta T_C \end{bmatrix}$$

for the toroidal-like part. The solution to these equations are

$$\begin{bmatrix} A_1 \\ A_2 \\ -A_3 \\ -A_4 \end{bmatrix} = \varepsilon_R^{-1}(r_o) \begin{bmatrix} 0 \\ 0 \\ \Delta T_P \\ \Delta T_B \end{bmatrix} \qquad (3\text{-}9a)$$

and

$$\begin{bmatrix} B_1 \\ -B_2 \end{bmatrix} = \varepsilon_L^{-1}(r_o) \begin{bmatrix} 0 \\ \Delta T_c \end{bmatrix} \qquad (3\text{-}9b).$$

Solving equations (3-9) for the values of ΔT_P, ΔT_B, and ΔT_c determined for a point force source in each of the coordinate directions gives the displacement field $\vec{u}$ by equation (3-4a) for each source. Let $\vec{u}^r$ be the displacement due to a unit point force located at $\vec{r}_o = (r_o, \theta_o, \phi_o)$ and pointing in the $\hat{r}$ direction,

and similarly define $\vec{u}^{\theta}$ and $\vec{u}^{\phi}$. $\vec{u}^{r}$, $\vec{u}^{\theta}$, and $\vec{u}^{\phi}$ were each determined by explicitly solving equations (3-9). The actual expressions are not duplicated here since they are quite long. The Green's dyadic when dotted into the source vector gives the displacement field due to a point force, that is

$$\vec{u}^{r} = \underline{G}_{\infty} \cdot \hat{r}_o$$

$$\vec{u}^{\theta} = \underline{G}_{\infty} \cdot \hat{\theta}_o$$

and $$\vec{u}^{\phi} = \underline{G}_{\infty} \cdot \hat{\phi}_o \quad .$$

By inspection of the forms for $\vec{u}^{r}$, $\vec{u}^{\theta}$, and $\vec{u}^{\phi}$ derived as described above the form of $\underline{G}_{\infty}$ was deduced to be[1]

[1] In the form for $\underline{G}_{\infty}$ and throughout the text the superscript * denotes complex conjugate.

$$
\underline{G}_{\infty} = \begin{cases}
\displaystyle\sum_{\ell=0}^{\infty} \sum_{m=-\ell}^{\ell} \frac{1}{8\pi\mu} \frac{(\ell-|m|)!}{(\ell+|m|)!} \left\{ \frac{\vec{E}^{1}_{m,\ell+1}(\vec{r})\ \vec{N}^{2*}_{m,\ell+1}(\vec{r}_o)}{\kappa(\ell+1)(2\ell+3)} + \frac{\vec{N}^{1}_{m,\ell-1}(\vec{r})\ \vec{E}^{2*}_{m,\ell-1}(\vec{r}_o)}{\kappa(\ell)(2\ell-1)} + \frac{2}{\ell(\ell+1)}\ \vec{M}^{1}_{m,\ell}(\vec{r})\ \vec{M}^{2*}_{m,\ell}(\vec{r}_o) \right\} & r \leqslant r_o \\
\displaystyle\sum_{\ell=0}^{\infty} \sum_{m=-\ell}^{\ell} \frac{1}{8\pi\mu} \frac{(\ell-|m|)!}{(\ell+|m|)!} \left\{ \frac{\vec{E}^{2}_{m,\ell-1}(\vec{r})\ \vec{N}^{1*}_{m,\ell-1}(\vec{r}_o)}{\kappa(\ell)(2\ell-1)} + \frac{\vec{N}^{2}_{m,\ell+1}(\vec{r})\ \vec{E}^{1*}_{m,\ell+1}(\vec{r}_o)}{\kappa(\ell+1)(2\ell+3)} + \frac{2}{\ell(\ell+1)}\ \vec{M}^{2}_{m,\ell}(\vec{r})\ \vec{M}^{1*}_{m,\ell}(\vec{r}_o) \right\} & r \geqslant r_o
\end{cases}
$$

$\underline{G}_\infty$ was obtained by a procedure which was essentially that of the Thomson-Haskell matrix formulation. The same procedure could be used to obtain the Green's dyadic for a sphere, but it is more convenient to view the problem slightly differently. A sufficient amount of the homogeneous solution which is regular at the origin (the vectors superscripted 1 in expression (2-22)) can be added to satisfy the boundary condition that the stress = 0 at r = a. This latter part was called $\underline{G}_H$ in Chapter 2. Assume the form

$$\underline{G}_s = \underline{G}_\infty + \sum_{m,\ell} \left[\vec{E}^1_{m,\ell+1}(\vec{r})\, \vec{A}_o + \vec{N}^1_{m,\ell-1}(\vec{r})\, \vec{B}_o + \vec{M}^1_{m,\ell}(\vec{r})\, \vec{C}_o \right]$$

where $\vec{A}_o$, $\vec{B}_o$, and $\vec{C}_o$ are undetermined vectors. The stress operator is applied from the right to the $\vec{r}$ coordinates giving

$$\hat{r}\cdot\underline{T}\,(\underline{G}_s) = \hat{r}\cdot\underline{T}\,(\underline{G}_\infty) + \hat{r}\cdot\underline{T}\left\{ \sum_{m,\ell} \left[\vec{E}^1_{m,\ell+1}\, \vec{A}_o + \vec{N}^1_{m,\ell-1}(\vec{r})\, \vec{B}_o + \vec{M}^1_{m,\ell}(\vec{r})\, \vec{C}_o \right] \right\} \qquad (3\text{-}10).$$

$\vec{A}_o$, $\vec{B}_o$, and $\vec{C}_o$ must be expressed in terms of the unit vectors $\hat{r}_o$, $\hat{\theta}_o$, $\hat{\phi}_o$ and the coordinates r_o, θ_o, ϕ_o. Setting r = a in equation (3-10) and requiring that $\hat{r}\cdot\underline{T}\,(\underline{G}_s) = 0$ determines $\vec{A}_o$, $\vec{B}_o$, and $\vec{C}_o$. The resulting expression for $\underline{G}_s$ is

$$\underline{G}_S = \underline{G}_\infty + \sum_{\ell=0}^{\infty} \sum_{m=-\ell}^{\ell} \frac{1}{8\pi\mu} \frac{(\ell-|m|)!}{(\ell+|m|)!}$$

$$\left\{ \frac{\vec{E}^1_{m,\ell+1}(\vec{r})}{2\kappa\Delta} \left[a^{-2\ell-3} \frac{(\ell+2)(2\ell+1)}{(\ell+1)(2\ell+3)} \vec{E}^{1*}_{m,\ell+1}(\vec{r}_o) - a^{-2\ell-1} (\ell+2) \vec{N}^{1*}_{m,\ell-1}(\vec{r}_o) \right] \right.$$

$$+ \frac{\vec{N}_{m,\ell-1}(\vec{r})}{2\kappa\Delta} \left[a^{-2\ell+1} \frac{(2\ell+1)\ \Psi}{\ell(\ell-1)(2\ell-1)} \vec{N}^{1*}_{m,\ell-1}(\vec{r}_o) - a^{-2\ell-1} (\ell+2) \vec{E}^{1*}_{m,\ell+1}(\vec{r}_o) \right]$$

$$\left. + 2\ \vec{M}^1_{m,\ell}(\vec{r}) \left[a^{-2\ell-1} \frac{(\ell+2)}{\ell(\ell+1)(\ell-1)} \vec{M}^{1*}_{m,\ell}(\vec{r}_o) \right] \right\}$$

where

$$\Delta = \frac{1}{2} \left[2(\ell+1)(\ell+2) - \kappa(2\ell+1) \right]$$

$$\Psi = (\ell-1)(\ell)(\ell+1)(\ell+2) + 4\kappa - \kappa^2$$

Surface Displacements due to a Buried Dislocation

The integral kernel in equation (2-12) gives the field due to a particular point dislocation surface. Explicit formulas from which the integral kernel

$$\left[\underline{T}_o \ (\underline{G}) \cdot \hat{n} \right] \cdot \Delta \hat{u}$$

can be easily derived are given in Appendix 6.

The resultant series representation for the displacement field for two cases is given below. The expressions are for $\theta_o = 0$, $\phi_o = 0$ and $r = a$. With the notation

$$\left[\underline{T}_o \ (\underline{G}_s) \cdot \hat{n} \right] \cdot \Delta \hat{u} \equiv \vec{u}(\hat{n}, \Delta \hat{u})$$

then $\vec{u}(\hat{\theta}_o, -\hat{\phi}_o)$ is the point source approximation for a buried right lateral strike slip fault with fault plane with normal $\hat{\theta}_o$, or for a buried left lateral strike slip fault with fault plane with normal $-\hat{\phi}_o$; and $\vec{u}(\hat{\theta}_o, \hat{r}_o)$ is the point source approximation for a buried dip slip fault with fault plane with normal $\hat{\theta}_o$ with the south side moving up, or for a buried horizontal thrust fault with fault plane with normal $\hat{r}_o$ with the upper surface thrust to the south (see Figure 3-1 for the conventions used in these descriptions). The results are

$$\vec{u}(\hat{\theta}_o, -\hat{\phi}_o) = \sum_{\ell=2}^{\infty} \frac{(2\ell+1)}{16\pi a^2} \left\{ \left\{ \hat{r} \sin 2\phi \; P_\ell^2 \frac{t^\ell}{\Delta} \left[L_3 - \frac{L_7 \, t^{-2}}{(\ell-1)} \right] \right. \right.$$

$$+ \hat{\theta} \sin 2\phi \left\{ \frac{\partial P_\ell^2}{\partial \theta} \alpha_1 - \frac{2 P_\ell^2}{\sin \theta} \alpha_2 \right\}$$

$$\left. \left. + \hat{\theta} \cos 2\phi \left\{ \frac{2 P_\ell^2}{\sin \theta} \alpha_1 - \frac{\partial P_\ell^2}{\partial \theta} \alpha_2 \right\} \right\} \right\}$$

(3-11a)

$$\vec{u}(\hat{\theta}_o, \hat{r}_o) = \sum_{\ell=1}^{\infty} \frac{(2\ell+1)}{8\pi a^2} \left\{ \left\{ \hat{r} \cos\phi \; P_\ell^1 \frac{L_7 \, t^\ell}{\Delta} \left[t^2 - 1 \right] \right. \right.$$

$$+ \hat{\theta} \cos \phi \left\{ \frac{\partial P_\ell^1}{\partial \theta} \alpha_3 + \frac{P_\ell^1}{\sin \theta} \alpha_4 \right\}$$

$$\left. \left. + \hat{\theta} \sin \phi \left\{ - \frac{P_\ell^1}{\sin\theta} \alpha_3 - \frac{\partial P_\ell^1}{\partial \theta} \alpha_4 \right\} \right\} \right\}$$

(3-11b)

where

$$\alpha_1 = \frac{t^{\ell}}{\Delta}\left[\frac{L_5\, t^{-2}}{(\ell-1)(\ell)} - \frac{L_3}{(\ell+1)}\right]$$

$$\alpha_2 = 4\,\frac{t^{\ell-1}}{(\ell-1)(\ell)(\ell+1)}$$

$$\alpha_3 = \frac{t^{\ell}}{\Delta}\left[\frac{L_7}{(\ell+1)} - \frac{L_5\, t^{-2}}{\ell}\right]$$

$$\alpha_4 = 2\,\frac{t^{\ell-1}}{\ell(\ell+1)}$$

$$t = \frac{r_o}{r}$$

and the argument of the Legendre function is $\cos\theta$.

The radial component of $\vec{u}(\hat{\theta}_o, -\hat{\phi}_o)$ has been partially summed to obtain a rapidly converging series. Let the radial component of $\vec{u}(\hat{\theta}_o, -\hat{\phi}_o)$ be denoted by $u_r(\hat{\theta}_o, -\hat{\phi}_o)$. As detailed in Appendix 7 $u_r(\hat{\theta}_o, -\hat{\phi}_o)$ can be written

$$u_r(\hat{\theta}_o, -\hat{\phi}_o) = \frac{\sin 2\phi}{128\pi} \left\{ \left[-27 - 6t^{-2} + 5t^{-4} + \cos\theta\,(74t^{-1} - 30t^{-3}) \right] 2\csc^2\theta + 27 - 9t^{-2} - 16t^{-1}\cos\theta \right.$$

$$+ \frac{1}{T^{1/2}} \left\{ \left[101 - 24t^{-2} - 5t^{-4} + \cos\theta\,(-27t - 80t^{-1} + 35t^{-3}) \right] 2\csc^2\theta \right.$$

$$\left. -144 + 18t^{-2} + 10t^{-4} + \cos\theta\,(75t^{-1} - 25t^{-3}) \right\}$$

$$+ \frac{1}{T^{3/2}} \left\{ 116 - 14t^{-2} - 10t^{-4} + \cos\theta\,(-27t - 110t^{-1} + 45t^{-3}) \right.$$

$$\left. + 50\,(-3 + t^{-2})\sin^2\theta \right\}$$

$$+ \frac{1}{T^{5/2}} \left\{ 48\,(t^2 - 1)\sin^2\theta \right\}$$

$$\left. + \sum_{\ell=2}^{\infty} \frac{22.5\,(3t^2-1)\,t^{\ell-2}}{\Delta} \frac{P_\ell^2}{\ell(\ell+1)(\ell+2)} \right\} \qquad (3\text{-}12)$$

where

$$T = 1 - 2t\cos\theta + t^2 \quad .$$

The last expression for $u_r(\hat{\theta}_o, -\hat{\phi}_o)$ converges approximately like $\ell^{-7/2}$. Using this expression with a equal to one, the quantity

$$U_s = \frac{8\pi\, u_r(\hat{\theta}_o, -\hat{\phi}_o)}{\sin 2\theta}$$

was calculated. To show the effect of sphericity the results were compared with the displacement due to the same source in a homogeneous elastic half space. The ratio U_s/U_H was calculated where

$$U_H = \frac{8\pi\, u_{rH}}{\sin 2\phi}$$

and u_{rH} is the vertical displacement field on the surface of the half space for a source depth equal to (1-t) and distance measured in units of θ. Using Maruyama's (1964) results for the half space, there follows

$$U_H = \frac{1}{\theta^2}\left\{2 - \frac{9(1-t)}{R^{1/2}} + \frac{13(1-t)^3}{R^{3/2}} - \frac{6(1-t)^5}{R^{5/2}}\right\}$$

where $R = \theta^2 + (1-t)^2$.

U_s/U_H is plotted in Figure 3-2 for various angular distances and for t = .995, t = .96, and t = .90. These values of t correspond to source depths of approximately 31 km., 255 km., and 637 km., respectively. The effect of sphericity is clearly not negligible at distances of 20° or greater for the case calculated. The

difference between the field on the sphere and in the halfspace for a given distance from the source increases as the depth of the source increases. This is physically to be expected since the deeper the source, the greater the influence of the surface of the sphere antipodal to the source. For distances less than roughly 10° and source depths less than roughly 30 km. the effect of sphericity on the displacement component calculated is less than a factor of two except very near the epicenter. The ratio U_S/U_H is a poor method of comparison very near the epicenter since a small change in the position of a zero crossing makes a large change in the ratio. Although the calculation given here shows the effects of sphericity very clearly because this is the only difference between the homogeneous sphere and the homogeneous halfspace, it does not show the effects of gravity or of varying the elastic constants with depth.

Takeuchi (1951, Chapter 7) has shown that the effect of gravity is negligible for distances where the ratio of the distance to the circumference of the earth is small. In Appendix 8 it is shown by comparing solutions by Longman (1962 and 1963) and Slichter and Caputo (1960) that the combined effect of the elastic parameters varying with depth and gravity is probably more important at distances greater than 20° than the effect of sphericity.

It is concluded that for the calculation of the static deformational field due to a shallow seismic source at less than about 10°, sphericity will not have an important effect, but variations in properties with depth may. For significantly greater distances or source depths variations of properties with depth, gravity, and sphericity should all be taken into account.

Chapter 4

SURFACE DEFORMATION DUE TO DISLOCATION SOURCES IN A LAYERED ELASTIC HALF-SPACE

Solution forms are derived for the displacement, tilt, and strain fields at the surface of a layered elastic half-space due to certain buried dislocation sources. In considering the effect of a buried weak layer on the surface fields expressions are needed for the same problem as described above except that the structure is a plate over a liquid. These are derived by a simple modification of the results for a layered half-space.

Construction of Representation of Static Deformational Fields for a Layered Elastic Half-Space

Again the general framework of Chapter 2 is used and the results given here are referenced to the appropriate equation in Chapter 2. Solutions to the vector harmonic equation (expression (2-20)) in circular cylindrical coordinates are given in Morse and Feshbach (1953). In a notation slightly different from theirs these are

$$\vec{M}^1_{mk} = e^{kz}\ \vec{C}_{mk}$$

$$\vec{M}^2_{mk} = e^{-kz}\ \vec{C}_{mk}$$

$$\vec{N}^1_{mk} = e^{kz}\ (\vec{P}_{mk} + \vec{B}_{mk})$$

$$\vec{N}^2_{mk} = e^{-kz}\ (\vec{P}_{mk} - \vec{B}_{mk})$$

$$\vec{G}^1_{mk} = e^{kz}\ \vec{P}_{mk}$$

$$\vec{G}^2_{mk} = e^{-kz}\ \vec{P}_{mk}$$

where

$$\vec{P}_{mk} = \hat{z}\ e^{im\theta}\ J_m\ (kr)$$

$$\vec{B}_{mk} = \frac{1}{k}\ \nabla \left[e^{im\theta}\ J_m\ (kr) \right]$$

$$\vec{C}_{mk} = \frac{1}{k}\ \nabla\ \times \left[\hat{z}\ e^{im\theta}\ J_m\ (kr) \right] .$$

Substituting $4(1-\sigma)$ times the solutions $\vec{G}^1_{mk}$ and $\vec{G}^2_{mk}$ into equation (2-19) gives the third homogeneous solution to equation (2-1).

$$\vec{E}^1_{mk} = (c-kz)\ e^{kz}\ \vec{P}_{mk} - kz\ e^{kz}\ \vec{B}_{mk}$$

$$\vec{E}^2_{mk} = (c + kz)\ e^{-kz}\ \vec{P}_{mk} - kz\ e^{-kz}\ \vec{B}_{mk}$$

where

$$c = 3 - 4\sigma \quad .$$

The stress across a face z = constant is derived using equation (2-6) together with the identities given in Appendix 3. The resulting expression are

$$\hat{z}\cdot\underline{T}\left(\vec{M}^1_{mk}\right) = \mu k\, e^{kz}\, \vec{C}_{mk} = \mu k\, \vec{M}^1_{mk}$$

$$\hat{z}\cdot\underline{T}\left(\vec{M}^2_{mk}\right) = -\,\mu k\, e^{-kz}\, \vec{C}_{mk} = -\,\mu k\, \vec{M}^2_{mk}$$

$$\hat{z}\cdot\underline{T}\left(\vec{N}^1_{mk}\right) = \mu 2k\, e^{kz}\, (\vec{P}_{mk} + \vec{B}_{mk}) = \mu 2k\, \vec{N}^1_{mk}$$

$$\hat{z}\cdot\underline{T}\left(\vec{N}^2_{mk}\right) = -\,\mu 2k\, e^{-kz}\, (\vec{P}_{mk} - \vec{B}_{mk}) = -\,\mu 2k\, \vec{N}^2_{mk}$$

$$\hat{z}\cdot\underline{T}\left(\vec{E}^1_{mk}\right) = \mu k\, e^{kz} \left\{ (c + 1 - 2kz)\, \vec{P}_{mk} + (c - 1 - 2kz)\, \vec{B}_{mk} \right\}$$

$$\hat{z}\cdot\underline{T}\left(\vec{E}^2_{mk}\right) = \mu k\, e^{-kz} \left\{ -(c + 1 + 2kz)\, \vec{P}_{mk} + (c - 1 + 2kz)\, \vec{B}_{mk} \right\} \quad .$$

To determine the coefficients in the expansions analogous to equation (2-25) it is convenient to have expressions for

$$\frac{\delta(r-r_o)\ \delta(\theta-\theta_o)}{r}\ \vec{n}$$

in terms of $\vec{P}_{mk}$, $\vec{B}_{mk}$ and $\vec{C}_{mk}$. The discontinuity in the radial function is then derived from the analog of equation (2-29). These expressions together with certain specializations which are needed in the following are given in Appendix 4.

To define $\varepsilon(z; m, k)$, the solution matrix, the expansions of the displacement field and the stress fields in terms of the surface vector harmonics $\vec{P}_{mk}$, $\vec{B}_{mk}$, and $\vec{C}_{mk}$ are needed. These are analogs of equations (2-32) and (2-33) and are, respectively,

$$\vec{u} = \sum_m \int_k \left[U_p \vec{P}_{mk} + U_B \vec{B}_{mk} + U_c \vec{C}_{mk} \right] dk \qquad (4\text{-}1a)$$

and

$$\vec{t} = \sum_m \int_k \left[T_p \vec{P}_{mk} + T_B \vec{B}_{mk} + T_c \vec{C}_{mk} \right] dk \qquad (4\text{-}1b).$$

Equations (4-1a, b) define U_α and T_α where α may be P, B, or C. In place of equation (2-34) there is

$$\begin{bmatrix} U_p \\ U_B \\ \frac{T_p}{k} \\ \frac{T_B}{k} \end{bmatrix} = \varepsilon_R(z;mk) \begin{bmatrix} A_1 \\ A_2 \\ A_3 \\ A_4 \end{bmatrix} \qquad (4\text{-}2a)$$

for the spheroidal-like field, and

$$\begin{bmatrix} U_C \\ \frac{T_C}{k} \end{bmatrix} = \varepsilon_L(z;m,k) \begin{bmatrix} B_1 \\ B_2 \end{bmatrix} \qquad (4\text{-}2b)$$

for the toroidal-like field. The solution matrices for these parts are, respectively,

$$\varepsilon_R(z) = \begin{bmatrix} (c-kz)\, e^{kz} & e^{kz} & (c+kz)\, e^{-kz} & e^{-kz} \\ -kz\, e^{kz} & e^{kz} & -kz\, e^{-kz} & -e^{-kz} \\ \mu(c+1-2kz)\, e^{kz} & \mu 2e^{kz} & -\mu(c+1+2kz)\, e^{-kz} & -\mu 2e^{-kz} \\ \mu(c-1-2kz)\, e^{kz} & \mu 2e^{kz} & \mu(c+1+2kz)\, e^{-kz} & \mu 2e^{-kz} \end{bmatrix}$$

and

$$\varepsilon_L(z) = \begin{bmatrix} e^{kz} & e^{-kz} \\ \mu e^{kz} & -\mu e^{-kz} \end{bmatrix} .$$

A development analogous to that leading from equation (2-36) to equation (2-44) gives for the spheroidal-like field

$$X_{PB}\, Y_{PB} = - D_{PB}^{s+1}\, \Delta U_{PB}$$

where

$$X_{PB} = \begin{bmatrix} D_{11} & D_{12} & \varepsilon_{13}(z_{n-1}) & \varepsilon_{14}(z_{n-1}) \\ D_{21} & D_{22} & \varepsilon_{23}(z_{n-1}) & \varepsilon_{24}(z_{n-1}) \\ D_{31} & D_{32} & \varepsilon_{33}(z_{n-1}) & \varepsilon_{34}(z_{n-1}) \\ D_{41} & D_{42} & \varepsilon_{34}(z_{n-1}) & \varepsilon_{44}(z_{n-1}) \end{bmatrix}$$

and

$$Y_{PB} = \begin{bmatrix} U_P(z_o) \\ U_B(z_o) \\ -A_{3,n} \\ -A_{4,n} \end{bmatrix}$$

The solution for the displacements at the surface $z = z_o$ is included in the solution

$$Y_{PB} = - X_{PB}^{-1} D_{PB}^{s+1} \Delta U_{PB} \quad . \tag{4-3a}$$

Similarly for the toroidal

$$X_C Y_C = - D_C^{s+1} \Delta U_C \tag{4-3b}$$

where

$$Y_C = \begin{bmatrix} D_{11} & \varepsilon_{12}(z_{n-1}) \\ D_{21} & \varepsilon_{22}(z_{n-1}) \end{bmatrix}$$

$$Y_C = \begin{bmatrix} U_C(z_o) \\ -B_{2,n} \end{bmatrix}$$

The elements of the propagator matrix (equation 2-38) are given in Appendix 5.

With the definitions

$$\Delta U_{PB} = \begin{bmatrix} \Delta U_P \\ \Delta U_B \\ \frac{\Delta T_P}{k} \\ \frac{\Delta T_B}{k} \end{bmatrix}$$

and

$$\Delta U_C = \begin{bmatrix} \Delta U_C \\ \frac{\Delta T_C}{k} \end{bmatrix}$$

for the source discontinuities, the following expressions are needed to compute the displacements at the surface.

$$U_P(z_o) = - KD_P^P(\Delta U_P) - KD_P^B(\Delta U_B) - KF_P^P\left(\frac{\Delta T_P}{k}\right) - KF_P^B\left(\frac{\Delta T_B}{k}\right) \qquad (4\text{-}4a)$$

$$U_B(z_o) = - KD_B^B(\Delta U_P) - KD_B^B(\Delta U_B) - KF_B^P\left(\frac{\Delta T_P}{k}\right) - KF_B^B\left(\frac{\Delta T_B}{k}\right) \qquad (4\text{-}4b)$$

$$U_C(z_o) = - KD_C^C(\Delta U_C) - KF_C^C\left(\frac{\Delta T_C}{k}\right) \qquad (4\text{-}4c).$$

ΔU_P, ΔU_B, and ΔU_C are the coefficients of $\vec{P}_{mk}$, $\vec{B}_{mk}$, and $\vec{C}_{mk}$, respectively, from the representation of a source which has a discontinuity in displacement (and continuity of stress) at the source depth z = h. ΔT_P, ΔT_B, and ΔT_C are the coefficients of $\vec{P}_{mk}$, $\vec{B}_{mk}$, and $\vec{C}_{mk}$, respectively, from the representation of a source which has a discontinuity in stress (and continuity of displacement) at the source depth z = h. The KD's and KF's are determined by equations (4-3). For example the first of the set of equations given by (4-3a) is equation (4-4a). Explicit algebraic expressions are given for the KD's and KF's for a homogeneous half-space in Appendix 9.

For a stack of elastic layers over a liquid the boundary conditions are the same as given for the above problem in Chapter 2 except at the liquid solid interface which is introduced at the depth $z = z_{n-1}$. The boundary conditions at z_{n-1} are

a) the tangential component of stress equals zero, and

b) the normal component of stress equals the negative of the product, liquid density (p) times gravitational field (g) times normal displacement.

The expressions given above are not altered except that the terms in equations (4-3) become

$$X_{PB} = \begin{bmatrix} D_{11} & D_{12} & -1 & 0 \\ D_{21} & D_{22} & 0 & -0 \\ D_{31} & D_{32} & \rho g & 0 \\ D_{41} & D_{42} & 0 & 0 \end{bmatrix} ,$$

$$Y_{PB} = \begin{bmatrix} U_P(z_o) \\ U_B(z_o) \\ U_P(z_{n-1}) \\ U_B(z_{n-1}) \end{bmatrix} ,$$

$$X_C = \begin{bmatrix} A_{11} & -1 \\ A_{21} & 0 \end{bmatrix} ,$$

and

$$Y_C = \begin{bmatrix} U_C(z_o) \\ U_C(z_{n-1}) \end{bmatrix} .$$

Except where explicitly noted the results given in the rest of this chapter are for a layered elastic half-space. The procedures apply as well to the problem of a layered elastic stack over a liquid.

Two examples of the construction of the final solution as an integral representation are given in detail.

For a force of magnitude F_z in the direction of $\hat{z}$ at $z = h$, $r = 0$, $\theta = 0$, the source term is

$$-F_z \delta(z-h) \frac{\delta(r)\ \delta(\theta)}{r} \hat{z} \quad .$$

The representation for $\frac{\delta(r)\ \delta(\theta)}{r} \hat{z}$ in Appendix 4 defines the source discontinuity as

$$\Delta T_p^{zF} = - p_{ok}^z = - \frac{k}{2\pi} \qquad (4\text{-}5)$$

with continuity of displacement and stress giving 0 for the other ΔU's and ΔT's. Substituting into equations (4-4) there follows

$$U_P(z_o) = KF_P^P \left(\frac{1}{2\pi}\right)$$

$$U_B(z_o) = KF_B^P \left(\frac{1}{2\pi}\right)$$

The kernel of equation (4-1a) is

$$\vec{U}_{PB} = \frac{1}{2\pi} \left[KF_P^P \vec{P}_{ok} + KF_B^P \vec{B}_{ok} \right] \quad .$$

With the notation $\vec{u}^{zF}$ for the displacement field due to a force $F_z \hat{z}$ at $z = k$, $r = o$, $\theta = o$, then the inverse transform of $\vec{U}_{PB}$ is

$$\vec{u}^{zF} = \frac{F_z}{2\pi} \left[\hat{z} \int_o^\infty KF_P^P \, J_o(kr) \, dk - \hat{r} \int_o^\infty KF_B^P \, J_1(kr) \, dk \right] .$$

For a source which has continuity of stress at $z = k$, but a discontinuity in the z component of displacement across a face parallel to $z = h$, the required discontinuity in the displacement field is

$$(\Delta u_z) \, \delta(z-h) \, \frac{\delta(r) \, \delta(\theta)}{r} \, \hat{z}$$

where Δu_z is the magnitude of the discontinuity in u_z. The representation for $\frac{\delta(r) \, \delta(\theta)}{r}$ gives the source discontinuity as

$$\Delta U_P^{zD} = p_{ok}^z = \frac{k}{2\pi} .$$

Continuity of displacement and stress give o for the other ΔU's and ΔT's. Then, as immediately above, with the notation $\vec{u}^{zD}$ for the field due to this source, there follows

$$\vec{u}^{zD} = \frac{(\Delta U_z)}{2\pi} \left[\hat{z} \int_o^\infty KD_P^P \, J_o(kr) \, k \, dk - \hat{r} \int_o^\infty KD_B^P \, J_1(kr) \, k \, dk \right] .$$

Other sources are treated similarly and integral expressions for the deformational fields for an arbitrary dislocation surface and an associated arbitrary jump in displacement can be derived.

Deformational Fields due to a Strike-Slip Source, A Dip-Slip Source, and A Dilatational Source

Explicit expressions are given for certain point sources which are used to model a seismic source. Figure 4-1 shows the coordinate system and the geometry of the elemental dislocation surface and the associated displacement discontinuity. For convenience each point source may be described using the terminology of faulting, the dislocation surface being identified with the fault surface and the displacement discontinuity being identified with the slip. Any slip vector in the plane of the dislocation surface can be obtained by superposition of the cases which are considered. The solution for a dilatational source is also given.

In constructing the solutions the displacement fields due to certain point forces are used. The notation $\vec{u}^{nF}$ is used for the displacement field at $z = o$ for a unit point force in the $\hat{n}$ direction. For a dislocation source specified by a surface with unit normal $\hat{n}$ and a unit jump in displacement $\Delta\hat{u}$ the displacement field at $z = o$ is denoted by $\vec{u}(\hat{n}, \Delta\hat{u})$.

First expressions are given for a vertical strike-slip fault (γ = o in Fig. 4-1a) and a vertical dip-slip fault (γ = o in Fig. 4-1b). The source is at a depth h in all cases although this appears explicitly only in the KD's and KF's.

Using the equivalence theorems of Burridge and Knopoff (1964), the displacement field for strike-slip motion on a vertical fault plane is

$$\vec{u}(\hat{y}, -\hat{x}) = \mu_s \left(\frac{\partial \vec{u}^{xF}}{\partial y} + \frac{\partial \vec{u}^{yF}}{\partial x} \right) \tag{4-6}$$

The derivatives in equation (4-6) and later in equation (4-8) are with respect to the field coordinates x and y, not with respect to the source coordinates x_o and y_o. The components of $\vec{u}(\hat{y}, -\hat{x})$ in circular cylindrical coordinates are

$$u_z(\hat{y}, -\hat{x}) = \frac{\mu_s}{2\pi} \sin 2\theta \int_o^\infty KF_P^B \, (-k \, J_2) \, dk \tag{4-6a}$$

$$u_r(\hat{y}, -\hat{x}) = \frac{\mu_s}{2\pi} \sin 2\theta \int_o^\infty \left\{ KF_B^B \left(-kJ_1 + \frac{2}{r} J_2 \right) + KF_C^C \left(- \frac{2}{r} J_2 \right) \right\} dk \tag{4-6b}$$

$$u_\theta(\hat{y}, -\hat{x}) = \frac{\mu_s}{2\pi} \cos 2\theta \int_o^\infty \left\{ KF_B^B \left(- \frac{2}{r} J_2 \right) + KF_C^C \left(-kJ_1 + \frac{2}{r} J_2 \right) \right\} dk \tag{4-6c}.$$

In the above and subsequent expressions μ_s is the rigidity of the source layer and the argument of the Bessel functions is kr.

The field, $\vec{u}(\hat{y}, -\hat{z})$, due to dip-slip motion on a vertical fault plane is the same as the field, $\vec{u}(-\hat{z}, \hat{y})$, due to a horizontal thrust. Since $\hat{z}$ is a separable coordinate surface in the latter field, the displacement dislocation can be constructed directly. The components of $\vec{u}(\hat{y}, -\hat{z})$ are

$$u_z(\hat{y}, -\hat{z}) = \frac{1}{2\pi} \sin\theta \int_0^\infty KD_P^B \left(kJ_1\right) dk \tag{4-7a}$$

$$u_r(\hat{y}, -\hat{z}) = \frac{1}{4\pi} \sin\theta \int_0^\infty \left\{ KD_B^B \left(kJ_o - kJ_2\right) + KD_C^C \left(kJ_o + kJ_2\right) \right\} dk \tag{4-7b}$$

$$u_\theta(\hat{y}, -\hat{z}) = \frac{1}{4\pi} \cos\theta \int_0^\infty \left\{ KD_B^B \left(kJ_o + kJ_2\right) + KD_C^C \left(kJ_o - kJ_2\right) \right\} dk \tag{4-7c}.$$

$\vec{u}^\Delta$ denotes the surface displacement field due to a dilatational source. Using the source equivalence theorems this can be shown to be

$$\vec{u}^\Delta = \vec{u}(\hat{z}, \hat{z}) - 2\mu_s \left(\frac{\partial \vec{u}^{xF}}{\partial x} + \frac{\partial \vec{u}^{yF}}{\partial y} \right) \tag{4-8}.$$

$\vec{u}^\Delta$ as given is for a unit source expansion. The components of $\vec{u}^\Delta$

are determined by

$$\vec{u}(\hat{z},\ \hat{z}) = \frac{\hat{z}}{2\pi}\int_o^\infty \left\{ KD_P^P\ (-k\ J_o) \right\}\ dk$$

$$+ \frac{\hat{r}}{2\pi}\int_o^\infty \left\{ KD_B^P\ \ (kJ_1) \right\}\ dk \qquad (4\text{-}9)$$

and

$$\frac{\partial \vec{u}^{xF}}{\partial x} + \frac{\partial \vec{u}^{yF}}{\partial y} = \frac{\hat{z}}{2\pi}\int_o^\infty \left\{ KF_P^B\ (k\ J_o) \right\}\ dk$$

$$+ \frac{\hat{r}}{2\pi}\int_o^\infty \left\{ KF_B^B\ (-kJ_1) \right\}\ dk \qquad (4\text{-}10).$$

For a strike-slip fault with a dipping fault plane the geometry of Figure 4-1a is used and the notation

$$\vec{u}^{ss} \equiv \vec{u}(\cos\gamma\ \ \hat{y} + \sin\gamma\ \hat{z},\ -\hat{x}) \quad .$$

Using the kernel, $[\underline{T}_o\ (\underline{G})\cdot\hat{n}]\cdot\Delta\vec{u}$, from equation (2-12) this can be written

$$\vec{u}^{ss} = \cos\gamma\ \vec{u}(\hat{y},\ -\hat{x}) + \sin\gamma\ \vec{u}(\hat{x},\ -\hat{z}) \qquad (4\text{-}11).$$

$\vec{u}(\hat{y},\ -\hat{x})$ is given by equations (4-7). $\vec{u}(\hat{x},\ -\hat{z})$ can be obtained by rotating the field $\vec{u}(\hat{y},\ -\hat{z})$ through $\frac{\pi}{2}$ about the z axis carrying y into x (i.e. replace θ by $\theta + \frac{\pi}{2}$ in equations (4-7a, b, c)).

For a dip-slip fault with dipping fault plane the geometry of Figure 4-1b is used and the notation

$$\vec{u}^{ds} \equiv \vec{u}(\cos\gamma\ \hat{y} + \sin\gamma\ \hat{z},\ \sin\gamma\ \hat{y} - \cos\gamma\ \hat{z}) \qquad (4\text{-}12).$$

Again using the kernel of equation (2-12) this can be written

$$\begin{aligned}\vec{u}^{ds} = {} & \cos 2\gamma\ \ \vec{u}(\hat{y},\ -\hat{z}) \\ & + \sin 2\gamma \left[\frac{1}{2}\ \vec{u}\left(\sqrt{2}(-\hat{x}+\hat{y})/2,\ \ -\sqrt{2}(\hat{x}+\hat{y})/2\right)\right. \\ & + \frac{(1-c_s)}{(1+c_s)}\ \vec{u}(\hat{z},\ \hat{z}\ ) \\ & \left. + \frac{\mu_s}{2}\,\frac{(c_s-7)}{(c_s+1)} \left(\frac{\partial \vec{u}^{xF}}{\partial x} + \frac{\partial \vec{u}^{yF}}{\partial y} \right) \right] \end{aligned} \qquad (4\text{-}13).$$

c_s is the parameter c in the source layer.

Expressions for $\vec{u}(\hat{y},\ -\hat{z})$, $\vec{u}(\hat{z},\ \hat{z})$, and $\frac{\partial \vec{u}^{xF}}{\partial x} + \frac{\partial \vec{u}^{yF}}{\partial y}$ are given in equation (4-7), (4-9), and (4-10), respectively. $u(\sqrt{2}(-\hat{x}+\hat{y})/2,\ -\sqrt{2}(\hat{x}+\hat{y})/2)$ can be obtained by rotating the field $\vec{u}(\hat{y},\ -\hat{x})$ through $\Pi/4$ about the z axis carrying x into y (i.e. replace θ by $\theta - \frac{\pi}{4}$ in equations (4-6a, b, c)).

Expressions for the components of tilt and strain for each of these sources are given in Appendix 11.

The KD's and KF's were generated numerically and approximated by a series

$$K(k) = \sum_{\ell} A_{\ell} \, k^{n_{\ell}} \, e^{-\alpha_{\ell} k} \qquad (4\text{-}14)$$

where A_{ℓ} and α_{ℓ} are numerically determined constants and n_{ℓ} is an integer. The resulting approximation can be integrated exactly to give displacement, tilt, and strain fields at the surface of the half-space, This is a simple adaptation of a procedure used by Biot (1935). The necessary integral is given in Erdelyi (1954) and the forms used for this work are listed in Appendix 10.

A more detailed discussion of the numerical procedure is given in Appendix 15; however, a few comments should be made here. The procedure used almost certainly does not converge. For a limited number of terms the integral kernels for certain structures can be approximated to within about a per cent over a wide range of k. Subject to certain qualifications which are discussed in Appendix 15, an approximation over a wide range of k gives results which are valid over a wide range of distances from the source. This allows a convenient calculation of the deformational field for those structures which can be approximated. Although the class of structures which can be treated satisfactorily is small, it allows establishment of the principal points to be made in this study. The cause of the difficulties for structures which cannot be handled

satisfactorily as well as a suggested integration procedure to improve upon the one given here are treated in Appendix 15.

The behavior of the solutions for large r can be obtained from the solution representations by taking the limit as $k \to o$ and integrating the resultant expressions. These are useful as a check on numerical calculations and for determining certain general properties of the solution fields. The limits are given for the surface displacement fields of equations (4-6, 7, 8) in Appendix 14.

Chapter 5

DISLOCATION MODELS OF FAULTING AND THE EFFECTS OF LAYERING ON THE DEFORMATIONAL FIELD IN A HALF-SPACE

Choice of Source Model

If the source region of an earthquake is surrounded by a surface Σ', then for some choice of Σ' it is usually assumed that outside Σ' the deformational field due to the earthquake is described by the equations of elasticity. The accumulated evidence from seismology indicates that this is certainly true over a large range of frequencies for the mantle of the earth. Archambeau (1967) reviews possible source mechanisms and concludes that reduction of stress on a surface Σ', as described above, is a satisfactory source description for the most likely mechanisms. To be specific an earthquake is assumed due to shear failure which can be described by simple Coulomb fracture or modified Coulomb fracture.

The above mechanism manifests itself as faulting. The association of faulting and earthquakes in the southern California region has been carefully documented by Allen *et al.* (1965). The static deformational field due to a fault is assumed to be essentially the same as the field due to the introduction of a stress free

surface into a prestressed elastic medium. The fault plane is taken to be a surface where the stress drops to zero, so that the surface Σ' above becomes the non-volume enclosing surface, Σ, of Chapter 2. Actually there need only be a reduction in stress over the fault surface, but for the problem considered here the distinction is not important.[1] The approximation of the volume enclosing surface Σ' by the non-volume enclosing surface Σ should be adequate as long as the zone of non-elastic behavior on either side of the fault surface is small compared to the length and width of the fault surface.

In Chapter 2 it was shown how a properly choosen dislocation source, $\Delta\vec{u}$, together with equation (2-12) can be used to calculate the displacement field due to the introduction of a stress free surface, Σ, into a prestressed medium. As was pointed out there a proper solution of the problem requires a knowledge of the prestress field which then, in principle at least, allows calculation of precisely that $\Delta\vec{u}$ which causes the surface Σ to be stress free. In practice dislocation theory has been used by choosing a $\Delta\vec{u}$ which is analytically convenient and which, on physical grounds, is expected to resemble the $\Delta\vec{u}$ for a particular type of faulting. This is the approach, for example, of Press (1965), Maruyama (1964),

[1]For some purposes, for example, the calculation of elastic strain energy release, the distinction may be quite important.

and Savage and Hastie (1966). The accuracy of this type of approximation can be tested against the few exact solutions for the introduction of a stress free surface into a prestressed medium. Knopoff (1957) gives the solution for a two dimensional strike slip fault in a homogeneous half-space. Keilis-Borok (1959) adapted a solution of Neuber's[2] (1946) for a slip fault in a whole space. This study is designed to evaluate the deformational field at intermediate[3] distances, so a detailed comparison of the exact solutions and the typical dislocation approximation of a constant $\Delta\vec{u}$ over Σ is not made. However, certain properties of the comparison which are important in justifying the models used are discussed below.

For a given plane fault surface Σ with total area Σ_A, if a constant $\Delta\vec{u}_c$ is chosen by

$$\Delta\vec{u}_c = \frac{\iint_{\Sigma} \Delta\vec{u}\, d\Sigma}{\Sigma_A} \qquad (5\text{-}1),$$

---

[2]There are some omissions in the solution as printed in Keilis-Borok's article, so that, if the complete details of the solution form are desired, it is advisable to use Neuber's book.

[3]The term "intermediate" distances is used here for distances of several fault lengths. When discussing a plate-like layer over a weak layer, "intermediate" is used to refer to distances of several plate thicknesses. The fault lengths and plate thicknesses which are appropriate are from 40 to 100 km.

then, for a homogeneous, isotropic whole space, the far field[4] from the model with this $\Delta\vec{u}_c$ is the same as the far field from the exact solution. This is easily verified for the Neuber solution. For a general plane fault surface in a homogeneous whole space the distribution of $\Delta\vec{u}$ is not known apriori, but if its average components are estimated, equation (5-1) can be applied. The reason for this is seen in equation (2-12). $[\underline{T}_o(\underline{G})\cdot\vec{n}]\cdot\Delta\vec{u}$ can be expanded in the form

$$\sum_{n=n_o}^{\infty} \frac{A_n}{r^n} \quad .$$

r is taken as a convenient measure of distance from the fault plane, say the distance from the center of Σ, and the expansion is valid outside of a surface centered at $r = o$ and enclosing Σ. Since the expression for $[\underline{T}_o(\underline{G})\cdot\vec{n}]\cdot\Delta\vec{u}$ is known explicitly for a homogeneous whole space, e.g. Maruyama (1964), this form is easily derived. A_{n_o} depends only on the direction to the observation point. The choice of $\Delta\vec{u}_c$ over Σ may or may not be a good approximation for the near and intermediate fields. This depends on the particular situation.

In order to further develop the nature of the approximations used here, considerations similar to those in the last paragraph

---

[4] By the far field is meant the asymptotic behavior of the field as distance from the fault goes to ∞.

are undertaken for a half-space. Only the deformational field at the surface of the half-space is considered. Two cases illustrate the ideas. Using the results in Appendix 14 for $\sigma = \frac{1}{4}$ the limits as $r \to \infty$ are

$$\vec{u}(\hat{y}, \hat{x}) = \frac{1}{r^2} \frac{1}{8\pi} \left\{ \hat{r}\ 5 \sin 2\theta + \hat{\theta}\ 2 \cos 2\theta + \hat{z}\ 2 \sin 2\theta \right\} + 0 \left(\frac{\vec{n}}{r^3}\right)$$

$$\vec{u}(\hat{y}, \hat{z}) = -\frac{h}{r^3} \frac{3}{2\pi} \hat{r} \sin\theta + 0 \left(\frac{\hat{r}}{r^4}\right)$$

$$+ \frac{h^2}{r^4} \frac{3}{2\pi} \hat{z} \sin\theta + 0 \left(\frac{\hat{z}}{r^5}\right) .$$

$\vec{u}(\hat{y}, \hat{x})$ is similar to the result for a whole space, but $\vec{u}(\hat{y}, \hat{z})$ contains terms of the form $\frac{h^n}{r^m}$. In this case the appropriate choice of $\Delta\vec{u}_c$ is

$$\Delta\vec{u}_c = \frac{\iint_{\Sigma} h^n \Delta\vec{u}\, d\Sigma}{\Sigma_A} \qquad (5\text{-}2).$$

As a simple example, if $\Delta\vec{u} = \Delta\vec{u}_o$ and Σ_A is defined by $-L \le X_1 \le L$, $H_1 \le h \le H_2$, then equation (5-2) is

$$\Delta\vec{u}_c = \frac{\Delta\vec{u}_o \int_{H_1}^{H_2} \int_{-L}^{L} h^n \, dX_1 dh}{2L\,(H_2-H_1)} = \Delta\vec{u}_o \frac{\left(H_2^{n+1} - H_1^{n+1}\right)}{(n+1)\,(H_2-H_1)}$$

If $n = 1$, $\Delta\vec{u}_c = \Delta\vec{u}_o \frac{(H_2+H_1)}{2}$ that is the point source is placed at the midpoint of the dislocation surface. The above approach amounts to the beginning of a multipole expansion of the source. The point to be made here is that for sufficiently large distance from the source a properly chosen point source approximation may give an adequate model of the deformational field for a dislocation model of faulting. A weak test of the accuracy of the approximation is given by the asymptotic expressions as above. If the integral kernel $[\underline{T}_o(\underline{G})\cdot\hat{n}]\cdot\Delta\vec{u}$ is known for all distances from the source, a strong test is made simply by choosing point sources at a few points on the dislocation surface. Comparison of the predicted field at a given location shows whether the field is sensitive to the distribution of $\Delta\vec{u}$ over Σ. For the latter case as many points sources as are necessary can be used in the approximation. This last procedure amounts to numerical integration.

The choice of the correct $\Delta\vec{u}$ over Σ is not determined by the above. Short of complete solution of the stress release problem

either field evidence or physical reasoning must be used to determine the appropriate $\Delta\vec{u}$. The closer the observation point is to Σ, the more important is the direction of $\Delta\vec{u}$ and its distribution over Σ. A point source approximation is used in the calculations for the models considered for Chapter 7. The adequacy of the source approximations is discussed with the individual cases.

Some Properties of the Surface Displacements in a Layered Half-Space

In this section some simple properties of the displacement field at the surface of a layered half-space are pointed out. These properties are derived from the asymptotic behavior for large r supplemented by some numerical results. Expressions for the asymptotic behavior of three source types in a layered half-space are given in Appendix 14. The formulas are not repeated in this section. The limits considered are surface displacement fields as r, the distance from the origin, increases.

For a vertical strike-slip fault as $r \to \infty$ each component of the field is dominated by a term which dies off as $\frac{1}{r^2}$. For a vertical dip-slip fault the r and θ components die off like $\frac{1}{r^3}$ while the z component dies off like $\frac{1}{r^4}$. Since tilts are derivatives of the r and θ components, the relative importance of these two field types at large distance can also be estimated.

All field components due to dip-slip motion on a vertical fault plane die off more rapidly away from the source than the same components due to strike-slip motion on a vertical fault plane. By source equivalence the same statement follows with slip motion on a horizontal thrust fault substituted for dip slip motion on a vertical fault plane. Reference to equation (4-13) shows that dip-slip motion on a dipping fault plane contains components which die off like $\frac{1}{r^2}$, so that the vertical fault plane is a very special case insofar as its far field behavior is concerned. Dip-slip motion on a nearly vertical fault plane is still a relatively poor excitor of far field compared to the same amount of strike-slip motion since the angular function is relatively small. For a dilatational source the r component dies off like $\frac{1}{r^2}$ and the z component like $\frac{1}{r^3}$.

In all the fields considered above those displacement components which die off like $\frac{1}{r^2}$ depend on the elastic properties of the bottom half-space and not upon the source depth. They do not depend on the elastic properties of the layers except for the rigidity of the source layer which acts like a factor which scales $\Delta\vec{u}$ from the source layer to the bottom half-space. It follows that as distance increases the largest deformational fields are controlled by the properties deeper in the medium. Those displacement components which die off as $\frac{1}{r^3}$ or faster depend upon source depth and the elastic properties of the layers as well as upon the elastic

properties of the bottom half-space.

For a single layer over a half-space those displacement fields which dominate at large distance, that is those which die off like $\frac{1}{r2}$, all contain the factor $\frac{\mu_1}{\mu_2}$. If c_1, c_2, and h are considered fixed, then increasing μ_2 decreases the fields at large distance and decreasing μ_2 increases them. To a first approximation the mantle has c constant with depth and μ increasing with depth. The implication from the asymptotic form is that the surface deformational fields on the earth will be reduced relative to those predicted for a half-space model with the source layer properties. The distance at which the asymptotic forms of Appendix 14 become dominant may be fairly large, so that at intermediate distances the deformational fields will not necessarily show the simple relative reduction which the first term in the asymptotic theory predicts. Physical reasoning suggests that the property of increasing rigidity with depth is the most important property of current mantle models insofar as the static deformational fields are concerned. Numerical calculations were made for a model in which the properties were the same with depth except that the region from a depth of 1 unit to 2 units had the rigidity doubled. The results were compared with a half-space model for three source types and displacement, tilt, and strain fields. More general comments concerning the effect of structure are made in the next section, but the point to be made here concerns the most important

displacement fields, those with a $\frac{1}{r^2}$ die off at large distance. At a distance of 2 to 3 units, where the effect of the layer of increased rigidity is a maximum, these fields generally show a reduction due to the layer of increased rigidity. Details due to local warping of the fields complicate the picture, but the conclusion is that conventional earth structure will generally decrease the important deformational fields with increasing distance even at intermediate distances.

The asymptotic forms yield no direct indication of the distance at which they are applicable. A comparison of asymptotic and numerical results is given in Table 5-1. The structure has two layers each of unit thickness over a half-space. The rigidity in the upper layer and the half-space is 1; the rigidity in the second layer is 0.5. Poisson's ratio is 0.25 everywhere. The results tabulated are for a strike-slip source at a depth of 0.1. The quantity UZ/UZH is the vertical displacement field normalized by the vertical field in a half-space with the properties of the source layer. R is the distance from the origin in units of layer thickness. The asymptotic form includes terms of order $\frac{1}{r^2}$ and $\frac{1}{r^3}$. This asymptotic result is good to about 5% at a distance of 20 and to about 1% at a distance of 30. At a distance of 10 it shows amplification of the field relative to the half-space where the numerical result shows reduction. For a more severe change in parameters an even larger value of r will be required before the

asymptotic form, to the order calculated, becomes a good approximation. For fields which die off more rapidly with distance, both higher order terms and probably more terms are required for a comparable estimate. For the distances and for the severe changes in elastic properties considered subsequently, the asymptotic forms are not sufficient although the general properties given in this section are still useful in appraising the results.

Nature of Weak Layer Model and Some Typical Results of Calculation

Among the possibilities that might explain the anomalously large tilt and strain observations is a weak or soft layer in the crust or mantle. A three layer model was used to investigate the effect of a weak layer on the static deformational fields due to a seismic source. The elastic constants in layers 1 and 3 (the bottom half-space) were fixed and equal. σ_1 and σ_3 were taken equal to .25. μ_3 was taken as the unit of rigidity. The elastic constants in layer 2, the source depth h, and the thickness of layer 2 were varied for three point source models, a vertical strike-slip fault, a vertical dip-slip fault, and a dilatational source. For convenience, in this section only, the first two sources will be called a "strike-slip source" and a "dip-slip source", respectively; it being understood that the fault plane is

vertical.

Displacement, tilt, and strain fields were calculated at the surface of the layered half-space and compared to the same fields in a homogeneous half-space with the properties of layer 1. Weakening of layer 2 either by reducing the rigidity, μ_2, at constant σ_2, or by reducing μ_2 with λ_2 constant can result in amplification of the deformational fields particularly at intermediate distances from the source. The amount and sign of the amplification (changes in the sense of the field at a given distance occur) is quite variable when different source types and different source depths are considered. Despite this diversity large amplification is usually achieved only by large variations in the rigidity or Poisson's ratio in layer 2. Exceptions to this occur for field types which show a high rate of fall off with distance in a half-space.

In order to achieve sufficiently large amplifications to relate the theoretical predictions to the field observations, the strength of layer 2 had to be reduced to the point where the effect of gravitational forces could not be neglected. To bound the variations in μ_2 and σ_2 calculations were done for a plate over a liquid as described in Chapter 4. It was found that the near and intermediate static field for a plate over a liquid is similar in shape and amplitude to the field for certain types of weakening of layer 2 of the 3 layer model. This similarity depends both on the values of μ_2 and σ_2 and the relative sizes of d_1 and d_2. The amount

by which μ_2 and σ_2 can be varied is limited by the numerical capabilities of the program. A numerically convenient method of achieving surface deformation fields which, for near and intermediate distances is similar to that of a plate over a liquid was

$$\mu_2 = .01 \ \mu_1$$
$$\sigma_2 = .25$$
$$d_1 = d_2 \approx 60 \text{ km.}$$

The numerical similarity is illustrated in Figure 5-1 in which the kernel KF_p^B is plotted as a function of k for several models. Models 1 and 2 are for a source in an elastic plate overlying a liquid. In both of these models the source depth is 1/4 the plate thickness, $\sigma = .25$, $\mu = 3.5 \times 10^{11}$ dynes/cm^2, and the product, density times gravitational field, is 3500 dynes/cm^3. In Model 1 the plate is 20 km thick. In Model 2 the plate is 100 km thick. Models 3, 4, and 5 are all two elastic layers over an elastic half-space. The elastic constants in layers 1 and 3 are fixed as indicated in the first paragraph of this section. Layers 1 and 2 are each one unit thick and the source is in layer 1 at a depth of .25. Model 3 has $\sigma_2 = .25$ and $\mu_2 = .01 \ \mu_1$; Model 4 has $\lambda_2 = \mu_1$ and $\mu_2 = .01 \ \mu_1$; and Model 5 has $\sigma_2 = .25$ and $\mu_2 = \mu_1$ (making it a homogeneous half-space). The kernel between about $k = .1$ and $k = 5$ determines the behavior of the solution at

intermediate distances. In this range of k Model 3 is intermediate between Models 1 and 2 while Model 4 is somewhat different.

The results described below are for $\sigma_2 = .25$ and μ_2 equal to some fraction of μ_1. This is intended to model decoupling by a gradual liquifying of the weak layer. The method is arbitrary, but should show the correct general patterns.

Figures 5-2, 5-3, 5-4, and 5-5 show some effects due to varying source type, source depth, rigidity of layer 2, and layer thickness. The ordinate in these figures is the ratio of the tilt (or strain) field in the layered half-space to the tilt (or strain) field in a uniform half-space with the properties of layer 1.

The abscissa is the distance along the surface in units of the thickness of layer 2. μ is the rigidity of layer 2 in units of the rigidity of layer 1; D is the thickness of layer 1; and H is the depth of the source below the surface. The fields were calculated in circular cylindrical coordinates. For tilts the curves labeled R and θ are for the radial and azimuthal components of tilt, respectively. For strains the curves labeled R, θ, and S are for strain components e_{rr}, $e_{\theta\theta}$, and $e_{r\theta}$, respectively.

Figure 5-2 shows the effect of different source types. The dip slip source shows by far the greatest amplification and this occurs with the sense of the tilts reversed compared to that in a half-space. The rigidity reduction in layer 2 by a factor of 10 is quite extreme when compared to the elastic parameters of current

earth models.

Figure (5-3) shows the effect of varying source depth for a dip-slip source. The amplification of the field is very sensitive to source depth for this case. For a dilatational source the effect of source depth is still moderately strong, while for a strike-slip source the effect is a small part of the total amplification.

Figure (5-4) shows the effect of varying the rigidity of layer 2 for a strike-slip source. Decreasing rigidity amplifies the tilt and causes the maximum tilt to occur slightly farther from the origin.

In Figure (5-5) the effect of decreasing the thickness of layer 1 is shown for a strike-slip source. The principal effect is a slight increase in the total strain amplification. For the other sources the strain amplification is usually less than that calculated for the strike-slip source.

The examples shown illustrate the most extreme effects found. Larger reduction in the rigidity, of course, gives larger amplifications. The tilt field for a shallow dip slip source shows rather startling amplifications at some distances, up to ± 1000 for $\mu_2 = .01\ \mu_1$. However, for a given source strength, the absolute field after amplification is of the same order as that for a strike-slip source. Even for the most extreme models considered the amplification can only approximately eliminate the difference in rates of fall off at intermediate distances from the source.

Chapter 6

A PERTURBATION PROCEDURE FOR CALCULATING THE EFFECTS OF LATERAL INHOMOGENEITIES ON THE EARTH'S FREE OSCILLATIONS

One of the problems associated with the hypothesis of a weak layer in the upper mantle or lower crust is the effect upon the dispersion of surface waves. Harkrider et al (1963) did some calculations showing the effect of thin weak or liquid layers on Rayleigh wave dispersion. They concluded that an exceedingly weak layer can be detected even if less than a kilometer thick if the layer is of sufficient lateral extent. For a layer in the lower crust or upper mantle the effect of lateral extent is critical. The agreement of low mode free oscillation data with theoretical models based on body wave structure argues against any shallow very weak zones of large lateral extent. For Love waves a weak zone at about 60 km depth should begin to have an appreciable effect on observed dispersion at periods between 30 and 50 seconds; the corresponding wave lengths being about 120 to 220 km. If the weak zone were only a few wave lengths long the effect of lateral extent could be quite important.

A Perturbation Procedure for Lateral Inhomogeneities

A perturbation technique is applied to the problem of the free oscillations of the earth. The problem is formulated so that the effect on the free oscillations of regional variations in physical properties can be calculated. This result is related to surface wave

dispersion through the implied great circular travel times. The problem is of interest independent of the question of the existence of weak zones in the earth since known differences in dispersion over continental, oceanic, and tectonic regions imply significant lateral differences. Backus (1964) has given a procedure for inverting great circular and great semi-circular phase velocity data for periods when a traveling wave view is appropriate. Toksöz and Anderson (1966) have interpreted observed phase velocity differences over different paths using path-averaging. Smith (1966) has presented free oscillation data showing different observed periods at different stations. The observed differences are probably due to regional variations in earth structure. The theory given here can aid in more precise interpretation of observed differences in free oscillation periods and in connecting free oscillation calculations with the traveling wave viewpoint. Backus and Gilbert (1961) calculated the rotational splitting of the free oscillations of the earth using a perturbation approach. The technique used here is essentially the same although the emphasis is upon an operator formalism which is convenient for lateral variations which occur over a distance which is short compared to the wave length considered.

Two types of perturbations are treated:

a) perturbations in λ and μ for a spherical, gravitating earth model;

b) perturbations in λ, μ, and ρ for a spherical, non-gravitating earth model.

The theory given allows calculation of the first order change in eigenfrequency, as would Rayleigh's principal, and also contains expressions for changes in the eigenfunction and expressions for higher order changes can be formed by simple extensions. The computational effort to obtain more than the first order change in eigenfrequency may be considerable.

For a complete treatment of the problem it is important to extend the theory to include perturbations in density and shape, and the effect of rotation. As mentioned, Backus and Gilbert (1961) have treated rotation and some aspects of perturbations in density have been considered by Backus (1967). The theory and results developed here should be adequate to give good estimates of the effects of lateral inhomogeneities on fundamental mode torsional eigenfrequencies.

The equations of motion for a spherically symmetric, gravitating earth are

$$\rho^\circ\nabla(\vec{g}^\circ\cdot\vec{u}_n^\circ) - \rho^\circ\vec{g}^\circ(\nabla\cdot\vec{u}_n^\circ) - (\lambda^\circ + 2\mu^\circ)\,\nabla(\nabla\cdot\vec{u}_n^\circ) + \mu^\circ\nabla\times(\nabla\times\vec{u}_n^\circ)$$

$$-(\nabla\lambda^\circ)(\nabla\cdot\vec{u}_n^\circ) - (\nabla\mu^\circ)\cdot(\nabla\vec{u}_n^\circ + \vec{u}_n^\circ\nabla) - \rho^\circ\nabla\psi_n^\circ = \sigma_n^\circ\,\rho^\circ\,\vec{u}_n^\circ \qquad (6\text{-}1a)$$

and

$$-4\pi\gamma\nabla\cdot(\rho^\circ\,\vec{u}_n^\circ) + \nabla\cdot(\nabla\psi_n^\circ) = 0 \qquad (6\text{-}1b)$$

Notations for equations used in Chapter 6 are given in Appendix 12 when not defined here. In equations (6-1 a, b) λ°, μ°, ρ° and g° are

functions of r only. If λ and μ are functions of θ and ϕ also, equations (6-1 a, b) become

$$\rho^\circ\nabla(\vec{g}^\circ\cdot\vec{u}_n) - \rho^\circ\vec{g}^\circ(\nabla\cdot\vec{u}_n)-(\lambda + 2\mu)\nabla(\nabla\cdot\vec{u}_n) + \mu\nabla \times (\nabla \times \vec{u}_n)$$

$$-(\nabla\lambda)(\nabla\cdot\vec{u}_n)-(\nabla\mu)\cdot(\nabla\vec{u}_n + \vec{u}_n\nabla) - \rho^\circ\nabla\psi_n = \sigma_n\rho^\circ\vec{u}_n \qquad (6\text{-}2a)$$

and

$$-4\pi\gamma\nabla\cdot(\rho^\circ\,\vec{u}_n) + \nabla\cdot(\nabla\psi_n) = 0 \qquad (6\text{-}2b).$$

Equations (6-1) are given in Alterman et al, (1959) among others; equations (6-2) are given in Hoskins (1920); both follow Love's derivation (Love, 1911; Chapter 7).

Let the differences in λ and μ which change equations (6-1) to (6-2) be small so that σ_n and $\vec{u}_n$, the eigenvalue and eigenfunction for the perturbed problem, are nearly equal to those of the unperturbed problem. Define the perturbations by

$$\lambda^1(r, \theta, \phi) = \lambda(r, \theta, \phi) - \lambda^\circ(r)$$

$$\mu^1(r, \theta, \phi) = \mu(r, \theta, \phi) - \mu^\circ(r) \quad .$$

Then for notational convenience the following definitions are made

$$L^\circ \equiv \begin{bmatrix} \rho^\circ\nabla(\vec{g}^\circ\cdot\underset{\sim}{\ }) - \rho^\circ\vec{g}^\circ(\nabla\cdot\underset{\sim}{\ }) - (\lambda^\circ + 2\mu^\circ)\nabla(\nabla\cdot\underset{\sim}{\ }) & -\rho^\circ \\ + \mu^\circ\nabla x(\nabla \times \underset{\sim}{\ }) - (\nabla\lambda^\circ)(\nabla\cdot\underset{\sim}{\ }) & \\ - (\nabla\mu^\circ)\cdot(\nabla\underset{\sim}{\ } + \underset{\sim}{\ }\nabla) & \\ -4\pi\gamma\nabla\cdot(\rho^\circ\underset{\sim}{\ }) & \nabla\cdot\underset{\sim}{\ } \end{bmatrix},$$

$$\underline{v}_n^\circ \equiv \begin{bmatrix} \vec{u}_n^\circ \\ \nabla\psi_n^\circ \end{bmatrix},$$

$$\underline{u}_n^\circ \equiv \begin{bmatrix} \vec{u}_n^\circ \\ 0 \end{bmatrix},$$

$$Q \equiv \begin{bmatrix} -(\lambda^1 + 2\mu^1)\nabla(\nabla\cdot\underset{\sim}{\ }) + \mu^1\nabla\times(\nabla\times\underset{\sim}{\ }) & 0 \\ -(\nabla\lambda^1)(\nabla\cdot\underset{\sim}{\ }) & \\ -(\nabla\mu^1)\cdot(\nabla\underset{\sim}{\ } + \underset{\sim}{\ }\nabla) & \\ 0 & 0 \end{bmatrix},$$

$$\underline{v}_n \equiv \begin{bmatrix} \vec{u}_n \\ \nabla\psi_n \end{bmatrix},$$

and

$$\underline{u}_n \equiv \begin{bmatrix} \vec{u}_n \\ 0 \end{bmatrix}.$$

The matrix operator $L_\circ$ is applied to the column vector $\underline{v}_n^\circ$ by using ordinary rules of matrix multiplication so that equations (6-1a, b) are written

$$L^\circ \underline{v}_n^\circ = \sigma_n^\circ \rho^\circ \underline{u}_n^\circ \qquad (6\text{-}1c) \quad ,$$

and equations (6-2a,b) are written

$$(L^\circ + Q)\underline{v}_n = \sigma_n \rho^\circ \underline{u}_n \qquad (6\text{-}2c) \quad .$$

A procedure is now followed analogous to that given in Dicke and Wittke (1960), (Chapter 14), or Mathews and Walker (1964), (Chapter 10). Equation (6-2c) is written

$$(L^\circ + \alpha Q)\,\underline{v}_n = \sigma_n \rho^\circ \underline{u}_n \qquad (6\text{-}2d)$$

where α is an arbitrary parameter which identifies the order of the terms in the assumed expansion

$$\underline{v}_n = \underline{v}_n^\circ + \alpha \underline{v}_n^1 + \alpha^2 \underline{v}_n^2 + \cdots \qquad (6\text{-}3a)$$

$$\underline{u}_n = \underline{u}_n^\circ + \alpha \underline{u}_n^1 + \alpha^2 \underline{u}_n^2 + \cdots \qquad (6\text{-}3b)$$

$$\sigma_n = \sigma_n^\circ + \alpha \sigma_n^1 + \alpha^2 \sigma_n^2 + \cdots \qquad (6\text{-}3c) \quad .$$

The column vectors $\underline{v}_n^i$ and $\underline{u}_n^i$ are defined by

$$v_n^i = \begin{bmatrix} \vec{u}_n^i \\ \nabla \psi_n^i \end{bmatrix}$$

and

$$\underline{u}_n^i = \begin{bmatrix} \vec{u}_n^i \\ \\ 0 \end{bmatrix} .$$

Substituting equations (6-3a, b, c) into equation (6-2d) and equating coefficients of the same power of α gives for the zero$^{\underline{th}}$ power of α

$$L^\circ \underline{v}_n^\circ = \sigma_n^\circ \rho^\circ \underline{u}_n^\circ \qquad (6\text{-}4) ,$$

for the first power of α

$$L^\circ \underline{v}_n^1 + Q \underline{u}_n^1 = \sigma_n^\circ \rho^\circ \underline{u}_n^1 + \sigma_n^1 \rho^\circ \underline{u}_n^\circ \qquad (6\text{-}5) ,$$

etc.

$\vec{u}_n^1$ is expanded in terms of the $\vec{u}_m^\circ$

$$\vec{u}_n^1 = \sum_m a_m \vec{u}_m^\circ \qquad (6\text{-}6)$$

where

$$a_m = (\vec{u}_m^{\circ *} , \vec{u}_n^1) .$$

The inner product is defined by

$$(\vec{u}_m^{\circ *} , \vec{u}_n^1) = \iiint \vec{u}_m^{\circ *} \cdot \vec{u}_n^1 \, \rho^\circ d(\text{vol})$$

and the $\vec{u}_m^\circ$ are normalized so that

$$(\vec{u}_m^{\circ *} , \vec{u}_m^\circ) = 1 .$$

Ottelet (1966) has shown that

$$(\vec{u}^{\circ *}_m , \vec{u}^{\circ}_\ell) = \delta_{m\ell} \quad .$$

It is assumed that

$$(\nabla\psi^1_n) = \sum_m a_m \nabla\psi^\circ_m \qquad (6\text{-}7) \quad .$$

The constant a_m in equation (6-7) is the same as the constant a_m in equation (6-6) and there has been no use of an orthogonality condition on the $\nabla\psi^\circ_m$ to obtain equation (6-7). Equation (6-2b) is satisfied by this assumption for all orders of α.

From equations (6-6) and (6-7) there follows

$$\underline{v}^1_n = \sum_m a_m \underline{v}^\circ_n \qquad (6\text{-}8a)$$

and

$$\underline{u}^1_n = \sum_m a_m \underline{u}^\circ_n \qquad (6\text{-}8b) \quad .$$

Substituting equations (6-8a, b) into equation (6-5) and using equation (6-4)

$$\sum_m \sigma^\circ_m a_m \rho^\circ \underline{u}^\circ_m + Q \underline{u}^\circ_n = \sigma^\circ_n \sum_m a_m \rho^\circ \underline{u}^\circ_m + \sigma^1_n \rho^\circ \underline{u}^\circ_n \qquad (6\text{-}9) \quad .$$

The fact that equation (6-2b) is satisfied for all orders of α results in the second of equations (6-9) being satisfied. The first of equations (6-9) is

$$\sum_m \sigma_m^\circ a_m \rho^\circ \vec{u}_m^\circ + Q_{11} \vec{u}_n^\circ = \sigma_n^\circ \sum_m a_m \rho^\circ \vec{u}_m^\circ + \sigma_n^1 \rho^\circ \vec{u}_n^\circ \qquad (6\text{-}10).$$

Taking the vector inner product of equation (6-10) from the right yields

$$\sigma_\ell^\circ a_\ell + (\vec{u}_\ell^{\circ *}, Q_{11} \vec{u}_n^\circ) = \sigma_n^\circ a_\ell + \sigma_n^1 \delta_{\ell n}$$

where

$$(u_\ell^{\circ *}, Q_{11} \vec{u}_n^\circ) = \iiint \vec{u}_\ell^{\circ *} \cdot (Q_{11} \vec{u}_\ell^\circ) \rho^\circ d(\text{vol}).$$

If $\ell = n$,

$$\sigma_n^1 = (\vec{u}_n^{\circ *}, Q^{11} \vec{u}_n^\circ) \quad , \qquad (6\text{-}11)$$

and if $\ell \neq n$

$$a_\ell = \frac{(\vec{u}_\ell^{\circ *}, Q^{11} \vec{u}_n^\circ)}{\sigma_n^\circ - \sigma_\ell^\circ} \qquad (6\text{-}12)$$

Equation (6-11) gives the first order perturbation in the eigenfrequency of the nth mode and equation (6-12) gives the coefficients for the first order change in the eigenfunctions. Further calculations here will involve only equation (6-11), but a few comments are made on the formalism developed above because of its possible use in other studies.

General application of equation (6-12) will involve considerable calculative effort since the inner products of the spheroidal and toroidal eigenfunctions over limited regions of a sphere are involved;

however, the results contain information about the amplitude of the eigenfunction over a slightly inhomogeneous sphere which should be useful in interpreting observed surface wave characteristics in terms of earth structure. Following Morse and Feshback (1953), (Chapter 9), the above procedure can be extended to include the effects of perturbations in boundary shape. This allows treatment of the effect of the varying elevation of the earth's surface. The above development has assumed non-degenerate eigenfunctions which are sufficient for the work which follows since the actual perturbations calculated are ϕ independent which allows choice of an appropriate zero order set of eigenfunctions by inspection. Treatment of more realistic earth models will require extension of the procedure to account for the degeneracy of the eigenfunctions. This is straightforward using known procedures, for example, in any of the last three references.

A simple modification of the above allows application of the formalism to a non-gravitating sphere including perturbations in the density ρ°. Dropping the terms which contain g°, g, ψ_n°, ψ in equations (6-1) and (6-2) and replacing ρ° by $\rho = \rho^\circ + \alpha\Delta\rho$, equation (6-2c) becomes

$$(L^\circ + \alpha Q)\, \underline{v}_n = \sigma_n(\rho^\circ + \alpha\Delta\rho)\, \underline{u}_n \quad .$$

L° and $\underline{v}_n^\circ$ become

$$L^\circ \equiv \begin{bmatrix} -(\lambda^\circ + 2\mu^\circ)\nabla(\nabla\cdot\sim) + \mu^\circ\,\nabla x(\nabla\, x\, \sim) & 0 \\ -(\nabla\lambda^\circ)(\nabla\cdot\sim) - (\nabla\mu^\circ)\cdot(\nabla\sim + \sim\nabla) & \\ 0 & 0 \end{bmatrix}$$

$$\underline{v}_n^\circ \equiv \begin{bmatrix} \vec{u}_n^\circ \\ 0 \end{bmatrix} .$$

The rest of the development is essentially as previously leading to the following expressions in place of equations (6-11) and (6-12)

$$\sigma_n^1 = (\vec{u}_n^{\circ *},\ Q_{11}\vec{u}_n^\circ) - \sigma_n^\circ\ (\vec{u}_n^{\circ *},\ \Delta\rho\ \vec{u}_n^\circ) \qquad (6\text{-}11a)$$

and

$$a_m^1 = \frac{(\vec{u}_m^{\circ *},\ Q_{11}\vec{u}_n^\circ) - \sigma_n^\circ\ (\vec{u}_m^{\circ *},\ \Delta\rho\ \vec{u}_n^\circ)}{\sigma_m^\circ - \sigma_n^\circ} \qquad (6\text{-}12a) .$$

Application of Perturbation Procedure to Torsional Oscillations

The formalism is now applied to the torsional oscillations of a layered, spherical earth model. Since an exact solution is developed for the radial part of the eigenfunctions the Thomson-Haskell matrix technique can be applied in a manner similar to that for the static solution given in Chapter 2. The matrix relations for the period equation for torsional oscillations of a sphere are given in Gilbert and MacDonald (1960) and are not repeated here. However, the solution function used here is different from that of Gilbert and MacDonald and this solution function with the necessary matrix results is given below and in Appendix 13. A derivation of the solution and a note on the sense in which it can be extended to spheroidal modes are given in Appendix 13.

For the torsional modes of either a gravitating or non-gravitating earth model equation (6-1d) becomes

$$\mu^\circ \nabla x(\nabla \times \vec{u}_n^\circ) - (\nabla\mu^\circ)\cdot(\nabla\vec{u}_n^\circ + \vec{u}_n^\circ \nabla) = \sigma_n^\circ \rho^\circ \vec{u}_n^\circ \quad .$$

The solution to this equation is of the form

$$\vec{u}_n^\circ = N_{m\ell p}\, u_{\ell p}(r)\, \vec{C}_{m\ell}(\theta,\phi) \quad .$$

As noted in Appendix 12 the subscript n is used for the mode type and for the three subscripts m, ℓ, and p. The $\vec{C}_{m\ell}$ have been defined

in Chapter 2 and the constant $N_{m\ell p}$ is defined below so that

$$\iiint_{\text{over sphere}} \vec{u}^{\circ *}_n \cdot \vec{u}^{\circ}_n \, \rho^{\circ} \, r^2 \sin\theta \, d\theta \, d\phi = 1 \quad .$$

For the solution in each layer μ° is a constant and $\rho^{\circ} = \frac{R^{\circ}}{r^2}$ where R° is a constant. The radial solution function is

$$u_{\ell p}(r) = A \, r^{-\frac{1}{2}} \, 2 \cosh ks + B \, r^{-\frac{1}{2}} \, 2 \sinh ks \qquad (6\text{-}13a)$$

if $(\ell + \frac{1}{2}) > \overline{\omega}$ and

$$u_{\ell p}(r) = A \, r^{-\frac{1}{2}} \, 2 \cos KS + B \, r^{-\frac{1}{2}} \, 2 \sin KS \qquad (6\text{-}13b)$$

if $(\ell + \frac{1}{2}) < \overline{\omega}$.

A and B are arbitrary constants and the following definitions apply

$$\overline{\omega} = \frac{R^{\circ}}{\mu^{\circ}} \sigma \qquad (6\text{-}14)$$

$$s = \ell n \, r \qquad (6\text{-}15)$$

$$k = \sqrt{(\ell + \tfrac{1}{2})^2 - \overline{\omega}} \qquad (6\text{-}16a) \text{ and}$$

$$K = \sqrt{\overline{\omega} - (\ell + \tfrac{1}{2})^2} \qquad (6\text{-}16b) \quad .$$

For a layered earth model with q layers numbered from 1 through q

$$N_{m\ell p} = \frac{1}{\left\{ \sum_{j=1}^{q} R_j^{\circ} \int_{r_j}^{r_{j-1}} u^2_{\ell p,j}\, dr \right\}^{\frac{1}{2}} \left\{ \frac{4\pi}{(2\ell+1)} \frac{(\ell+m)!}{(\ell-m)!} \ell(\ell+1) \right\}^{\frac{1}{2}}} \qquad (6\text{-}17)$$

The detailed from of $\int_{r_j}^{r_{j-1}} u^2_{\ell p,j}\, dr$ and the necessary matrix forms are given in Appendix 13.

A perturbation in rigidity within the ith layer is considered where

$$\mu_i^1 = \mu_i - \mu_i^{\circ} \quad \text{constant for} \quad r_L \leq r \leq r_u$$

$$\theta_L \leq \theta \leq \theta_u$$

$$0 \leq \phi \leq 2\pi$$

and

$\mu_i^1 = \mu_i - \mu_i^{\circ} = 0$ elsewhere. Results are also given for a perturbation in density of similar geometry but with the magnitude of the perturbation determined by

$$\rho_i^1 = \rho_i - \rho_i^{\circ} = \frac{(R_i - R_i^{\circ})}{r^2}$$

where R_i and R_i° are constants.

If $r_L = r_i$ and $r_u = r_{i-1}$, $\theta_L = 0$ and $\theta_u = \pi$, this perturbation is the same as a change μ_i^1 in the rigidity of the $i^{\underline{th}}$ layer of the sphere (or similarly for a change in density). This case was used as a check on the numerical calculations.

For torsional oscillations and these perturbations the perturbation in the operator, Q, is written

$$Q = Q_v + Q_s$$

where

$$Q_v = \begin{bmatrix} \mu_i^1 \nabla x(\nabla x \sim) & 0 \\ -2\mu_i^1 \nabla(\nabla \cdot \sim) & \\ 0 & 0 \end{bmatrix} \qquad \text{for } r_L \leqslant r \leqslant r_u \text{ , } \theta_L \leqslant \theta \leqslant \theta_u \text{ , } 0 \leqslant \phi \leqslant 2\pi$$

$$Q_v = 0 \text{ elsewhere} \quad ,$$

$$Q_s = \begin{bmatrix} -(\nabla\mu_i^1)\cdot(\nabla_\sim + \sim\nabla) & 0 \\ 0 & 0 \end{bmatrix}$$

and

$$\nabla\mu_i^1 = \hat{r}\,\mu_i^1 \{ \delta(r-r_L) - \delta(r-r_u) \} + \hat{\theta}\,\frac{\mu_i^1}{r} \{ \delta(\theta-\theta_L) - \delta(\theta-\theta_u) \}$$

Equation (6-11a) is then

$$\sigma_n^1 = (\vec{u}_n^{\circ *},\ Q_{11s}\ \vec{u}_n^{\circ}) + (\vec{u}_n^{\circ *},\ Q_{11v}\ \vec{u}_n^{\circ}) - \sigma_n^{\circ}\ (\vec{u}_n^{\circ *},\ \Delta\rho\ \vec{u}_n^{\circ}) \quad .$$

$$(\vec{u}_n^{\circ *},\ Q_v \vec{u}_n^{\circ}) = \frac{\mu_i^1}{\mu_i^{\circ}}\ \sigma_n^{\circ}\ \overline{\underline{R}}_v\ \Theta_v \quad ,$$

$$(\vec{u}_n^{\circ *},\ Q_s \vec{u}_n^{\circ}) = \frac{\mu_i^1}{R_i^{\circ}} \left\{ \overline{\underline{R}}_s\ \Theta_v + \overline{\underline{R}}_v\ \Theta_s \right\} \quad , \text{ and}$$

$$\sigma_n^{\circ}\ (\vec{u}_n^{\circ *},\ \Delta\rho \vec{u}_n^{\circ}) = \frac{(R_i^{\circ} - R_i)}{R_i}\ \sigma_n^{\circ}\ \overline{\underline{R}}_v\ \Theta_v$$

where

$$\overline{\underline{R}}_v = \frac{R_i^{\circ} \displaystyle\int_{r_L}^{r_u} u^2_{\ell p,i}\ dr}{\displaystyle\sum_{j=1}^{k} R_j^{\circ} \int_{r_j}^{r_{j-1}} u^2_{\ell p,j}\ dr} \quad ,$$

$$\Theta_v = \frac{\displaystyle\int_{\theta_L}^{\theta_u} \left[m^2 \left(\frac{P_\ell^m}{\sin\theta} \right)^2 + \left(\frac{\partial P_\ell^m}{\partial \theta} \right)^2 \right] \sin\theta\ d\theta}{\dfrac{2}{(2\ell+1)}\ \dfrac{(\ell+m)!}{(\ell-m)!}\ \ell(\ell+1)} \quad ,$$

$$\overline{\underline{R}}_s = \frac{R_i^\circ \left[t_{\ell p,i}\ u_{\ell p,i}\ r^2 \right]_{r_L}^{r_u}}{\sum_{j=1}^{k} R_j^\circ \int_{r_j}^{r_{j-1}} u_{\ell p,j}^2\ dr} \quad ,$$

$$\Theta_s = \frac{2 \left[\sin\theta \frac{\partial p_\ell^m}{\partial \theta}\ S_\ell^m + m^2\ P_\ell^m\ T_\ell^m \right]_{\theta_L}^{\theta u}}{\frac{2}{(2\ell+1)} \frac{(\ell+m)!}{(\ell-m)!}\ \ell(\ell+1)} \quad ,$$

$$t_{\ell p,i} = \frac{\partial u_{\ell p,i}}{\partial r} - \frac{u_{\ell p,i}}{r} \quad ,$$

$$S_\ell^m = -\frac{\cos\theta}{\sin\theta} \frac{\partial P_\ell^m}{\partial \theta} + m^2 \frac{P_\ell^m}{\sin^2\theta} - \frac{\ell(\ell+1)}{2} P_\ell^m \quad , \quad \text{and}$$

$$T_\ell^m = \frac{1}{\sin\theta} \frac{\partial P_\ell^m}{\partial \theta} - \frac{\cos\theta}{\sin^2\theta} P_\ell^m \quad .$$

Results of Calculations

The preceding expressions were programmed for an earth model with a perturbation in rigidity and a perturbation in density. The geometry of the perturbed region is shown in Figure 6-1. The calculated change in eigenperiod, ΔT, is compared with

$$\Delta T_{AVE} = \frac{2(\theta_u - \theta_L)}{2\pi} \quad (T_1 - T_o) \quad .$$

$T_1 - T_o$ is the change in eigenperiod for a change in rigidity extending from $\theta = 0$ to $\theta = \pi$. ΔT_{AVE} will be the change in eigenperiod if $T_1 - T_o$ is reduced in proportion to the angular distance actually covered by the inhomogeneity. Brune et al (1961) and earlier Jeans (1923) showed that the standing wave pattern of a free oscillation can be viewed as resulting from the interference of two traveling waves traveling in opposite directions around a sphere. For the geometry used here the estimate ΔT_{AVE} is appropriate for a source located at the pole with $m = 0$. In particular, for such a source, physical arguments indicate that ΔT_{AVE} should approach ΔT as the wave length of the associated traveling wave becomes small compared to $2(\theta_u - \theta_L)\, r_o$ where r_o is the radius of the sphere.

The particular perturbation used was a change in rigidity or a change in density in a layer 10 km thick centered at 55 km depth. The mantle model used for the results presented in Figure 6-2 was one of Prof. D. L. Anderson's models based on data from shield areas.

The conclusions drawn are not dependent upon small differences in the starting earth model. In Figure 6-2 for a perturbation from $\theta = 15°$ to $\theta = 90°$ the ratio of the breadth of the inhomogeneous region to the wave length appropriate to the standing wave pattern varies from about 1/2 at $\ell = 2$ to about 4 at $\ell = 20$. At $\ell = 2$ the estimate ΔT_{AVE} is good to about 20% while at $\ell = 20$ it is good to better than 5%. Similarly for a perturbation from $\theta = 75°$ to $\theta = 90°$ the same ratio varies from about 1/12 at $\ell = 2$ to about 9/10 at $\ell = 20$. For this case at $\ell = 2$ the estimate ΔT_{AVE} may be in error by a factor of 3 to 4, at $\ell = 10$ it is good to about 20%, while at $\ell = 20$ it is good to about 10%. Similar considerations for the case where the perturbation varies from $\theta = 45°$ to $\theta = 90°$ give intermediate results. The geometry of the perturbations for these cases is sufficiently simple that the relationship between the free oscillation result and a traveling wave view is easily seen. The change in free oscillation period can be directly interpreted in terms of phase velocity for a great circular path by the formula

$$C = \frac{2\pi\, r_o}{(\ell+\frac{1}{2})T} \quad .$$

The interpretation for other geometries is more complicated, but the above results should suffice for a test of the compatibility of the hypothesis of a regional weak layer in the upper mantle and observed surface wave dispersion.

To be specific the following discussion is limited to the case of a thin weak layer at about 60 km depth. In Table 6-1 the torsional

free oscillation periods for three models are listed for several values of the degree number ℓ. λ is the approximate wave length of traveling waves which would interfere to give the free oscillation. In the column "Model G" are the periods for a 35 layer approximation to a Gutenberg earth model. In the column "Model G3" are the periods for a model which is the same except with the rigidity reduced by a factor of 100 in a 1 km thick layer centered at 60.5 km depth. Column b, the percentage differences between the periods for Models G and G3, shows that a regional weak layer with the properties of Model G3 is easily consistent with the long period data. Observed differences for various great circular paths reported by Toksoz and Anderson (1966) are larger than the differences between Models G and G3 even without assuming that the weak layer of Model G3 is of limited extent.

In the column "Model G4" of Table 6-1 are the periods for a 60 km shell with the same properties as the uppermost 60 km of the Gutenberg Model G and with the lower boundary a free surface. Column c is the percentage difference between the periods for Models G and G4. The differences for the long periods are far larger than observational differences and show the expected unacceptability of a world encircling completely decoupling zone. As the period approaches 50 sec the differences in column c rapidly approach the size of observed differences. This results from the concentration of the energy in the mode above the 60 km level.

The results in Figure 6-2 and Table 6-1 give a basis for estimating the effect of a very thin, very weak regional layer on

surface wave dispersion. However, although the rigidity changes for models G3 and G4 are limited to a small region in the model, they are not a small proportion of the original rigidities. To evaluate the effect of this, the ratio of the actual period change to the estimate of the period change from perturbation theory is listed for several models in Table 6-2. The basic model is Model G. The column "Model G1" is based on a model like G, but with the rigidity reduced by one-half in a 1 km thick layer centered at 60.5 km depth. Similarly Model G2 has a rigidity reduction to one-tenth of the original value in the same layer. If the ratio given in Table 6-2 is near 1, the perturbation theory gives a good estimate. This is the case for the models with a rigidity reduction of 50% and 90% in a thin layer. With a rigidity reduction of 99% the perturbation estimate is too low by a factor of 3 at ℓ = 100 (T ~ 88 sec). When the rigidity is reduced to zero the perturbation estimate fails, as would be expected. However, the periods calculated for the shell model, listed for model G4, Table 6-1, can serve as estimates of the period which would be deduced from dispersion in a region with a completely decoupled outer layer which was many wave lengths long.

The above results are now combined to estimate the effect on surface wave dispersion of a very thin, very weak zone of limited lateral extent. Column's b and c, Table 6-1, give the period changes due to an earth encircling weak layer. Reference to Anderson's partial derivative tables (Anderson, 1964) shows that the percentage differences for ℓ = 160 are about as large as will occur for the model

considered here. The percentage change is reduced by the approximate ratio of the length of path containing the weak layer to the total length of path. Then it is increased by the approximate maximum ratio of $\Delta T/\Delta T_{AVE}$ for the appropriate ratio of inhomogeneity dimension to wave length. Table 6-3 lists the calculated percentage changes in period. These can also be interpreted as the percentage changes in phase velocity. For long periods the observational differences for different paths reported by Toksoz and Anderson (1966) are used as a measure of an acceptable variation in period. For shorter periods (about 40 to 80 sec) the variations in typical phase velocities for different regions summarized by Brune (1968) are used. These measures of acceptable variations in period are the maximum allowable since they include known regional structural differences other than a weak layer. The results for model G3, Table 6-3, are large but acceptable by the above criteria. For model G4 with ℓ = 20 results were included for all cases for completeness, but they are obviously inappropriate when the weak layer dimension and the path length are both 500 to 2000 km since dispersion for such a long wave length could not be measured over so short a path. For a weak layer dimension of 1000 km and a path length of 40,000 km a 0.83% change is predicted which, although large, is not outside observed limits. For model G4 with ℓ = 160 the changes again are comparable to observed limits.

The calculated changes in eigenperiod are sharply dependent upon the lateral extent, thickness, depth, and rigidity of the weak layer.

For a weak layer to have an appreciable effect on static tilts and strains, its lateral extent must be at least as great as the source to receiver distance, about 200 to 600 km for the observations considered here. To a first approximation the effect of a weak layer with non-zero rigidity is proportional to its thickness. The static models which showed deviations from the half-space tilts and strains which were large enough to correspond to the observations are essentially equivalent to complete decoupling such as characterized Model G4. The percentage variations for Model G4 are comparable with observed variations without accounting for regional differences other than a weak layer. Since other regional differences are undoubtedly important contributors to the observed phase velocity variations, their combination with a weak layer will tend to conflict with phase velocity observations. Although the calculations are uncertain at approximately the level of the discrepancy, the extreme weakening necessary in the static models appears to make some frequency dependence in the rigidity a necessity. Assuming that a weak layer is due to partial melting, the material may show appreciable rigidity at high frequencies and virtually no rigidity at low frequencies. Some rigidity at $\ell = 160$ ($T \approx 57$ sec) such as in Model G3 results in period variations of 0.5% to 2% which are judged acceptable. Longer wave lengths could measure a lower rigidity, but still be consistent with observed differences because of the longer paths necessary to measure them.

It is concluded that if decoupling is to be significantly

involved in explaining the static tilt and strain observations and also be consistent with surface wave dispersion data, the decoupling region must have the following properties:

a) the zone or zones of severe decoupling must be very thin, of the order of 1 km or less; and

b) the effective rigidity of the decoupling zone must show frequency dependence.

Chapter 7

COMPARISON OF OBSERVATIONS AND RESULTS FROM THEORETICAL MODELS

In this Chapter the observed tilts and strains are tabulated. Models are chosen for the source mechanism. The results from several theoretical models are then tabulated and compared with the observations. The implications of the comparisons are discussed.

Observations

The observed permanent tilts and strains for the Parkfield, Baja, and Borrego Mountain earthquakes are listed in Table 7-1. The possible variation listed after each observation is the author's estimate of the maximum possible variation in the observed value which will still be consistent with the record. This estimate includes a qualitative evaluation of line width, noise level, and longer term trends in the recording. The listed variation is not intended as an estimate of standard error.

Some additional comments on the observations are contained in Appendix 16 where some other observations are recorded. However, certain critical information is also given here. An attempt was made to estimate a time interval at the beginning of which there was no evidence of offset and at the end of which the permanent offset had definitely occurred. For the Parkfield earthquake it was

estimated that the offset had definitely occurred within 6 minutes. While for the Baja earthquake the offsets had definitely occurred in 6 to 15 minutes. The possible reading error is about 2 minutes and all the records are consistent with the offset having occurred instantaneously. The records which allow the greatest precision of reading give the smallest times. These time estimates are important in comparing the source dimensions implied by the static field versus the source dimensions implied by the dynamic field.

The implications of the other observations reported in Appendix 16 are as discussed below.

Fault Mechanisms for Parkfield, Baja, and Borrego Mountain Earthquakes

The Parkfield earthquake has been intensively studied resulting in a unique collection of information on the source mechanism. The critical parameters for this study are the dimensions and geometry of the fault plane and the magnitude and direction of slip on the fault plane together with its spatial distribution. The data considered in determining the parameters adopted are given below.

McEvilly, et al. (1967), bound the fault plane solution with the following two solutions:

	Fault Plane		
	Strike	Dip	Motion
(1)	N 35° W	88° NE	Right lateral 13° upward component on SW block.
(2)	N 29° W	85° SW	Right lateral 26° upward component on SW block.

The ambiguity concerning the determination of the fault plane is clearly removed by the field evidence.

Brown et al. (1967) mapped surface rupture and tectonic fracture patterns along a zone 38 km long which may be 5 to 8 km longer. The mapping shows two offset fault traces. For purposes of calculating static fields an "average" trace somewhere between N 40° W and N 45° W is indicated. In the same paper aftershocks are reported at depths from 2 to 12 kilometers.

Eaton (1967) presented data on aftershocks of the Parkfield earthquake which showed almost all of the aftershocks at less than 15 km depth and the great majority above about 12 km depth. The density of aftershocks was greatest from roughly 5 km depth to within 1 or 2 km of the surface. There were few if any aftershocks very near the surface which is presumably associated with the presence of relatively weak sedimentary fill. The aftershock epicenters are closely associated with the surface trace of the fault indicating a nearly vertical fault plane.

Allen and Smith (1966) report that the white line on the highway 1.5 km east of Cholame was offset 4.5 cm in a right lateral sense

10 hours following the main shock with the offset increasing in time. Brown et al. (1967) measured up to 10 cm of right lateral separation, locally and up to 7 cm of vertical displacement, locally. The vertical displacement was not believed to be tectonic and the measurements were made days to weeks after the earthquake.

Aki (1967) deduced a dislocation with a 50 cm offset at depth of 3 km moving at 2.2 km/sec by comparing a theoretically calculated seismogram with observed strong motion records. Hofmann (1967) reported about 20 cm relative right lateral movement between stations about 5 to 10 km from the fault. The time interval between measurements was about six months and includes the occurrence of the Parkfield earthquake. Hoffman's data was used together with Knopoff's (1957) fault model to obtain an estimate, which is roughly an upper bound, of the average displacement and depth of faulting. The details are given in Appendix 17, but for the purpose here a depth of 12 km and a right lateral offset of 26 cm are accepted.

On the basis of the above the source model given in Table 7-2 was chosen. The variations given for azimuths, distance, and dip indicate what are judged to be reasonable variations consistent with the observations. They were used as guides when varying the parameters in theoretical models, but not as strict constraints.

There are no studies available for the source mechanism of the Baja earthquake. A fault plane solution was carried out using the long period instruments of the World Wide Net and the long period

instruments of the local network of the Seismological Laboratory of the California Institute of Technology. The fault plane solution is given in Appendix 18. The data are judged consistent with the following solutions:

Nodal Planes		
N 53° E	$\delta = 90°$	(could vary to $\delta = 83°$ NE dip which changes the azimuth to N 59° E)
N 37° W	$\delta = 72° \pm 5°$	($\pm 15°$ is possible but less likely)

The fault plane solution and epicentral location are consistent with the earthquake being caused by movement on one or both of the branches of the San Jacinto fault near the head of the Gulf of California. The interpretation adopted here is:

Fault Plane		Motion
Strike	Dip	
N 37° W	72° SW	Right lateral with from 0° to 8° upward on the SW block.

The map in Kovach et al. (1962) showing the San Jacinto fault near the head of the Gulf of California was also used in determining the probable azimuth of the fault plane.

The depth of the Baja earthquake is important, but ill

determined. The USC and GS Preliminary Determinations of Epicenter cards give 33 km, but this is a restricted depth, not based on a direct determination. The City Clerk of San Luis, Mexico, stated that there were reports of ground fissuring and sand geysers. It is not clear if these were associated with primary surface rupture or secondary effects due to shaking (Prof. S. W. Smith - personal communication). Many of the seismograms which were used in the fault plane solution showed a "double event" which appeared to be due to two pulses separated by about 4 sec. This may be due to source complications such as two events on the same fault trace or events on the two fault traces shown in Kovach et al. (1962). Alternatively, it may be due to the depth of the source. The accumulated evidence of earthquakes on the San Andreas fault system favors a shallow source, but a source at a greater depth than usual is not ruled out. A shallow source was assumed for the model given in Table 7-2, but the possibility of a deeper source was also considered. The fault length, fault depth (dimension from the surface to the bottom of the fault), and amount of slip were arbitrarily fixed so that the maximum possible strains at the distance of Isabella, California, were approximately equal to the observed strains.

The source model for the Borrego Mountain earthquake is based on the report of Allen et al. (1968). The maximum right lateral, strike-slip motion reported was 38 cm; therefore, the assumption here of an average motion of 38 cm is several times what an average

of observed surface displacements would give. Preliminary determinations of aftershock locations give depths of less than 15 km.

The California Institute of Technology's Isabella station is at 35.663° North Latitude, 118.476° West Longitude. The azimith of the NW-SE tiltmeter and strainmeter is 321.61°. The azimuth of the NE-SW tiltmeter and strainmeter is 51.61°.

Comparison with Results of Theoretical Calculations

Source models essentially like those given in Table 7-2 were used to predict the tilt and strain fields at Isabella. The results given in Press (1965) were first used to try to fit the data. The strong disagreement of the prediction and the data led to the consideration of structural effects. As pointed out in Chapters 3 and 5 a conventional earth structure, if anything, increases the difficulties compared to a half-space. The effect of a weak layer at a depth of about 50 km was investigated by calculating theoretical deformational fields for models like those described in the last section of Chapter 5. A variety of parameters were varied for each earthquake. The parameters considered and the amount of variation were determined in each case by comparing the results of the calculations with the observations. Point source approximations for strike-slip, dip-slip, and dilatational sources were assumed. The dip of the fault, the depth of the source,

the source-station angle (θ in Figure 7-1), the station-instrument angle (β in Figure 7-1), and the distance from the source to the station were varied. Deformational fields were calculated for a half-space model and for a model with a layer of unit thickness and rigidity, overlying a layer of unit thickness and reduced rigidity, overlying a uniform half-space. For the results presented the models had Poisson's ratio equal to $\frac{1}{4}$ in all layers. By allowing a wide range of source-station distances for each calculation the possibility of rescaling the model to obtain a better fit to the data was included. Since there is considerable interplay between the nature and thickness of the weak layer and the thickness of the overlying layer this procedure effectively permits consideration of a wide variety of models.

For each model the deformational fields due to a strike-slip, a dip-slip, and a dilatational source were calculated. The field evidence and the fault plane solutions indicated that dip-slip motion for the three earthquakes is small compared to strike-slip motion. An extremely weak decoupling layer and a dip-slip source leads to a great diversity of results. Nonetheless it was generally true that the values of the deformational fields, due to the dip-slip motion assumed, were relatively small compared to those due to the strike-slip motion assumed. This is basicaly due to the smaller source strength assumed for dip-slip motion. Within the class of models considered there is no indication that dip-slip motion can

make an important contribution toward explaining the observations. An arbitrary expansion or compression in the source region was modeled by a point dilatational source. Such a source did not consistently aid in explaining the important features of the observations. The results discussed below and presented in Figures 7-2, 7-3, and 7-4 are all for strike-slip models.

The large source strengths implied by the observations are illustrated by comparing the predictions from one of Press's strike-slip models with the observations. The model assumed had the fault half-length equal to 19 km, a total source strength of 8.1×10^{13} cm^3, and an orientation 10° different than that given in Table 7-2. The term "source strength" is used for the product of fault length, fault breadth, and average slip. The ratios of the observed tilts to the theoretical were:

$$\text{NW-SE} \qquad \frac{\text{observed tilt}}{\text{theoretical tilt}} \approx +150$$

$$\text{NE-SW} \qquad \frac{\text{observed tilt}}{\text{theoretical tilt}} \geq +40$$

This fault model has a source which is compatible with the field evidence. The predicted tilts have the correct sign, but are much too small.

The predicted tilt fields for four models for the Parkfield earthquake are plotted in Figure 7-2. The models are listed in Table 7-3. Aki (1967b) reports a seismic moment of 10^{25} dyne-cm. Assuming a rigidity of 3.33×10^{11} dyne/cm, this gives a source

strength of 3×10^{13} cm^3. Model D is a shallow point source with this source strength. It shows the same order of discrepancy with the observations as the results from Press's model. Model C is the same with the source strength increased to 1.14×10^{14} cm^3. This is considered a very strong source. Smith and Wyss (1968) associate a source of about one-half this strength with the main shock at Parkfield. Models B and A show the effect of reducing the rigidity of the second layer in the model to 1/10 and 1/100 of that in the top layer. Model A predicts a field which is still over two times smaller than the observations. A closer fit can of course be achieved, e.g. by increasing the source strength, but this is not deemed important. The important point is the degree of weakening which is necessary to substantially improve the fit. In either A or B the zone of reduced rigidity must be viewed as a convenient way of modeling a relatively thin, very weak layer. Model A is close to a model of a plate over a liquid layer.

In varying the depth of the source in layer 1 when layer 2 was weakened, it was found that the most important feature was the relative position of the source in layer 1. A source in the upper 1/3, near the middle, and in the lower 1/3 of layer 1 give essentially different features in the deformational fields. A point source at a given depth in layer 1 is roughly equivalent to a source which is centered at the point source location and distributed over a depth range of about 2/10 of the thickness of the layer. Considering the

extreme features of the structural models necessary to achieve some correspondence between the theoretical models and the data, detailed depth distributions and a detailed fit of the data were not attempted for Parkfield or for the other earthquakes discussed below.

Deformational fields for sources located at either end of the surface fault trace were calculated for the Parkfield model. It was determined that integration of the source in the horizontal direction does not have a strong effect on the field predicted at Isabella.

As an example of the nature of the observations from the Baja earthquake compared to a half-space model one of Press's strike-slip models was used to predict the tilt and strain fields at Isabella. The source-station angle was taken as 6°, the half-length of the fault as 50 km, and the source strength as 1.22×10^{16} cm^3. The ratios of observed to theoretical fields were

$$\text{NW-SE strain} \qquad \frac{\text{observed strain}}{\text{theoretical strain}} = +1.0$$

$$\text{NE-SE strain} \qquad \frac{\text{observed strain}}{\text{theoretical strain}} = +3.0$$

$$\text{NW-SE tilt} \qquad \frac{\text{observed tilt}}{\text{theoretical tilt}} = +10.$$

$$\text{NE-SW tilt} \qquad \frac{\text{observed tilt}}{\text{theoretical tilt}} = -3.2$$

Two points are important. First, the source strength adapted is considered quite large. For example, using the numbers listed in Brune and Allen (1967), source strengths for four earthquakes of magnitude 7.1 to 7.2 vary from .6 x 10^{15} cm^3 to 6 x 10^{15} cm^3. The Baja earthquake has a magnitude of 6.3. By analogy with the Parkfield earthquake, detailed observations might indicate a rather larger source than expected. Second, all of the observed components are very close to a nodal line except the NE-SW tilt, and this tilt has the opposite sign from that predicted. The most critical factor in trying to obtain a model to fit the Baja data are the sign and approximate magnitude of the NE-SW tilt. For a half-space model a change of over 30° in the azimuth of the fault plane given in Table 7-2 is necessary to obtain the sign of this tilt. The relative magnitudes and signs of the other observations are next in importance, but the nearby nodal line makes the other tilt and strains change very rapidly for relatively small changes in angle.

The tilts and strains calculated for four models for the Baja earthquake are shown in Figure 7-3. The parameters of the models are given in Table 7-4. In this figure the solid lines are calculated fields which have the same sign as the observed fields; the dashed lines are calculated fields which have the opposite sign from the observed fields. The same convention is used in Figures 7-2 and 7-4. The most important point for half-space models, like Model D in Figure 7-3a, is that the NE-SW tilt has the opposite sign from

the observation. Also all the fields are small compared to the observations. Of all the models tried no half-space model gave the same sign as the observation for the NE-SW tilt. Model C has the wrong sign at the scaling used, but can be rescaled to give the correct sign. For example rescaling model C so that the unit of length is about 50 km instead of 60 km and the source strength remains the same, gives

$$\text{NE-SW tilt} = + 1.1 \times 10^{-9}$$

$$\text{NW-SE tilt} = - 2.0 \times 10^{-10}$$

$$\text{NW-SE strain} = + 5.7 \times 10^{-10}$$

$$\text{NE-SW strain} = + 3.0 \times 10^{-10}$$

at Isabella. The NE-SW tilt has the correct sign, but is too small. To match this observation would require increasing the already large source strength by 40 times. Models A and B show the effect of having the source appreciably below the middle of layer 1. Both models show the same sign for the NE-SW tilt as the observation, and both show relatively large amplification of the size of this tilt relative to a half-space. A source strength about 5 times larger is necessary to match the observed NE-SW tilt. For the other tilt and two strains neither Model A nor B has all the signs and relative amplitudes in agreement with the observations. No model tested was satisfactory in this respect. Model A gives as good a fit

as any to the relative sizes of the observations, but the strains have the wrong sign. The thickness of layer 1 and the absolute source depth in models A and B could probably be reduced by using a source relatively lower in the plate.

Figure 7-4 shows the results from four models for the Borrego Mountain earthquake. The parameters for the models are given in Table 7-5. Since there was no observation to determine the sign, the arbitrary convention was adopted that a solid line represents SE up in Figure 7-4a and a solid line represents SW up in Figure 7-4b. Model D is a half-space model. It shows reversed signs from the strain observations and, if scaled to match the strain observations, the NE-SW tilt would tend to violate the observational bound. These two features, reversed signs and tilt which tends to be too large, characterized all the models attempted which had a geometry within a few degrees of that given in Table 7-2. A half-space model which showed the same signs as the strain observations and also had sufficiently small tilts had a fault plane azimuth of 332° compared with 318° for the preferred model in Table 7-2.

Borrego Mountain models with a weak layer and a shallow source strong enough to give the strain amplitudes generally gave a NE-SW tilt which was larger than the observed bound. However, a node in the tilt field of these models allowed a scaling which could accomodate the absence of tilts and give the correct sign and magnitude for the strains. This is illustrated by model C.

Models A and B show that a source near the midpoint of layer 1 results in a reduction of the tilt fields over a wide range in distances from the source. This would explain the lack of tilt observation under less restricted scaling than model C, but considerable deviation from the preferred fault plane azimuth in Table 7-4 is still necessary in order to get the proper signs for the strains. All these models, despite the large source strength assumed fall somewhat short of the observed magnitudes for the strains.

Discussion of Results

For the three earthquakes studied the use of half-space models to predict the tilts and strains leads to substantial disagreement between calculated fields and observations. Including the possibility of a weak or decoupling layer which begins at a depth of about 40 km to 100 km improved the ability to fit some important features of the data, but did not lead to a completely satisfactory fit. All models required a larger source than other evidence supports although models with a weak layer did not generally require as strong a source as half-space models. In particular the observed tilts from the Parkfield earthquake can be fit by either a half-space model or a model with a weak layer. A substantially weaker source can be used in the weak layer model. All important features of the

Baja earthquake cannot be fit by any of the models tried. Proximity to a nodal line for three of the observations from this earthquake tends to negate their value in constraining the model. No half-space model for the Baja earthquake showed the proper sign for the critical NE-SW tilt, but some models with a weak layer did. The Borrego Mountain observations could be roughly fit with or without a weak layer. For all models considered for the Borrego Mountain earthquake a change in fault plane azimuth from that inferred from field evidence was necessary to obtain the proper sign for the observed strains. The necessary change is large compared to what the field evidence indicates and could be due to appreciable lateral variations in earth structure. Assuming a half-space model, the similarity of source type and source-station geometry for the Baja and Borrego Mountain earthquakes implies that the NE-SW tilt at Isabella should be comparable for the two earthquakes. Changes in the sign of the field, which a weak layer causes, help to explain the observation that the two reponses are not similar.

In order to give an appreciably improved fit to the data the degree of decoupling in the weak layer had to be extreme. The degree of weakening is the principal objection to the models used. The thickness of the weak layer in the models calculated here is only an aid in the computational scheme. The model which served as motivation to test the weak layer hypothesis is that of a partially molten region in the upper mantle. The precise rheology

of such a layer is not known, but it is assumed here to act as a decoupling layer. The models calculated are very simple, but the interplay of source depth, layer thickness, and variation in rigidity should give a good idea of the nature of the deformational fields due to a decoupling layer.

An important associated problem is that an extremely weak layer, even if very thin, should have an appreciable effect on surface wave dispersion. The results of the calculations using the perturbation theory of Chapter 6 do not apply directly to the problem because the theory tends to break down for an extremely strong perturbation and because the calculations made include only very long wave lengths. Nevertheless the results indicate that path averaging, slightly modified for short paths, to determine the effect on phase velocity can be used. This combined with some frequency dependence in the properties of the weak layer material will not violate surface wave data. A recent article by Aki (1968) bears on this question and supports the possibility of very thin, weak layers in the upper mantle or crust.

The emphasis in the structural models used is on variations in the physical properties of the material which occur over a limited vertical range and a relatively large horizontal dimension. The observations from the Baja and Borrego Mountain earthquakes suggest that strong vertical variations in earth structure with a relatively small horizontal dimension may also be involved. The scale, the

contrast in physical properties, and the orientation of possible structural effects has all gradations from regional to local. For example the rigid plate tectonics of Morgan (1968) or McKenzie and Parker (1967) involves structural units much larger than the source-receiver distance for the observations considered here. Effects due to regional tectonics on a scale of hundreds of kilometers, as suggested by Tomaschek (1957), or the "jostling" of fault blocks suggested by Hamilton and Myers (1966) (e.g. page 534), have an appropriate distance scale. Effects due to local geologic structure with a length scale of hundreds of meters, as reported by Nishimura (1950), could dominate. Finally very local effects due to the geometry or physical nature of the recording site are also a possibility. The last two cases are clearly unrelated to the weak layer models considered here.

The size of effects due to local conditions at the recording site is an important problem. The instruments are located in an abandoned mine tunnel. Topography at the recording site and the geometry of the tunnel will certainly have some effect. Neuber's (1946) results show that distortion of the strain field from that predicted for a half-space model can be expected to be roughly proportional to the curvature of the topographic surface or the tunnel interior. Such distortions should diminish rapidly away from the surfaces and were judged to be small. Two very simple models show that this argument may not be sufficient. Using Neuber's (1946)

solution for a spherical cavity in a medium under tension the effect of the cavity on a strain measurement was estimated. The true strain, ε_T, was defined as the difference between the displacement fields at two points along the axis of tension in a infinite medium. The strain measured in cavity, ε_m, was defined as the difference between the displacement fields at the same points, but on the surface of a spherical cavity. These geometries are illustrated in Figure 7-5a, b. The ratio of the strains is $\frac{\varepsilon_m}{\varepsilon_T} \approx +1.5$.

Another simple example was calculated using Starr's (1928) solution for a two dimensional elliptical surface in a uniform shear field. The true tilt, t_T, was defined as the difference between displacement field components at two points in an infinite medium. The tilt measured in a two dimensional cavity, t_m, was defined as the same difference in displacement field components, but on the surface of an elliptical cavity. The geometries are illustrated in Figure 7-5 c, d. The ratio of the tilts is

$$\frac{t_m}{t_T} = - \frac{(\lambda+2\mu)}{(\lambda+\mu)} e^{2\xi_o} \tanh \xi_o \quad .$$

The parameter ξ_o is a measure of the ellipticity of the cavity. The "measured" tilt shows a change in sign. A variation in the size of a measured strain by + 1.5 is not important in this study. A reversal in the sign of the tilt is quite important. The simple

geometries considered are not adequate to give an evaluation of the effect of tunnel geometry at the Isabella recording site, but they do illustrate the fact that it cannot be excluded as a potentially important factor.

Another local factor which may be important is movement along joints or cracks in or near the tunnel. An extension of the base of one of the strainmeters of less than a micron gives a strain of 10^{-9}. During some periods of time offsets of 10^{-9} to 10^{-8} occur on some of the strain or tilt records. They are not related to evident seismic events. Their origin is not known. A tilt of 10^{-7} which was recorded for an Alaskan earthquake (see the Fox Island Earthquake, Table A16-2, Appendix 16) is so large that it indicates a relatively local effect. On the other hand of the earthquakes checked there are many more which do not have an offset than there are which do, and many of these had larger amplitude waves at Isabella than the Fox Island earthquake. A detailed study of possible effects at the recording site is an important remaining problem.

The source model adopted here although greatly simplified is considered adequate insofar as the field evidence defines the nature and dimensions of the source. The question of source strength, the product of rupture length, rupture width, and average offset, is the most critical point. The unusual amount, quality and variety of information on the Parkfield earthquake indicated a source

strength which is larger than might have otherwise been determined. It is certainly possible that there are complications in the source which escape detection. The inclusion of a dilatational source in the calculations was a simple test of the hypothesis that there might be regional changes in volume associated with earthquakes. The apparent spreading in the Gulf of California (e.g. Hamilton and Myers, 1966, p. 524) and apparent compression reported by Burford (1968) suggest this source type. One possible complication, although postulated on an ad hoc basis, is deemed sufficiently pertinent to be discussed. The extent of the aftershock zone, horizontally and vertically, is taken to define the fault plane surface. The concurrence with surface evidence of rupture confirms this in the horizontal dimension. Vertically it is less certain. A vertical weak zone, or in the most extreme case, a vertical free surface at depth associated with the fault zone could give an appreciably greater effective depth than the aftershock depths indicate. The net result when observed from a distance is a larger apparent source strength. One of the cases treated analytically by Walsh (1968), that of deepening of an already existing fault surface, illustrates this. The geometry treated by Walsh is different than that suggested above, but the effect several fault depths away should be similar.

For the three earthquakes considered the source strength which the static observations suggest and the rapidity with which the static field attained its new value at Isabella imply strong surface

wave excitation. The fact that the bounds on the time intervals during which the offsets occur are essentially determined by record quality allows for time durations considerably less than the estimates. Assuming a short time duration for offset and using the magnitude-moment relationship of Brune (1968), the source strength of a 5½ magnitude earthquake is about 1.7×10^{13} cm^3; that of a 6 3/4 magnitude earthquake about 2.7×10^{14} cm^3. Using magnitude as the basis, this would give source strengths some 2 to 20 times smaller than those used in the models calculated. Brune (1968) pointed out that there are uncertainties in applying the magnitude-moment relationship to individual earthquakes, but the amount of discrepancy, particularly for the Baja earthquake, is a difficult point. Some additional considerations can help to explain this. If there is a vertical weak region associated with the fault zone, as discussed above, this region may have little stored strain energy associated with it, and therefore little seismic radiation generated by its movement. Also the nature of a dynamic stress release source, as opposed to a step dislocation in time, particularly with a weak layer present, may not generate strong surface waves when constrained by the time intervals during which the static offset occurred.

A unique demonstration of source complications was documented by Allen et al. (1968) for the Borrego Mountain earthquake. Offsets of 1 to 2 cm were observed on small theodolite nets spanning Superstition Hills fault, Imperial fault, and Banning-Mission Creek fault. The time of occurrence of these offsets

is not certain, but they are apparently associated with strain release triggered by the Borrego Mountain earthquake. These particular sources are not strong enough to have an appreciable effect at Isabella compared to the Borrego Mountain earthquake. For example a model of the Banning-Mission Creek fault based on the data in Allen et al. (1968) (fault length 20 km, offset 1 cm, fault depth assumed to be 20 km) gave strains at least a factor of 10 less than most Borrego Mountain models. A source of this strength at roughly a distance of 100 km could dominate the offset at Isabella. Smaller sources which are closer could be equally important, and this notion eventually scales to movement on joints in the tunnel constituting very local sources.

The discussion above shows that there are important problems remaining to be solved in order to achieve a definite explanation for the observations. The scale of the spatial variations of the observed tilt and strain fields, particularly with respect to the question of local versus regional effects, is the most important problem. Although each recording site and regional structure is an individual case, the same problem is pertinent for other observations of the type considered here.

Chapter 8

CONCLUSIONS

The use of dislocation theory to model the static deformational field due to seismic sources was investigated. An earthquake is assumed to be due to faulting which results in a reduction in stress in a prestressed region. It is shown that if a stress free surface is introduced into a prestressed medium, the resulting deformational field is identical with that of a suitable dislocation source. The validity of a dislocation source representation can be investigated by using point dislocation models to test the effects of spatial source distribution.

A representation of the Green's function for a homogeneous elastic sphere is derived and used to show that for shallow seismic sources sphericity cannot be neglected beyond about 20°. For sources over about 50 km deep sphericity is important at even shorter distances.

Integral representations for the static surface deformational fields due to certain dislocation sources in a layered, elastic half-space are derived. The point source equivalents of a strike-slip fault, a dip-slip fault, and a volume change are treated. The asymptotic forms of the solutions and numerical results from some simple layered models are used to show some general properties of the surface deformational fields. At distances of a few degrees

the effect of earth structure is generally a reduction in the field compared to the field in a half-space due to the increase in rigidity with depth.

Predicted tilt and strain fields from dislocation fault models are compared with observed fields for three earthquakes. The discrepancy between observations and prediction led to an investigation of the hypothesis that a weak layer in the lower crust or upper mantle might be dominating the observations. Theoretical models showed that, if a weak layer is to help significantly in explaining the observations, the degree of weakening must be quite severe. A perturbation procedure was developed to calculate the effect of lateral inhomogeneities on the earth's free oscillations. This was applied to test the compatibility of thin, weak zones of limited lateral extent and observed surface wave dispersion. It is concluded that extremely weak, thin layers in the lower crust or upper mantle are consistent with observed surface wave dispersion, but, for the degree of weakening used in the static earth structure models, some frequency dependence in the elastic properties is required.

The comparison of theoretical and observed tilts and strains for shallow seismic source at distances of about 200 km to 600 km does not distinguish between the weak layer hypothesis and a number of alternatives. The situation is summarized by the following conclusions.

a. Half-space models require a much larger source than other evidence indicates. Structural models where the mantle has a higher rigidity than the crust generally increase the source size necessary. Weak layer models also require a larger source than other evidence indicates, but generally smaller than that required by half-space models.

b. The hypothesis of a weak or decoupling layer in the lower crust or upper mantle improves the ability of the theoretical models to fit the important features of the observed tilts and strains. The improvement is significant only if the weakening is extreme, so that the weak layer approaches a model of a thin liquid layer.

c. None of the half-space or weak layer models show a completely satisfactory compatibility with the evidence as to the nature of the source, the predicted deformational fields, and the observed fields. This can be due to regional structural effects, source complications, or local effects at the recording site. Observations on the spatial variability of the tilt and strain fields are necessary to distinguish between the alternatives.

REFERENCES

Aki, Keiiti, Seismological Evidences for the Existence of Soft Thin Layers in the Upper Mantle under Japan, J. Geophys. Res., 73, 585-594, 1968.

Aki, K., Source Mechanisms of the Parkfield Earthquake, presented at the Conference on Geologic Problems of the San Andreas Fault System, Stanford University, September 16, 1967a.

Aki, Keiiti, Scaling Law of Seismic Spectrum, J. Geophys. Res., 72, 1217-1231, 1967b.

Allen, C. R., A. Grantz, J. N. Brune, M. M. Clark, R. V. Sharp, T. G. Theodore, E. W. Wolfe, and M. Wyss, The Borrego Mountain, California, Earthquake of 9 April 1968: A Preliminary Report, Bull. Seismol. Soc. Am., (in press), 1968.

Allen, C. R., P. St. Amand, C. F. Richter, and J. N. Nordquist, Relationship Between Seismicity and Geologic Structure in the Southern California Region, Bull. Seismol. Soc. Am., 55, 753-797, 1965.

Allen, C. R., and S. W. Smith, Pre-Earthquake and Post-Earthquake Surficial Displacements, Bull. Seismol. Soc. Am., 56, 966-967,1966.

Alterman, Z., H. Jarosch, and C. L. Pekeris, Oscillations of the Earth, Proc. Roy. Soc., A 252, 80-96, 1959.

Anderson, D. L., Universal Dispersion Tables, 1. Love Waves Across Oceans and Continents on a Spherical Earth, Bull. Seismol. Soc. Am., 54, 681-726, 1965.

Archambeau, Charles B., Elastodynamic Source Theory: Part 1. General Theory, Rev. of Geophys. (in press), 1967.

Backus, George E., Converting Vector and Tensor Equations to Scalar Equations in Spherical Coordinates, Geophys. J. Roy. Astr. Soc., 13, 71-101, 1967.

Backus, George E., Geographical Interpretation of Measurements of Average Phase Velocities of Surface Waves over Great Circular and Great Semi-Circular Paths, Bull. Seismol. Soc. Am., 54, 571-610, 1964.

Backus, G., and F. Gilbert, The Rotational Splitting of the Free Oscillations of the Earth, Proc. Natl. Acad. Sci., U.S., 47, 363-371, 1961.

Ben-Menahem, A., and S. J. Singh, Eigenvector Expansions of Green's Dyads with Application to Geophysical Theory, unpublished manuscript, 71 pp., 1968.

Ben-Menahem, Ari, Deformation of a Non-Gravitation Elastic Sphere by a Finite Internal Dislocation, unpublished manuscript, 52 pp, 1965.

Bergman, Stefan, and M. Schiffer, Kernel Functions and Elliptic Differential Equations, in Mathematical Physics, Academic Press Inc., New York, pp 219-222, 1953.

Biot, M. A., Effect of Certain Discontinuities on the Pressure Distribution in a Loaded Soil, Physics, G, 367-375, 1935.

Bolt, Bruce A., and Otto W. Nuttli, P Wave Residuals as a Function of Azimuth, J. Geophys. Res., 71, 5977-5985, 1966.

Brown, R. D., Jr., J. G. Vedder, R. E. Wallace, E. F. Roth, R. F. Yerkes, R. O. Castle, A. O. Waananen, R. W. Page, and J. P. Eaton, The Parkfield-Cholame California Earthquakes of June-August 1966 - Surface Geologic Effects, Water-Resources Aspects, and Preliminary Seismic Data, Geological Survey Professional Paper 579, 66 pp, 1967.

Brune, James N., Seismic Moment, Seismicity, and Rate of Slip along Major Fault Zones, J. Geophys. Res., 73, 777-784, 1968a.

Brune, James N., Surface Waves and Crustal Structure, in press, 1968b.

Brune, James N., and Clarence R. Allen, A Low-Stress Drop, Low-Magnitude Earthquake with Surface Faulting: The Imperial, California, Earthquake of March 4, 1966, Bull. Seismol Soc. Am., 57, 501-514, 1967.

Brune, James N., John E. Nafe and Leonard E. Alsop, The Polar Phase Shift of Surface Waves on a Sphere, Bull. Seismol. Soc. Am., 51, 247-257, 1961.

Burford, Robert O., Recent Strain Changes Across the San Andreas Fault and Coast Ranges at Hollister and Cholame, California, Preprint, 74 pp., 1968.

Burridge, R., and L. Knopoff, Body Force Equivalents for Seismic Dislocations, Bull. Seismol. Soc. Am., 54, 1875-1888, 1964.

Carder, D. S., D. W. Gordon, and J. N. Jordan, Analysis of Surface-Foci Travel Times, Bull. Seism. Soc. Am., 56, 815-840, 1966.

Chinnery, M. A., The Deformation of the Ground Around Surface Faults, Bull. Seism. Soc. Am., 51, 355-372, 1961.

Cleary, J., and A. L. Hales, An Analysis of the Travel Times of P-waves to North American Stations, in the Distance Range 32° to 100°, Bull. Seism. Soc. Am., 56, 467-489, 1966.

Dicke, R. H., and J. P. Wittke, Introduction to Quantum Mechanics, Addison-Wesley Publishing Company, Inc., Reading, Mass., 369 pp, 1960.

Doyle, H. A., and A. L. Hales, An analysis of the Travel Times of S Waves to North American Stations, in the Distance Range 28° to 82°, Bull. Seism. Soc. Am., 57, 761-771, 1967.

Eaton, J. P., Dependence of Hypocenter Determinations on the distribution of Recording Stations and the Precision of the Seismic Velocity Model of the Earth's Crust in the Parkfield-Cholame Region, presented at Conference on Geologic Problems of the San Andreas Fault System, Stanford University, Sept. 16, 1967.

Erdelyi, A., Editor, Tables of Integral Transforms, Vol. II, McGraw-Hill Book Company, Inc., New York, p. 28, 1954.

Gilbert, Freeman, and George Backus, Propagator Matrices in Elastic Wave and Vibration Problems, Geophysics, 31, 326-332, 1966.

Gilbert, F., and G. J. F. MacDonald, Free Oscillations of the Earth, I. Toroidal Oscillations, J. Geophys. Res., 65, 675-693, 1960.

Hales, A. L., A Weak Layer in the Mantle?, Geophys. J. Roy. Astr. Soc., 4, 312-319, 1961.

Hales, A. L., and H. A. Doyle, P and S Travel Time Anomalies and Their Interpretation, Geophys. J. of the Roy. Astr. Soc., 13, 403-415, 1967.

Hamilton, Warren, and Bradley W. Myers, Cenozoic Tectonics of the Western United States, Rev. Geophys., 4, 509-549, 1966.

Harkrider, David G., Surface Waves in Multilayered Elastic Media, I. Rayleigh and Love Waves from Buried Sources in a Multilayered Elastic Half-Space, Bull. Seismol. Soc. Am., 54, 627-670, 1964.

Harkrider, D. G., A. L. Hales, and F. Press, On Detecting Soft Layers in the Mantle with Rayleigh Waves, Bull. Seismol. Soc. Am., 53, 539-548, 1963.

Herrin, Eugene, James Taggert, and Anton Hales, Regional Variations in P Travel Times, preprint, 10 pp plus tables and figures, 1968.

Hildebrand, F. B., Advanced Calculus for Engineers, Prentice-Hall, Inc., New York, 594 pp, 1949.

Hofmann, R.B., Recent Changes in California Fault Strain from the Department of Water Resources Geodimeter Strain-Monitoring Program, presented at Conference on Geologic Problems of the San Andreas Fault System, Stanford University, Sept. 16, 1967.

Hoskins, L. M., The Strain of a Gravitating Sphere of Variable Density and Elasticity, Trans. Amer. Math. Soc., 21, 1-43, 1920.

Jeans, J. H., The Propagation of Earthquake Waves, Proc. Roy. Soc. London, (A), 102, 554-574, 1923.

Jordan, James, Rudolph Black, and Charles C. Bates, Patterns of Maximum Amplitudes of P_n and P Waves over Regional and Continental areas, Bull. Seis. Soc. Am., 55, 693-720, 1965.

Keilis-Borok, V., On Estimation of the Displacement in an Earthquake Source and of Source Dimensions, Ann. Geofis. Rome, 12, 205-214, 1959.

Knopoff, Leon, Energy Release in Earthquakes, Geophys. J. of the Roy. Astro. Soc., 1, 44-52, 1957.

Kovach, Robert L., Clarence R. Allen, and Frank Press, Geophysical Investigations in the Colorado Delta Region, J. Geophys. Res., 67, 2845-2871, 1962.

Love, A. E. H., A Treatise on the Mathematical Theory of Elasticity, Dover Publications, New York, p 183, 1944.

Love, A. E. H., Some Problems of Geodynamics, Republished by Dover Publications, Inc., New York, 180 p, 1911.

Longman, I. M., A Green's Function for Determining the Deformation of the Earth under Surface Mass Loads, 2. Computations and Numerical Results, J. Geophys. Res., 68, 485-596, 1963.

Longman, I. M., A Green's Function for Determining the Deformation of the Earth under Surface Mass Loads, 1. Theory, J. Geophys. Res., 67, 845-850, 1962.

Lur'e, A. I., Three-Dimensional Problems of the Theory of Elasticity, Interscience Publishers, New York, 44-46, 1964.

Maruyama, Takuo, Statical Elastic Dislocations in an Infinite and Semi-Infinite Medium, Bull. Earthqk. Res. Inst., 42, 289-368, 1964.

Mathews, J., and R. L. Walker, Mathematical Methods of Physics, W. A. Benjamin, Inc., New York, 475 pp, 1964.

McEvilly, T. V., W. H. Bakun, and K. B. Casaday, The Parkfield, California Earthquakes of 1966, Bull. Seismol. Soc. Am., 57, 1221-1244, 1967.

McKenzie, D. P., and R. L. Parker, The North Pacific: An Example of Tectonics on a Sphere, Nature, 216, 1276-1280, 1967.

Morgan, W. Jason, Rises, Trenches, Great Faults, and Crustal Blocks, J. Geophys. Res., 73, 1959-1982, 1968.

Morse, P. M., and Herman Feshbach, Methods of Theoretical Physics, Part II, McGraw-Hill Book Company, Inc., New York, 979 pp, 1953.

Neuber, Heinz, Theory of Notch Stresses, translated by F. A. Raven, J. W. Edwards, Ann Arbor, Michigan, Chapter 5, 1946.

Nishimura, E., On Earth Tides, Trans. Amer. Geophys. Union, 31, 357-376, 1950.

Ottelet, I., A Variational Principle Governing the Free Oscillations of a Gravitating Elastic Compressible Planet, The Astrophysical Journal, 143, 253-258, 1966.

Powell, Tom, and Donald Fries, Handbook: World-Wide Standard Seismograph Network, Revised July 1966, Institute of Science and Technology, The University of Michigan, pg. vii, 1966.

Press, Frank, Displacements, Strains and Tilts at Teleseismic Distances, J. Geophys. Res., 70, 2395-2412, 1965.

Richter, Charles F., John M. Nordquist, Violet Taylor, and Clarence Allen, Local Bulletin of Earthquakes in the Southern California Region, 1 January 1963 to 31 December, 1966, Seismological Laboratory, Division of Geological Sciences, California Institute of Technology, 34 pp, 1967.

Ritsema, A. R., (i,Δ)-Curves for Bodily Seismic Waves of a Focal Depth, Kementerian Perhubungen, Lembaga Meteorologi Ian Geofisik, Djakarta, Republik Indonesia, Verhandelingen No. 54, 10 pp, 1958.

Savage, J. C., and L. M. Hastie, Surface Deformation Associated with Dip-Slip faulting, J. Geophys. Res., 71, 4897-4904, 1966.

Slichter, L. B., and Michele Caputo, Deformation of an Earth Model by Surface Pressure, J. Geophys. Res., 65, 4151-4156, 1960.

Smith, Stewart W., and Max Wyss, Displacement on the San Andreas Fault Initiated by the 1966 Parkfield Earthquake, manuscript submitted to the Bull. Seismol. Soc. Am., 1968.

Smith, Stewart W., Free Oscillations Excited by the Alaskan Earthquake, J. Geophys. Res., 71, 1183-1193, 1966.

Starr, A. T., Slip in a Crystal and Rupture in a Solid due to Shear, Proc. Camb. Phil. Soc., 24, 489-500, 1928.

Steketee, J. A., Some Geophysical Aplications of the Elasticity Theory of Dislocations, Canadian J. of Physics, 36, 1168-1198, 1958.

Swanson, Jack G., Magnitude Studies Conducted Under Projects VT/5054 and VT/5055, Technical Report No. 66-73, sponsored by

ARPA, Nuclear Test Detection Office, ARPA Order No. 624, Prepared by Teledyne Industries, Geotech Division, 34 pp, 1966.

Sykes, Lynn R., Mechanism of Earthquakes and Nature of Faulting on the Mid-Ocean Ridges, J. Geophys. Res., 72, 2131-2153, 1967.

Takeuchi, Hitoshi, On the Earth Tide, J. of the Faculty of Sci., Univ. of Tokyo, Sec. II, vol. 7, Part II, 7-153, 1951.

Teledyne Industries, Geotech Division, The Registration of Earthquakes, prepared for the Air Force Technical Application Center, Washington, D. C., under ARPA Project Vela-Uniform, May through August, vol. 5, Nos. 5, 6, 7, 8, 1966a.

Teledyne Industries, Geotech Division, Seismological Bulletin Long-Range Seismic Measurements Program, May through August, Nos. 53, 54, 55, 56, 1966b.

Toksoz, M. N., and D. L. Anderson, Phase Velocities of Long-Period Surface Waves and Structure of the Upper Mantle, J. Geophys. Res., 71, 1649-1658, 1966.

Tomaschek, Rudolf, Tides of the Solid Earth, Section G., 839-842, in Encylcopedia of Physics, edited by S. Flugge, vol. XLVIII, 1957.

Walsh, J. B., Mechanics of Strike-Slip Faulting with Friction, J. Geophys. Res., 73, 761-776, 1968.

Wideman, C. J., and M. W. Major, Strain Steps Associated with Earthquakes, Bull. Seism. Soc. Am., 57, 1429-1448, 1967.

Appendix 1

A PILOT INVESTIGATION OF UPPER MANTLE ABSORPTION OF SEISMIC ENERGY USING DATA FROM THE ARPA PROJECT VELA-UNIFORM

Summary

The unified magnitude, the ratio of the amplitudes of S to P waves, and travel time residuals were compiled from published data for five seismological stations. Using one of the stations as a reference, a relative measure of the above quantities was calculated for each of the other stations for each of a number of earthquakes. The results can be interpreted as consistent with regions of upper mantle with a low Q and possibly a high Poisson's ratio; however, a considerably more detailed study is indicated before the interpretation and reliability of the results can be considered as established.

Introduction

Tiltmeter and strainmeter offsets associated with earthquakes led to the hypothesis of a regional "soft" or "weak" layer in the crust or upper mantle. A "weak" layer can reasonably be expected to be characterized by relatively high absorption of seismic energy, particularly high absorption of shear energy compared to dilatational energy, and by relatively large delay times for seismic phases. Professor D. L. Anderson suggested the use of published amplitude data available in the "Registration of Earthquakes", Teledyne Industries (1966), and the "Seismological Bulletin of the Long-Range Seismic Measurements Program," Teledyne Industries (1966), to calculate a measure of energy absorption. The results reported

here, which were intended as a feasibility study, were developed by Professor Anderson and the author.

Data

The principal source for the data used was "The Registration of Earthquakes at Blue Mountains Seismological Observatory (BMO), Cumberland Plateau Seismological Observatory (CPO), Tonto Forest Seismological Observatory (TFO), Uinta Basin Seismological Observatory (UBO), and Wichita Mountain Seismological Observatory (WMO)", Teledyne Industries (1966a). The location of the observatories is given in Figure A1-1. The data used here are from either the short period instruments which are peaked at about .35 seconds or from the long period instruments which are peaked at about 30 seconds. Some data were taken from the "Seismological Bulletin Long-Range Measurements Program," Teledyne Industries (1966b), for stations at Kanab, Utah (KU); Mina, Nevada (MN); Jasper, Alberta (JP); and Prince George, British Columbia (PG). The location of the stations is shown in Figure A1-2. The instruments are essentially the same as for the observatories. Details can be found in the bulletins.

Three quantities were calculated:

a) the ratio of S-amplitude to P-amplitude at each station relative to the same ratio at UBO;

b) the ratio of the P-amplitude at each station relative to the P-amplitude at UBO;

c) the travel time residual at each station relative to the travel time residual at UBO.

S/P Ratio for TFO, WMO, CPO, BMO

Calculation of the S/P ratio was restricted to earthquakes for which the station to epicenter azimuth differed by less than 11° from the UBO to epicenter azimuth and neither the station nor UBO was greater than 96° from the epicenter. Data were taken from the Registration of Earthquakes, Teledyne Industries (1966a), for May through August. The amplitudes given in the bulletins are corrected for instrument response. The amplitudes of the P and S arrivals were normalized (i.e. divided) by the dominant period of the pulse. The P-amplitude was always taken from a short period instrument and the S-amplitude from a long period instrument. The P pulses used generally report a period near 1 sec (about .5 to 2 sec) while the S pulses used generally show a period near 20 sec (about 15 to 30 sec). No correction was made for the distance of the station to the epicenter. The largest possible difference in distance (using UBO as a reference) is about 20° for CPO. The restriction on azimuth difference and the restriction that the data at the station and at UBO come from the same earthquake should tend to remove radiation pattern and source region effects. The ratio of normalized S to normalized P for the station was divided by the ratio of normalized S to normalized P for UBO. These twice normalized

amplitude ratios will be called the "S/P ratio" for the station. Data were not available or did not meet the restrictions for all stations from every earthquake, so the results for each station are based on a somewhat different sample of earthquakes.

S/P Ratio for KN, MN, JP, PG

Calculation of the S/P ratio for these stations was as above except the azimuth and distance restrictions were not applied. Data were taken from the Seismological Bulletin Long-Range Measurements Program, Teledyne Industries (1966b), for May through August.

P-ratio for TFO, WMO, CPO, BMO

In the Registration of Earthquakes, Teledyne Industries (1966a), the unified magnitude is given for all suitable P arrivals. Corrections for hypocentral depth and distance to the earthquake are applied. No station correction is made. For each earthquake the magnitude at UBO was differenced from the magnitude at each station giving the magnitude difference relative to UBO. The $\log_{10}$ of the relative magnitude gives the ratio of the P-amplitude at the station to the P-amplitude at UBO (the amplitude ratio being implicitly corrected for the same effects as the magnitude) and will be called the "P-ratio" for the station. No correction was made for radiation pattern. Data were taken from about the first half of August, 1966.

P-residual for TFO, WMO, CPO, BMO

The travel time residual with reference to the 1958 Jeffreys-Bullen Travel Time Tables is also given in The Registration of Earthquakes. This travel time residual for P arrivals was corrected according to the "Average Surface Focus Travel Time Curve" given by Carder *et al*. (1966) For each earthquake the corrected P travel time residual at UBO was subtracted from the corrected P travel time residual at the station to give the "P-residual" for the station. The data used were from the same time period as for the P-ratio.

Results and Discussion

The results and some statistical measures are given in Table A1-1. A summary of the results used in the discussion of Q is given in Table A1-2. The P-residuals were assumed normally distributed. For the observations which are ratios a logarithmic normal distribution was assumed (*i.e.* the logarithms of the measurements are assumed noramlly distributed). The statistical measures identified as "standard deviation factor" and "standard error factor" are the antilogs of the standard deviation of the logarithms and the standard error of the mean of the logarithms. They are intended to be used as multiplicative factors with an intuitive interpretation

analogous to the standard deviation and standard error.[1]

Figures A1-3 through A1-6 show all of the data for some of the stations. The indicated quantity is plotted versus epicentral distance from UBO and histograms are constructed for the same data. Qualitatively the histograms leave some doubt about the assumption of a normal distribution. Observations indicated by an arrow were excluded in calculating the results given in Table A1-1.

A simple interpretation of the results is that the S/P-ratio and P-ratio are very rough measures of upper mantle absorption at each station relative to upper mantle absorption at UBO - higher ratios corresponding to lower absorption. The P-residuals are independent, but it is reasonable to expect more positive P-residuals to correlate with high absorption. On this basis TFO is clearly distinguished as the most absorptive station, but other stations, for example BMO, show a low P-ratio but a high S/P-ratio. Complications in this obviously oversimplified interpretation are discussed later, but for now a calculation is attempted neglecting the complications and the inconsistency between P-ratios and S/P-ratios.

Under many assumptions a quantitative estimate of the relative absorption at the different stations can be made. Let all the

---

[1]For example the P-ratio for TFO is .6 with a "standard deviation factor" of 2.6, and this is taken to imply that about 67% of the measurements lie between .6 x 2.6 = 1.6 and .6 ÷ 2.6 = .2. The "standard error factor" of 1.1 for this measurement implies that the true P-ratio is more likely to lie between .6 x 1.1 = .7 and .6 ÷ 1.1 = .5 than not.

absorption for a given station occur in a single layer with quality factor Q^i, thickness X, and velocity v^i for waves of period T^i, and let crustal structure and site effects be included in a "crustal factor" A_c^i - where i = p for compressional waves, s for shear waves. Then the amplitude observed at station 1 is

$$A_1^i = A_{1o}^i A_{1c}^i \quad \exp(-k_1^i X)$$

where A_o^i is the amplitude at the source and

$$k_1^i = \frac{\pi}{Q_1^i v_1^i T_1^i} \quad .$$

Straightforward algebra gives

$$R_1 \equiv \frac{A_1^p}{A_2^p} \frac{A_{1c}^p}{A_{2c}^p} \exp\left[-(k_1^p - k_2^p) X_1\right]$$

for the amplitude of P waves at station 1 relative to station 2, and

$$R_2 \equiv \frac{A_1^p / A_1^s}{A_2^p / A_2^s} = \frac{A_{1c}^p A_{2c}^s}{A_{2c}^p A_{1c}^s} \exp\left\{-\left[(k_1^p - k_2^p) - (k_1^s - k_2^s)\right] X_1\right\}$$

for the P/S ratio at station 1 relative to station 2. Assuming that the crustal factors are the same for all stations

$$Q_1^p = \frac{\pi}{v^p T^p} \frac{1}{\left(k_2^p - \frac{\ln R_1}{X_1}\right)}$$

and

$$Q_1^s = \frac{\pi}{v^s T^s} \frac{}{\left(k_1^p - k_2^p + k_2^s + \frac{\ln R_2}{X_1}\right)}$$

If the Q_2^i are known or assumed the Q_1^i can be calculated. The results of such calculations are given in Table A1-3. Q^i values were assumed for WMO. The results for $Q_2^i = \infty$ at WMO would be upper bounds on Q at TFO if the assumptions were correct. Locations in Table A1-3 which are filled with a dash gave negative Q values which shows that the assumed conditions are incompatible with the data for these cases.

The ratio Q^p/Q^s can be written

$$Q^p/Q^s = \left(\frac{\alpha}{\beta}\right)^2 \left[\frac{\mu^*}{k^* + 4\mu^*/3}\right]$$

$$= \frac{2(1-\sigma)}{1-2\sigma} \left[\frac{\mu^*}{k^* + 4\mu^*/3}\right]$$

where k^* and μ^* are the imaginary parts of the bulk and shear moduli, σ is Poisson's ratio, and α and β are the compressional and shear velocities. Clearly $Q^P/Q^S \to \infty$ as $\sigma \to 1/2$. If all losses are in shear $k^* = 0$ and $Q^P/Q^S = \frac{3(1-\sigma)}{2(1-2\sigma)}$. For $\sigma = 1/4$, $Q^P/Q^S = 2.25$ and for $\sigma = 0.4$, $Q^P/Q^S = 6$. A high ratio of Q^P to Q^S indicates a high value of Poisson's ratio. The derived values of Q^P, Q^S, and Q^P/Q^S in Table A1-3 show either very low Q, very high Q^P/Q^S, or both. Increasing X_1 tends to increase the Q estimates and decrease Q^P/Q^S, but the derived values in Table A1-3 are dominated by the P-ratio. Comparing any two stations with P amplitude differences as large as the difference between TFO and WMO gives similar results. Jordan et al (1965) have contoured amplitude patterns for P waves of about 1 second period and have shown that P amplitudes can vary within the limits in Table A1-2 due to local effects at the receiver and the source. Therefore the individual entries for relative P amplitudes are liable to be controlled by the structure at the recording site. However, Jordan et al (1965) point out that there are indications of regional systematics with amplitudes lower in the western part of the United States than in the eastern part. It is difficult to associate a quantitative value with the difference, but a 3 to 2 ratio as shown for WMO and TFO in Table A1-2 appears reasonable. The results in Table A1-3 show that such an amplitude difference requires a very low Q or high Poisson's ratio under the assumed conditions. Either result indicates

an approach to fluid-like behavior. It should be noted that the lowest Q values in a given column in Table A1-3 are determined essentially by the assumed values at WMO rather than by the station observations. There is also the possibility that regional structural differences determine regional P amplitude differences so that the inference of low Q or high Poisson's ratio is only suggestive.

An estimate of the S-ratio, defined in a manner analogous to the P-ratio, can be derived by multiplying the P-ratio times the S/P-ratio. This has been done to give the S-ratio in the third column of Table A1-2. It should be noted that the S/P-ratio and P-ratio were determined from different sets of data. Since the S-waves typically have about a 20 second period, the S-ratio should be much less sensitive to local structural variations than the P-ratio. On the basis of S-ratio relative to UBO the stations can be separated into two groups - UBO and TFO with an S-ratio of 1 or less, and WMO, CPO, and BMO with an S-ratio of 2 or greater. Using the same derivation as given for Q_1^p previously, but with s substituted for p, the Q^s at one station can be assumed and the Q^s at other stations calculated. the results of such a calculation when Q^s values were assumed at BMO are given in Table A1-5. For X_1 = 100 km. the upper bounds on Q^s at UBO and TFO are less than 50. Similar bounds result if WMO or CPO are used as a reference station. The thickness of the layer in which Q differences are allowed is important in determining the

bound as is shown by the increase in the upper bound at UBO and TFO when X_1 = 400 km. As in Table A1-3 the lowest Q^S values in each column are determined essentially by the assumed values at BMO. If the assumptions in the calculations were correct, the inference is a fairly low Q^S under TFO and UBO or substantial Q^S differences through regions of at least several hundred kilometers extent.

An absolute P-residual was determined from the relative P-residuals in Table A1-1 by assuming Carder et al's (1966) correction curve to the Jeffreys-Bullen travel times has an average of -2.0 seconds. The resulting P-residuals, Table A1-4, correlate with the S-ratios as expected if the S-ratios are due to regional differences in Q^S. UBO and TFO show a positive residual and WMO, CPO, and BMO show negative residuals. P-residuals given by Carder et al (1966), Cleary and Hales (1966), and Herrin et al (1968) are also listed in Table A1-4. The correlation of the S-ratios with the other determinations of station residuals given in Table A1-4 is not perfect, but only the determination of Carder et al (1966) for UBO is in substantial disagreement.

Introducing an S-delay, as would be implied by relatively long transit times for S waves in an absorbing layer, tends to reduce the high Q^P/Q^S ratios in Table A1-3. However, this is equivalent to assuming a high Poisson's ratio. A cursory examination of S arrival times reported in the Registration of Earthquakes does not exclude the possibility of large

relative S-delay. The study of Doyle and Hales (1967) implies relative S-delays of 3 - 4 sec for TFO and UBO relative to BMO. Their results can be interpreted, Hales and Doyle (1967), to give a Poisson's ratio of about .325 for X = 100 km or .275 for X = 400 km in the region of UBO and TFO. Such changes in S-delay or Poisson's ratio do not change the basic pattern of low Q and high Q^P/Q^S in Table A1-3.

No attempt is made at a complete listing of factors which may influence the data, but the following illustrate the important difficulties. Since the S/P-ratios are not corrected for distance there could be an important distance effect. Figure A1-4 supports the idea that the ratios for WMO and CPO decrease with average distance from the epicenter. Bolt and Nuttli's (1966) study indicates some large azimuthal effects. Misidentification of phases and source radiation patterns could bias the data. Although the statistical measures indicate an adequate sample size for the stations represented in Table A1-2, the assumptions underlying these estimates may not be satisfied. A statistical study of magnitudes by Swanson (1966) based on a much larger sample size leads to P-ratios within .1 of those in Table A1-2 except for BMO. Swanson's results give $P_{BMO}/P_{UBO} \approx 1.1$.

Conclusions and Recommendations

The results of this study are consistent with a very low Q upper mantle and possibly a very high Poisson's ratio in the Basin and Range Province. The analysis used is by no means conclusive. The data in The Registration of Earthquakes and the Seismological Bulletin of the Long-Range Seismic Measurement Program are available in a computer compatible form. Computer processing would allow easy use of all the data and relative ease of application of corrections, for example, a distance correction for S-amplitude. Statistical checks on the reliability of the data could be easily made. This should certainly be an improvement over this pilot study, but some effects require a separate, rather detailed investigation. In particular, the effect of local crustal structure and possibly the recording site should be investigated as well as the reliability of the identification of phases. Even without this more detailed work, the results of this pilot project indicate that a similar study based on all the data should be useful. Such a study should be capable of singling out areas where possible Q anomalies in the upper mantle could be investigated by other methods.

Appendix 2

ENERGY CONSIDERATIONS UPON INTRODUCING A DISLOCATION INTO A PRESTRESSED MEDIUM

In Chapters 2 and 5 the change in the strain field due to faulting in the earth has been related to the change in strain field caused by the introduction of a dislocation surface into a prestressed medium. When an earthquake occurs, it is supposed that the strain energy in the medium is reduced - the change in strain energy going into inelastic processes and seismic radiation. An acceptable mathematical model of a seismic source should allow a reduction in the stored strain energy. Steketee (1958) concluded that, for boundary conditions which are appropriate to the earth, a dislocation model results in a strain energy increase. He states, "... we have to recognize that the surface of the earth is essentially free and if a dislocation is made under these circumstances, Colonnetti's Theorem shows that the strain energy can only increase." It should be noted that Steketee pointed out the possibility of strain energy reduction with certain boundary conditions. However, he rejected the particular cases he considered as unrealistic. As shown below the inclusion of more general conditions, in particular, the possibility of prestressing by body forces, allows the possibility of strain energy reduction.

Tensor notation is used in this appendix with the symbol

definition patterned after Steketee (1958, Section 6. The Strain Energy of the Dislocation). The symbols are

τ_{ij} stress tensor ;

e_{ij} strain tensor ;

ω_{ij} rotation tensor ;

u_i displacement field;

T_i^{ν} traction across a surface element with normal ν_i ;

f_i body forces ;

S exterior surface of the body ;

Σ any interior surface across which a dislocation exists ;

W^* the total stored strain energy due to prestressing alone, that is the total stored strain energy before introduction of the dislocation surface modeling the fault ; and

W' the total stored strain energy after introduction of the dislocation surface modeling the fault.

The development here closely follows that in Steketee with the important differences being pointed out.

The total strain energy in a body with volume V is

$$W = \int_V \tau_{ij}\, e_{ij}\, dV \qquad \text{(A2-1)}.$$

The equilibrium equation is

$$\tau_{ij,j} + f_i = 0$$

Using $\tau_{ij}\, \omega_{ij} = 0$ and the identity

$$(\tau_{ij}\, u_i)_{,j} = \tau_{ij,j}\, u_i + \tau_{ij}\, u_{i,j}$$

equation (A2-1) can be written

$$W = \frac{1}{2} \int_V (\tau_{ij}\, u_i)_{,j}\, dV + \frac{1}{2} \int_V f_i\, u_i\, dV \qquad \text{(A2-2)}$$

It is assumed that the body is bounded by an external surface, S, with tractions $\overset{\nu}{T}_i$ and may have internal surfaces, Σ, with displacement dislocations Δu_i. Using the divergence theorem equation (A2-2) can be written

$$W = \frac{1}{2} \int_S u_i\, \overset{\nu}{T}_i\, dS + \frac{1}{2} \int_\Sigma \Delta u_i\, \overset{\nu}{T}_i\, d\Sigma + \frac{1}{2} \int_V f_i\, u_i\, dV \qquad \text{(A2-3).}$$

Equation (A2-3) is the same as Steketee's equation (6.4) except that the inclusion of body forces adds the last term.

If the body is prestressed by body forces, internal dislocations, and tractions on S,

$$W^* = \frac{1}{2}\int_S u_i^* \overset{\nu}{T}{}_i^* \, dS + \frac{1}{2}\int_{\Sigma^*} \Delta u_i^* \overset{\nu}{T}{}_i^* \, d\Sigma^* + \frac{1}{2}\int_V f_i^* u_i^* \, dV \qquad \text{(A2-4)}.$$

If a new dislocation surface is introduced, then

$$W' = \frac{1}{2}\int_S \left(u_i^* + u_i\right)\left(\overset{\nu}{T}{}_i^* + T_i\right) dS + \frac{1}{2}\int_V f_i^* \left(u_i^* + u_i\right) dV$$

$$+ \frac{1}{2}\int_{\Sigma^*} \Delta u_i^* \left(\overset{\nu}{T}{}_i^* + \overset{\nu}{T}{}_i\right) d\Sigma^* + \frac{1}{2}\int_{\Sigma} \Delta u_i \left(\overset{\nu}{T}{}_i^* + \overset{\nu}{T}{}_i\right) d\Sigma \qquad \text{(A2-5)}$$

where Σ is the new dislocation surface and

a) the boundary condition on S changes from $\overset{\nu}{T}{}_i^*$ to $\overset{\nu}{T}{}_i^* + \overset{\nu}{T}{}_i$;

b) Δu_i^* is assumed fixed on Σ^* ; and

c) the f_i^* are assumed constant.

Subtracting equation (A2-4) from (A2-5) yields

$$W' - W^* = \frac{1}{2}\int_{\Sigma} \Delta u_i \left(\overset{\nu}{T}{}_i + \overset{\nu*}{T}{}_i\right) d\Sigma$$

$$+ \frac{1}{2}\int_{\Sigma^*} \Delta u_i^* \overset{\nu}{T}{}_i \, d\Sigma^* + \frac{1}{2}\int_S u_i \left(\overset{\nu}{T}{}_i + \overset{\nu*}{T}{}_i\right) dS$$

$$+ \frac{1}{2}\int_S u_i^* \overset{\nu}{T}{}_i \, dS + \frac{1}{2}\int_V f_i^* u_i \, dV \qquad \text{(A2-6)} \; .$$

$W' - W^*$ is the change in stored strain energy caused by introduction of the dislocation surface Σ. If $f_i^* = 0$ and $\Sigma \equiv \Sigma^*$, equation (A2-6) is equivalent to either of Steketee's equations (6.10). If it is further assumed that $\Delta u_i^* = 0$ and $\overset{\nu}{T}{}_i^* = 0$ on S, then the theorem of Colonnetti follows as Steketee shows. Steketee states the result as follows: "... the work performed by the initial forces over Σ while making the dislocation is equal and opposite to the work performed by the initial forces on S when the dislocation is made." Under these circumstances the total strain energy in the body must increase when the dislocation is made. It should be noted that with $f_i^* = 0$, $\Sigma \equiv \Sigma^*$, $\Delta u_i^* = 0$ and $\overset{\nu}{T}{}_i = 0$ on S the only prestressing mechanisms possible are the tractions $\overset{\nu}{T}{}_i^*$ on S. If S is the surface of the earth and $\overset{\nu}{T}{}_i^* = 0$, there is no prestress.

A sufficiently general case to demonstrate the possibility of energy decrease with geophysically relevant boundary conditions follows if

a) the boundary conditions on S are

$$\overset{\nu}{T}{}_i = \overset{\nu}{T}{}_i^* = 0 \quad ;$$

b) Δu_i^* is assumed non-zero on Σ^* and does not change; and

c) the f_i^* are assumed non-zero and constant.

$$W' - W^* = \frac{1}{2}\int_{\Sigma} \Delta u_i \left(\overset{\nu}{T}_i + \overset{\nu}{T}{}^*_i\right) d\Sigma + \frac{1}{2}\int_{\Sigma^*} \Delta u_i^* \overset{\nu}{T}_i \, d\Sigma^*$$

$$+ \frac{1}{2}\int_{V} f_i^* u_i \, dV \qquad \text{(A2-7)} \quad .$$

Although equation (A2-7) can allow either an increase or a decrease in strain energy, the result that the stored strain energy must increase no longer follows. Even if the Δu_i^* are zero the last integral in equation (A2-7) may be either positive or negative, so, if the prestress is due to body forces, there may be a decrease in energy without the necessity for $\overset{\nu}{T}_i$ to be non-zero on S.

As a rather trivial example to demonstrate explicitly the possibility of energy decrease, let $f_i^* = 0$, $\Sigma^* \equiv \Sigma$ and $\Delta u_i = - \Delta u_i^*$. Equation (A2-7) is then

$$W' - W^* = \frac{1}{2}\int_{\Sigma} \Delta u_i \overset{\nu}{T}{}^*_i \, d\Sigma = - \frac{1}{2}\int_{\Sigma} \Delta u_i^* \overset{\nu}{T}{}^*_i \, d\Sigma \quad .$$

The stored strain energy is decreased by just the amount of energy it took to form Δu_i^* initially as it must be since the prestressing dislocation was just reduced to zero.

Appendix 3

IDENTITIES FOR STATIC ELASTIC SOLUTIONS IN SPHERICAL AND CIRCULAR CYLINDRICAL COORDINATES

The identities given here can be derived simply by executing the indicated operations. Many of these results are given in Morse and Feshbach (1953, Chapter 13).

Spherical Coordinates

The notation, $\vec{M}$, refers to either the vector $\vec{M}^1_{m,\ell}$ or the vector $\vec{M}^2_{m,\ell}$; and similarly for the notations $\vec{N}$, $\vec{G}$, and $\vec{E}$.

$$\nabla\cdot\vec{P}_{m\ell} = \frac{2}{r}\, S^m_\ell$$

$$\nabla\cdot\vec{B}_{m\ell} = \frac{L}{r}\, S^m_\ell$$

$$\nabla\cdot\vec{C}_{m\ell} = 0$$

$$\nabla \times \vec{P}_{m\ell} = \frac{L}{r}\, \vec{C}_{m\ell}$$

$$\nabla \times \vec{B}_{m\ell} = -\frac{1}{r}\, \vec{C}_{m\ell}$$

$$\nabla \times \vec{C}_{m\ell} = \frac{1}{r}\left(L\, \vec{P}_{m\ell} + \vec{B}_{m\ell}\right)$$

$$\nabla\left(\nabla\cdot\vec{P}_{m\ell}\right) = \frac{2}{r^2}\left(-\vec{P}_{m\ell} + L\, \vec{B}_{m\ell}\right)$$

$$\nabla\left(\nabla\cdot\vec{B}_{m\ell}\right) = \frac{L}{r^2}\left(\vec{P}_{m\ell} - L\, \vec{B}_{m\ell}\right)$$

$$\nabla\left(e^{im\phi}\ P_\ell^m\right) = \frac{L}{r}\ \vec{B}_{m\ell}$$

$$\nabla \times \left(\hat{r}\ e^{im\phi}\ P_\ell^m\right) = \frac{L}{r}\ \vec{C}_{m\ell}$$

$$\nabla\cdot\vec{M} = \nabla\cdot\vec{N} = 0$$

$$\nabla\cdot\vec{G}^1_{m,\ell+1} = -\ (2\ell+3)(\ell+1)\ r^\ell\ S_\ell^m$$

$$\nabla\cdot\vec{G}^2_{m,\ell-1} = -\ (2\ell-1)\ \ell\ r^{-\ell-1}\ S_\ell^m$$

$$\nabla\cdot\vec{E}^1_{m,\ell+1} = 2(2\ell+3)(\ell+1)(1-K)\ r^\ell\ S_\ell^m$$

$$\nabla\cdot\vec{E}_{m,\ell-1} = 2(2\ell-1)\ell(1-K)\ r^{-\ell-1}\ S_\ell^m$$

$$\nabla \times \vec{M}^1_{m,\ell} = (\ell+1)\ \vec{N}^1_{m,\ell-1}$$

$$\nabla \times \vec{M}^2_{m,\ell} = -\ \ell\ \vec{N}^2_{m,\ell+1}$$

$$\nabla \times \vec{N} = 0$$

$$\nabla \times \vec{G}^1_{m,\ell+1} = -\ (2\ell+3)\ \vec{M}^1_{m,\ell}$$

$$\nabla \times \vec{G}^2_{m,\ell-1} = (2\ell-1)\ \vec{M}^2_{m,\ell}$$

$$\nabla \times \vec{E}^1_{m,\ell+1} = -\ 2(2\ell+3)\ K\ \vec{M}^1_{m,\ell}$$

$$\nabla \times \vec{E}^2_{m,\ell-1} = 2(2\ell-1)\ K\ \vec{M}^2_{m,\ell}$$

$$\frac{\partial \vec{E}^1_{m,\ell+1}}{\partial r} = (\ell+1)\, r^{-1}\, \vec{E}^1_{m,\ell+1}$$

$$\frac{\partial E_{m,\ell-1}}{\partial r} = -\,\ell\, r^{-1}\, \vec{E}^2_{m,\ell-1}$$

$$L = \sqrt{\ell(\ell+1)}$$

$$S^m_\ell = e^{im\phi}\, P^m_\ell\, (\cos\,\theta)$$

$$K = 2(1-\sigma)$$

.

Circular Cylindrical Coordinates

The notation, $\vec{M}$, refers to either the vector $\vec{M}^1_{km}$ or the vector $\vec{M}^2_{km}$; and similarly for $\vec{N}$, $\vec{G}$, and $\vec{E}$.

$$\nabla\, T^m_k = k\, \vec{B}_{mk}$$

$$\nabla \times (\hat{z}\, T^m_k) = k\, \vec{C}_{mk}$$

$$\nabla\cdot\vec{M} = \nabla\cdot\vec{N} = 0$$

$$\nabla\cdot\vec{G}^1_{km} = k\, e^{kz}\, T^m_k$$

$$\nabla\cdot\vec{G}^2_{km} = -\,k\, e^{-kz}\, T^m_k$$

$$\nabla \cdot \vec{E}^1_{km} = (c-1)\, k\, e^{kz}\, T^m_k$$

$$\nabla \cdot \vec{E}^2_{km} = -\,(c-1)\, k\, e^{-kz}\, T^m_k$$

$$\nabla \times \vec{M} = k\, \vec{N}$$

$$\nabla \times \vec{N} = 0$$

$$\nabla \times \vec{G} = k\, \vec{M}$$

$$\nabla \times \vec{E} = (c+1)\, k\, \vec{M}$$

$$\nabla \times (\nabla \times \vec{G}) = k^2 \vec{N} = \nabla(\nabla \cdot \vec{G})$$

$$\frac{\partial \vec{E}^1_{km}}{\partial z} = k\left(\vec{E}^1_{km} - \vec{N}^1_{km}\right)$$

$$\frac{\partial \vec{E}^2_{km}}{\partial r} = -\,k\left(\vec{E}^2_{km} - \vec{N}^2_{km}\right)$$

$$T^m_k = e^{im\theta}\, J_m\,(kr)$$

$$c = 3-4\sigma$$

Appendix 4

EXPANSIONS OF THE DELTA FUNCTION IN VECTOR SPHERICAL AND CYLINDRICAL HARMONICS

Spherical Coordinates

Let

$$\underline{I}_{m\ell} = \vec{P}^*_{m\ell}(\theta_o,\phi_o)\ \vec{P}_{m\ell}(\theta,\phi) + \vec{B}^*_{m\ell}(\theta_o,\phi_o)\ \vec{B}_{m\ell}(\theta,\phi) + \vec{C}^*_{m\ell}(\theta_o,\phi_o)\ \vec{C}_{m\ell}(\theta,\phi)$$

and $\hat{n}$ be a unit vector, then

$$\frac{\delta(\theta-\theta_o)\delta(\phi-\phi_o)}{\sin\theta}\ \hat{n} = \sum_{\ell=0}^{\infty}\ \sum_{m=-\ell}^{\ell} N_{m\ell}\ \hat{n}\cdot\underline{I}_{m\ell}$$

where

$$N_{m\ell} = \frac{(2\ell+1)}{4\pi}\ \frac{(\ell-m)!}{(\ell+m)!}$$

Circular Cylindrical Coordinates

Let

$$\underline{I}_{mk} = \vec{P}^*_{mk}(r_o,\theta_o)\ \vec{P}_{mk}(r,\theta) + \vec{B}^*_{mk}(r_o,\theta_o)\ \vec{B}_{mk}(r,\theta) + \vec{C}^*_{mk}(\theta_o,\phi_o)\ \vec{C}_{mk}(\theta,\phi)$$

and $\hat{n}$ be a unit vector, then

$$\frac{\delta(r-r_o)\delta(\theta-\theta_o)}{r}\,\hat{n} = \frac{1}{2\pi}\sum_{m=-\infty}^{\infty}\int_o^{\infty}\hat{n}\cdot\underline{I}_{mk}\;\; k\;\; dk \quad .$$

For $r_o = 0$ and $\theta_o = 0$

$$\frac{\delta(r)\;\delta(\theta)}{r}\;\hat{z} = \int_o^{\infty}\vec{P}^x\,dk \quad ,$$

$$\frac{\delta(r)\;\delta(\theta)}{r}\;\hat{x} = \int_o^{\infty}\left[\vec{B}^x + \vec{C}^x\right]dk \quad ,$$

$$\frac{\delta(r)\;\delta(\theta)}{r}\;\hat{y} = \int_o^{\infty}\left[\vec{B}^y + \vec{C}^y\right]dk \quad ,$$

where

$$\vec{P}^x = p^z_{ok}\,\vec{P}_{ok} \quad ,$$

$$\vec{B}^x = b^x_{1k}\,\vec{B}_{1k} + b_{-1k}\,\vec{B}_{-1k} \quad ,$$

$$\vec{C}^x = c^x_{1k}\,\vec{C}_{1k} + c^x_{-1k}\,\vec{C}_{-1k} \quad ,$$

$$\vec{B}^y = b^y_{1k}\,\vec{B}_{1k} + b^y_{-1k}\,\vec{B}_{-1k} \quad ,$$

$$\vec{C}^y = c^y_{1k}\,\vec{C}_{1k} + c^y_{-1k}\,\vec{C}_{-1k} \quad ,$$

or

$$\vec{P}^x = \frac{k}{2\pi}\,\hat{z}\,J_0 \quad ,$$

$$\vec{B}^x = \frac{k}{4\pi}\left\{\hat{r}\cos\theta\left[J_0 - J_2\right] - \hat{\theta}\sin\theta\left[J_0 + J_2\right]\right\} \quad ,$$

$$\vec{C}^x = \frac{k}{4\pi}\left\{\hat{r}\cos\theta\left[J_0 + J_2\right] - \hat{\theta}\sin\theta\left[J_0 - J_2\right]\right\} \quad ,$$

$$\vec{B}^y = \frac{k}{4\pi}\left\{\hat{r}\sin\theta\left[J_0 - J_2\right] + \hat{\theta}\cos\theta\left[J_0 + J_2\right]\right\} \quad ,$$

$$\vec{C}^y = \frac{k}{4\pi}\left\{\hat{r}\sin\theta\left[J_0 + J_2\right] + \hat{\theta}\cos\theta\left[J_0 - J_2\right]\right\} \quad .$$

The argument of J_0 and J_2 is kr .

Appendix 5

ELEMENTS OF PROPAGATOR MATRICES

SPHERICAL COORDINATES

For a layer (or spherical shell) whose elastic properties are $K = 2(1-\sigma)$ and μ and which is bounded below by r_q and above by r_{q-1}, the elements of the propagator matrix are denoted A_{ij}. The A_{ij} propagate the solution from $r = r_{q-1}$ to $r = r_q$. For the motion expressible with the $\vec{P}_{m,\ell}$ and $\vec{B}_{m,\ell}$, let

$$D_{ij} = R^{-\ell} A_{ij} \quad ,$$

$$R = \frac{r_q}{r_{q-1}} \quad ,$$

$$M = \frac{\mu}{r_{q-1}}$$

$\mathcal{B}$, $\mathcal{C}$, and L_1 through L_8 are defined in Chapter 3.

$$D_{11} = R \left[- (\ell+1)\, b_{11} + \ell\, c_{11} \right]$$

$$D_{12} = \ell(\ell+1)\, R \left[b_{12} + c_{12} \right]$$

$$D_{13} = R\, m^{-1} \left[- (\ell+1)\, b_{13} - \ell\, c_{13} \right]$$

$$D_{14} = \ell(\ell+1)\, R\, m^{-1} \left[b_{14} - c_{14} \right]$$

$$D_{21} = R \left[- b_{21} - c_{21} \right]$$

$$D_{22} = R \left[\ell\, b_{22} - (\ell+1)\, c_{22} \right]$$

$$D_{23} = R\, m^{-1} \left[- b_{23} + c_{23} \right]$$

$$D_{24} = R\, m^{-1} \left[\ell\, b_{24} + (\ell+1)\, c_{24} \right]$$

$$D_{31} = m \left[- (\ell+1)(\ell+2)\, b_{31} - \ell(\ell-1)\, c_{31} \right]$$

$$D_{32} = m \left[\ell(\ell+1)(\ell+2)\, b_{32} - (\ell-1)(\ell)(\ell+1)\, c_{32} \right]$$

$$D_{33} = - (\ell+1)\, b_{33} + \ell\, c_{33}$$

$$D_{34} = \ell(\ell+1) \left[b_{34} + c_{34} \right]$$

$$D_{41} = m \left[- (\ell+2)\, b_{41} + (\ell-1)\, c_{41} \right]$$

$$D_{42} = m \left[\ell(\ell+2)\, b_{42} + (\ell-1)(\ell+1)\, c_{42} \right]$$

$$D_{43} = - b_{43} - c_{43}$$

$$D_{44} = b_{44} - c_{44} \quad .$$

Let

$$B_{ij} = \mathcal{B}^{-1}\, b_{ij} \quad ,$$

$$C_{ij} = \mathcal{C}^{-1}\, R^{2\ell+3}\, c_{ij} \quad ,$$

$$\rho_1 = R^{-(2\ell+3)} \quad ,$$

$$\rho_2 = R^{2\ell+1} \quad .$$

$$B_{11} = (\ell+2)\ L_1 + L_5\ \rho_1$$

$$B_{12} = (\ell+2)\ L_1 - L_7\ \rho_1$$

$$B_{13} = L_1 - L_1\ \rho_1$$

$$B_{14} = L_1 + L_3\ \rho_1$$

$$B_{21} = (\ell+2)\ L_3 - L_5\ \rho_1$$

$$B_{22} = (\ell+2)\ L_3 + L_7\ \rho_1$$

$$B_{23} = L_3 + L_1\ \rho_1$$

$$B_{24} = L_3 - L_3\ \rho_1$$

$$B_{31} = L_5 - L_5\ \rho_1$$

$$B_{32} = L_5 + L_7\ \rho_1$$

$$B_{33} = L_5 + (\ell+2)\ L_1\ \rho_1$$

$$B_{34} = L_5 - (\ell+2)\ L_3\ \rho_1$$

$$B_{41} = L_7 + L_5\ \rho_1$$

$$B_{42} = L_7 - L_7\ \rho_1$$

$$B_{43} = L_7 - (\ell+2)\ L_1\ \rho_1$$

$$B_{44} = L_7 + (\ell+2)\ L_3\ \rho_1$$

The C_{ij} can be derived from the above formulas for the B_{ij} by the replacements

$$B_{ij} \to C_{ij}$$

$$(\ell+2)\ L_i \to (\ell-1)\ L_{i+1}$$

$$L_i \to L_{i+1}$$

$$\rho_1 \to \rho_2 \quad .$$

For example

$$C_{11} = (\ell-1)\ L_2 + L_6\ \rho_2$$

$$C_{12} = (\ell-1)\ L_2 - L_8\ \rho_2$$

$$C_{13} = L_2 - L_2\ \rho_2$$

etc.

For the motion expressible with the $\vec{C}_{m,\ell}$ let

$E_{ij} = (2\ell+1)\ R^{-\ell} A_{ij}$.

$$E_{11} = (\ell+2) + (\ell-1)\ \rho_2^{-1}$$

$$E_{12} = m \left[1 - \rho_2^{-1} \right]$$

$$E_{21} = (\ell-1)(\ell+2)\ m\ R^{-1} \left[1 - \rho_2^{-1} \right]$$

$$E_{22} = R^{-1} \left[(\ell-1) + (\ell+2)\ \rho_2^{-1} \right] \quad .$$

Circular Cylindrical Coordinates

For a layer whose elastic properties are $c = 3 - 4\sigma$ and μ and which is bounded below by z_q and above by z_{q-1}, the elements of the propagator matrix are denoted A_{ij}. The A_{ij} propagate the solution from $z = z_{q-1}$ to $z = z_q$. For the motion expressible with the $\vec{P}_{mk}$ and $\vec{B}_{mk}$, let

$$F_{ij} = 2(c+1)\, e^{-D} A_{ij} \quad ,$$

$$D = k\, d \quad ,$$

$$d = z_q - z_{q-1} \quad .$$

$$F_{11} = (c+1-2D) + (c+1+2D)\, e^{-2D}$$

$$F_{12} = -(c-1-2D) + (c-1+2D)\, e^{-2D}$$

$$F_{13} = \mu^{-1}\left[(c-D) - (c+D)\, e^{-2D} \right]$$

$$F_{14} = \mu^{-1}\left[D - D\, e^{-2D} \right]$$

$$F_{21} = -(c-1+2D) + (c-1-2D)\, e^{-2D}$$

$$F_{22} = -(c+1+2D) + (c+1-2D)\, e^{-2D}$$

$$F_{23} = -F_{14}$$

$$F_{24} = \mu^{-1}\left[(c+D) - (c-D)\, e^{-2D} \right]$$

$$F_{31} = 4\mu\left[(1-D) - (1+D)\, e^{-2D} \right]$$

$$F_{32} = 4\,\mu\left[\,D - D\,e^{-2D}\,\right]$$

$$F_{33} = F_{11}$$

$$F_{34} = F_{21}$$

$$F_{41} = -\,F_{32}$$

$$F_{42} = 4\,\mu\left[\,(1+D) - (1-D)\,e^{-2D}\,\right]$$

$$F_{43} = -\,F_{12}$$

$$F_{44} = F_{22} \quad .$$

For the motion expressible with the $\vec{C}_{mk}$, let

$$G_{ij} = 2\,e^{-D}\,A_{ij} \quad .$$

$$G_{11} = 1 + e^{-2D}$$

$$G_{12} = \mu^{-1}\left[\,1 - e^{-2D}\,\right]$$

$$G_{21} = \mu\left[\,1 - e^{-2D}\,\right]$$

$$G_{22} = G_{11} \quad .$$

Appendix 6

FORMULAE FOR COMPUTING $\left[\underline{T}_o(\underline{G}_s)\cdot\hat{n}\right]\cdot\Delta\vec{u}$ in SPHERICAL COORDINATES

Let $\vec{X}^1_{m,\ell}$ be any of the vectors $\vec{M}^1_{m,\ell}$, $\vec{N}^1_{m,\ell}$, or $\vec{E}^1_{m,\ell}$. Similarly define $\vec{X}^2_{m,\ell}$. Inspection of the form of $\underline{G}_s$ in Chapter 3 shows that each of its components is of the form $a\,\vec{X}^1_{m,\ell}(\vec{r})\;\vec{X}^{2*}_{m,\ell+i}(\vec{r}_o)$ where a is a constant, i an integer and the superscripts 1 and 2 may be interchanged. Since $\hat{n}\cdot\underline{T}_o\,(\vec{X}^j_{m,\ell}(\vec{r})) = 0$, only $\hat{n}\cdot\underline{T}_o(\vec{X}^{j*}_{m,\ell}(\vec{r}_o))$ is needed. The expressions below are actually for $\hat{n}\cdot\underline{T}(\vec{X}^j_{m,\ell}(\vec{r}))$. Replacing $\vec{r}$ by $\vec{r}_o$ and taking the complex conjugate gives $\hat{n}\cdot\underline{T}_o(\vec{X}^{j*}_{m,\ell}(\vec{r}_o))$. The form of $\hat{n}\cdot\underline{T}(\vec{u})$ is given in equation (2-6). Expressions for $\hat{r}\cdot\underline{T}\,(\vec{X}^j_{m,\ell}(\vec{r}))$ are given in equation (3-3). The additional expressions which are necessary follow.

Define the symbols ∇_α by

$$\nabla_r\vec{u} = \frac{\partial\vec{u}}{\partial r}$$

$$\nabla_\theta\vec{u} = \frac{1}{r}\frac{\partial\vec{u}}{\partial\theta}$$

$$\nabla_\phi\vec{u} = \frac{1}{r\sin\theta}\frac{\partial\vec{u}}{\partial\phi}\quad .$$

$$\hat{\theta}\cdot\underline{T}(\vec{M}^1_{m,\ell}) = 2\mu\ \nabla_r\ \vec{M}^1_{m,\ell}$$

$$+ \mu(\ell+1)\ r^{\ell-1}\left[\, i\ m\ S_3\ \hat{r} - \ell S\ \hat{\phi}\,\right]$$

$$\hat{\theta}\cdot\underline{T}(\vec{M}^2_{m,\ell}) = 2\mu\ \nabla_r\ \vec{M}^2_{m,\ell}$$

$$+ \mu\ell\ r^{-\ell-2}\left[\, -\ im\ S_3\ \hat{r} - (\ell+1)\ S\ \hat{\phi}\,\right]$$

$$\hat{\theta}\cdot\underline{T}(\vec{N}^1_{m,\ell-1}) = 2\mu\ \nabla_\theta\ \vec{N}^1_{m,\ell-1}$$

$$\hat{\theta}\cdot\underline{T}(\vec{N}^2_{m,\ell+1}) = 2\mu\ \nabla_\theta\ \vec{N}^2_{m,\ell+1}$$

$$\hat{\theta}\cdot\underline{T}(\vec{E}^1_{m,\ell+1}) = 2\mu\ \nabla_\theta\ \vec{E}^1_{m,\ell+1}$$

$$+ 2(2\ell+3)\ r^{\ell}\left[\,\mu K\ S_1\ \hat{r} + \lambda(1-K)(\ell+1)\ S\ \hat{\theta}\,\right]$$

$$\hat{\theta}\cdot\underline{T}(\vec{E}^2_{m,\ell-1}) = 2\mu\ \nabla_\theta\ \vec{E}^2_{m,\ell-1}$$

$$+ 2(2\ell-1)\ r^{-\ell-1}\left[\,-\mu K\ S_1\ \hat{r} + \lambda(1-K)\ \ell S\ \hat{\theta}\,\right]$$

$$\hat{\phi}\cdot\underline{T}(\vec{M}^1_{m,\ell}) = 2\mu\ \nabla_\phi\ \vec{M}^1_{m,\ell}$$

$$+ \mu(\ell+1)\ r^{\ell-1}\left[\, -S_1\ \hat{r} + \ell S\ \hat{\theta}\,\right]$$

$$\hat{\phi}\cdot\underline{T}(\vec{M}^2_{m,\ell}) = 2\mu\ \nabla_\phi\ \vec{M}^2_{m,\ell}$$

$$+ \mu\ell\ r^{-\ell-2}\left[\ S_1\ \hat{r} + (\ell+1)\ S\ \hat{\theta}\ \right]$$

$$\hat{\phi}\cdot\underline{T}(\vec{N}^1_{m,\ell-1}) = 2\mu\ \nabla_\phi\ \vec{N}^1_{m,\ell-1}$$

$$\hat{\phi}\cdot\underline{T}(\vec{N}^2_{m,\ell+1}) = 2\mu\ \nabla_\phi\ \vec{N}^2_{m,\ell+1}$$

$$\hat{\phi}\cdot\underline{T}(\vec{E}^1_{m,\ell+1}) = 2\mu\ \nabla_\phi\ \vec{E}^1_{m,\ell+1}$$

$$+ 2(2\ell+3)\ r^{\ell}\left[\ \mu K\ \text{im}\ S_3\ \hat{r} + \lambda(1-K)(\ell+1)\ S\ \hat{\phi}\ \right]$$

$$\hat{\phi}\cdot\underline{T}(\vec{E}^2_{m,\ell-1}) = 2\mu\ \nabla_\phi\ \vec{E}^2_{m,\ell-1}$$

$$+ 2(2\ell-1)\ r^{-\ell-1}\left[\ -\mu K\ \text{im}\ S_3\ \hat{r} + \lambda(1-K)\ \ell S\ \hat{\phi}\ \right]$$

$$\nabla_\theta\vec{M}^1_{m,\ell} = r^{\ell-1}\left\{-\text{im}\ S_3\ \hat{r} + T_1\ \hat{\theta} - S_2\ \hat{\phi}\right\}$$

$$\nabla_\theta\vec{M}^2_{m,\ell} = r^{\ell-2}\left\{-\text{im}\ S_3\ \hat{r} + T_1\ \hat{\theta} - S_2\ \hat{\phi}\right\}$$

$$\nabla_\theta\vec{N}^1_{m,\ell-1} = r^{\ell-2}\left\{(\ell-1)\ S_1\ \hat{r} + \left[S_2 + \ell S\right]\ \hat{\theta} + T_1\ \hat{\phi}\right\}$$

$$\nabla_\theta\vec{N}^2_{m,\ell+1} = r^{-\ell-3}\left\{-(\ell+2)\ S_1\ \hat{r} + \left[S_2 - (\ell+1)\ S\right]\ \hat{\theta} + T_1\ \hat{\phi}\right\}$$

$$\nabla_\theta \vec{E}^1_{m,\ell+1} = r^\ell \left\{ \left[(\ell+1)^2 - 2(\ell+2)\ K \right] S_1\ \hat{r} \right.$$

$$\left. + \left[L_3\ S_2 + (\ell+1)\ L_1\ S \right] \hat{\theta} + L_3\ T_1\ \hat{\phi} \right\}$$

$$\nabla_\theta \vec{E}^2_{m,\ell-1} = r^{-\ell-1} \left\{ \left[\ell^2 + 2(\ell-1)\ K \right] S_1\ \hat{r} \right.$$

$$\left. + \left[- L_4\ S_2 + \ \ell L_2\ S \right] \hat{\theta} - L_4\ T_1\ \ \hat{\phi} \right\}$$

$$\nabla_\phi \vec{M}^1_{m,\ell} = r^{\ell-1} \left\{ S_1\ \hat{r} + T_2\ \hat{\theta} - T_1\ \hat{\phi} \right\}$$

$$\nabla_\phi \vec{M}^2_{m,\ell} = r^{-\ell-2} \left\{ S_1\ \hat{r} + T_2\ \hat{\theta} - T_1\ \hat{\phi} \right\}$$

$$\nabla_\phi \vec{N}^1_{m,\ell-1} = r^{\ell-2} \left\{ \text{im}\ (\ell-1)\ S_3\ \hat{r} + T_1\ \hat{\theta} + \left[T_2 + \ell S \right]\ \hat{\phi} \right\}$$

$$\nabla_\phi \vec{N}^2_{m,\ell+1} = r^{-\ell-3} \left\{ - \text{im}(\ell+2)\ S_3\ \hat{r} + T_1\ \hat{\theta} + \left[T_2 - (\ell+1)\ S \right] \hat{\phi} \right\}$$

$$\nabla_\phi \vec{E}^1_{m,\ell+1} = r^\ell \left\{ \text{im} \left[(\ell+1)^2 - 2(\ell+2)\ K \right]\ S_3\ \hat{r} \right.$$

$$\left. + L_3\ T_1\ \hat{\theta} + \left[L_3\ T_2 + (\ell+1)\ L_1\ S \right] \hat{\phi} \right\}$$

$$\nabla_\phi \vec{E}^2_{m,\ell-1} = r^{-\ell-1} \left\{ \text{im} \left[\ell^2 + 2(\ell-1)\ K \right] S_3\ \hat{r} \right.$$

$$- L_4 \hat{\theta} - \left[L_4 T_2 - \ell L_2 S \right] \hat{\phi} \Big\}$$

where

$$S = S_\ell^m = e^{im\phi} P_\ell^m (\cos \theta)$$

$$S_1 = \frac{\partial S_\ell^m}{\partial \theta}$$

$$S_2 = \frac{\partial^2 S_\ell^m}{\partial \theta^2}$$

$$S_3 = \frac{S_\ell^m}{\sin \theta}$$

$$T_1 = \frac{im}{\sin \theta} \left[S_1 - \cos \theta \, S_3 \right]$$

$$T_2 = \frac{1}{\sin \theta} \left[\cos \theta \, S_1 - m^2 S_3 \right] \quad ,$$

λ and μ are Lame's constants,

and the L_i and K are defined with equations (3-2) and (3-3). In order to complete the list of the derivatives of the $\vec{X}^j_{m,\ell}$ the radial derivatives are listed below.

$$\nabla_r \vec{X}^1_{m,} = \ell r^{-1} \vec{X}^1_{m,\ell}$$

$$\nabla_r \vec{X}^2_{m,} = -(\ell+1)\, r^{-1} \vec{X}^2_{m,\ell} \quad .$$

Appendix 7

PARTIAL SUMMATION OF EXPRESSION FOR $u_r(\hat{\theta}_o, -\hat{\phi}_o)$ TO OBTAIN A RAPIDLY CONVERGING FORM

By straightforward algebraic rearrangement of the radial component of equation (3-11a), there follows

$$u_r(\hat{\theta}_o, -\hat{\phi}_o) = \sum_{\ell=2}^{\infty} \frac{1}{16\pi a^2} \sin 2\phi \, P_\ell^2(\cos\theta) \, t^{\ell-2} \left\{ (t^2-1) - \frac{2}{(\ell-1)} + (1-3t^2) \left[(1-2k) \frac{\ell}{\Delta} + \frac{(1-k)}{\Delta} \right] \right\} .$$

Then use of the relations (for $\sigma = 1/4$)

$$\frac{1}{\Delta} = \frac{\frac{1}{2}}{\ell} + \frac{\frac{1}{4}}{(\ell+1)} - \frac{1}{(\ell+2)} + \frac{\frac{1}{4}}{(\ell+3)} - \frac{\frac{33}{8}}{(\ell+1)(\ell+2)(\ell+3)\Delta}$$

$$- \frac{\frac{15}{4}}{(\ell)(\ell+1)(\ell+2)(\ell+3)\Delta} ,$$

$$\frac{\ell}{\Delta} = -\frac{\frac{11}{16}}{\ell} + \frac{\frac{29}{16}}{(\ell+1)} - \frac{\frac{1}{16}}{(\ell+2)} - \frac{\frac{1}{16}}{(\ell+3)} + \frac{\frac{39}{16}}{(\ell+1)(\ell+2)(\ell+3)\Delta}$$

$$+ \frac{\frac{165}{32}}{(\ell)(\ell+1)(\ell+2)(\ell+3)\Delta} ,$$

$$\sum_{\ell=2}^{\infty} t^{\ell-2} P_\ell^2(\cos\theta) = \frac{3\sin^2\theta}{T^{5/2}} \quad ,$$

$$\sum_{\ell=2}^{\infty} \frac{t^{\ell-1}}{(\ell-1)} P_\ell^2(\cos\theta) = \cos\theta(3 + 2\,\mathrm{ctn}^2\theta) + \frac{(t-\cos\theta)}{T^{1/2}}\left[\frac{2}{\sin^2\theta} + \frac{1}{T}\right] \quad ,$$

$$\sum_{\ell=2}^{\infty} \frac{t^{\ell}}{\ell} P_\ell^2(\cos\theta) = 1 + 2\,\mathrm{ctn}^2\theta + \frac{(t\cos\theta-1)}{T^{3/2}} + \frac{2\cos\theta\,(t-\cos\theta)}{\sin^2\theta\, T^{1/2}} \quad ,$$

$$\sum_{\ell=2}^{\infty} \frac{t^{\ell+1}}{(\ell+1)} P_\ell^2(\cos\theta) = 2\cos\theta\ \csc^2\theta + \frac{[(t-\cos\theta) - 2t\sin^2\theta]}{T^{3/2}}$$

$$+ \frac{(2\csc^2\theta - 1)(t-\cos\theta)}{T^{1/2}} \quad ,$$

$$\sum_{\ell=2}^{\infty} \frac{t^{\ell+2}}{(\ell+2)} P_\ell^2(\cos\theta) = 2\csc^2\theta + \frac{[2t^2\cos^2\theta - 3t(t-\cos\theta) - 2]}{T^{3/2}}$$

$$+ \frac{[(2\csc^2\theta + 1)\, t\cos\theta - 2\,\mathrm{ctn}^2\theta]}{T^{1/2}} \quad ,$$

and

$$T = 1 - 2t\cos\theta + t^2 \quad ,$$

together with further algebraic rearrangement leads to equation (3-12).

Appendix 8

EFFECTS OF EARTH STRUCTURE AND GRAVITY ON THE STATIC DEFORMATION OF THE EARTH AT LARGE DISTANCE

The static deformation of the earth is affected by the variation of elastic properties with depth and self-gravitation. Two published solutions allow estimation of the importance of these effects at distances greater than 20°. Longman (1963) computed the deformation due to a point mass loading a Gutenberg earth model. Slichter and Caputo (1960) derived a solution for the deformation of an elastic shell enclosing a compressible fluid due to antipodal pressure caps. Their solution does not contain gravitational effects.

Slichter and Caputo's solution is considered first. In their model λ_1 is the compressibility of a homogeneous, liquid core, and λ_2 and μ_2 are Lame's constants for a homogeneous, isotropic, elastic mantle. They give numerical results for $\frac{\lambda_2}{\mu_2} = \frac{14}{11}$ (Poisson's ratio = 0.28), $\frac{\lambda_1}{\mu_2} = 8$, and $\mu_2 = 10^{12}$ dynes/cm^2. These results can be scaled for varying μ_2 and λ_1 with Poisson's ratio in the mantle fixed. The earth model is deformed by uniform antipodal pressure caps. The numerical results are for a specified pressure and for caps which subtend half-angles of 25°, 16°, 8°, and 4° at the center of the model. To obtain the figures quoted

below the pressure was normalized so that the net pressure in each cap was 1 dyne. The limit, as the half-angle goes to zero, of the normalized vertical displacement is the displacement for antipodal point forces. This limit was estimated from the numerical results in the paper for three observational positions. Let the point forces be at the north and south pole. Let $u_r^s(\theta)$ be the vertical displacement at colatitude θ (e.g. u_r^s (90°) is the vertical displacement at the equator). Then for antipodal point forces of 1 dyne

$$u_r^s\ (30^\circ) \approx\ -\ 4.3 \times 10^{-22}\ \text{cm.}$$

$$u_r^s\ (60^\circ)\ \approx\ 1.3 \times 10^{-22}\ \text{cm.}$$

and

$$u_r^s\ (90^\circ)\ \approx 3.1 \times 10^{-22}\ \text{cm.}$$

If μ_2 is varied with $\frac{\lambda_1}{\mu^2}$ and $\frac{\lambda_2}{\mu^2}$ fixed, inspection of the solution given by Slichter and Caputo shows that the values of u_r are proportional to $\frac{1}{\mu_2}$. For example under these conditions at $\theta = 90^\circ$

$$u_r^s \approx 9.2 \times 10^{-22}\ \text{cm.} \quad \text{for} \quad \mu_2 = 3 \times 10^{11}\ \text{dynes/cm}^3.$$

$$u_r^s \approx 3.1 \times 10^{-22}\ \text{cm} \quad \text{for} \quad \mu_2 = 10^{12}\ \text{dynes/cm}^3.$$

$$u_r^s \approx 1.0 \times 10^{-22}\ \text{cm} \quad \text{for} \quad \mu_2 = 3 \times 10^{12}\ \text{cynes/cm}^3.$$

Varying the elastic constants through a range from crustal values to lower mantle values produces a change in displacement values which

is significant compared to the sphericity effect determined in Chapter 3. For the problem considered by Slichter and Caputo one expects a lower average rigidity to be appropriate near the source and a higher average rigidity to be appropriate near $\theta = 90^{\circ}$, although precisely what values should be used cannot be determined without solving the complete problem.

Longman (1962 and 1963) computed the response of a gravitating Gutenberg earth model with a point mass load. By scaling the numerical results which he gives to a 1/980.7 gram mass one obtains approximately a 1 dyne point force at the surface. By superposing solutions for such a mass at the north and south poles of the earth modle, a solution is obtained which is comparable to Slichter and Caputo's but includes gravitational effects and a realistic variation of elastic parameters. With a notation similar to that above the vertical displacement for antipodal 1/980.7 gram masses is

$$u_r^{\ell}(30^{\circ}) \approx -.81 \times 10^{-22} \text{ cm.}$$

$$u_r^{\ell}(60^{\circ}) \approx .20 \times 10^{-22} \text{ cm}$$

$$u_r^{\ell}(90^{\circ}) \approx .33 \times 10^{-22} \text{ cm.}$$

Comparing these with the displacements from Slichter and Caputo's solutions one obtains

$$\frac{u_r^s}{u_r^\ell}\ (30^\circ) = 5.3$$

$$\frac{u_r^s}{u_r^\ell}\ (60^\circ) = 6.5$$

$$\frac{u_r^s}{u_r^\ell}\ (90^\circ) = 9.3 \quad .$$

Although some of the difference is due to the gravitational attraction of the mass load, it still seems likely that the earth's self-gravitation and structural effects are appreciable.

From these comparisons it is concluded that, at large distances from the source, neither the effects of elastic constants varying with depth nor gravitation can be neglected compared with the effect of sphericity alone.

Appendix 9

INTEGRAL KERNELS FOR A HOMOGENEOUS HALF-SPACE

For a homogeneous half-space with rigidity μ and $c = 3-4\sigma$, where σ is Poisson's ratio, the integral kernels for equations (4-4) are

$$KD_P^P = (1 + kh)\, e^{-kh}$$

$$KD_P^B = -\, kh\, e^{-kh}$$

$$KD_B^P = kh\, e^{-kh}$$

$$KD_B^B = (1 - kh)\, e^{-kh}$$

$$KF_P^P = \frac{1}{4\mu}(c + 1 + 2kh)\, e^{-kh}$$

$$KF_P^B = \frac{1}{4\mu}(c - 1 - 2kh)\, e^{-kh}$$

$$KF_B^P = \frac{1}{4\mu}(c - 1 + 2kh)\, e^{-kh}$$

$$KF_B^B = \frac{1}{4\mu}(c + 1 - 2kh)\, e^{-kh}$$

$$KD_C^C = e^{-kh} \qquad KF_C^C = \frac{1}{\mu}\, e^{-kh}$$

Appendix 10

INTEGRALS USED IN APPROXIMATIONS TO HALF-SPACE DEFORMATIONAL FIELDS

For the surface deformational fields in a layered half-space an approximation to the integral kernels of the form of equation (4-14) can be integrated exactly. The results below all follow from a general Hankel transform in Erdelyi (1954, Chapter VIII, Section 8.6, Formula 3). All the forms which were actually used in calculating the results in the text are given here.

$$F(n,m) = \int_0^\infty k^n \, e^{-hk} \, J_m(kr) \, dk \quad ,$$

$$X^2 = h^2 + r^2 \quad ,$$

$$z^2 = \frac{h^2}{X^2} \quad ,$$

if n is even, $a_n = (-1)^{\frac{n}{2}} \, x^{-n-1}$,

if n is odd, $a_n = (-1)^{\frac{(n-1)}{2}} \, h \, x^{-n-2}$,

A_n, B_n, and C_n are polynomials in z^2, and d_{An}, d_{Bn}, and d_{Cn} are constants. For $m = 0$ and $0 \leq n \leq 12$,

$$F(n,o) = d_{An} \; a_n \; A_n \quad .$$

For $m = 1$ and $n = 0$,

$$F(0,1) = r \; X^{-1} \; (X + h)^{-1} \quad .$$

For $m = 1$ and $1 \leq n \leq 12$,

$$F(n,1) = -r \; d_{Bn} \; a_{n+1} \; B_n \quad .$$

For $m = 2$ and $-1 \leq n \leq 1$,

$$F(-1,2) = \frac{r^2}{2} \; (X + h)^{-2}$$

$$F(0,2) = r^2 \; X^{-1} \; (X + h)^{-2}$$

$$F(1,2) = r^2 \; X^{-3} \; (X + h)^{-2} \; (2X + h) \quad .$$

For $m = 2$ and $2 \leq n \leq 11$,

$$F(n,2) = r^2 \; d_{Cn} \; a_{n+2} \; C_n \quad .$$

d_{An}, d_{Bn} and d_{Cn} are given in Table A10-1.

The coefficients for the polynomials A_n, B_n, and C_n are given in Tables A10-1, A10-2, and A10-3, respectively. Each row in these

tables gives one polynomial. The column labeled "n" identifies the polynomial and the other columns give the coefficients for the power of z which heads the column. The polynomials alternate in sign with the first term positive. For example the polynomial B_6 is

$$B_6 = 5 - 30\, z^2 + 33\, z^4$$

and $F(6, 1)$ is

$$F(6,1) = - r\, d_{B_6}\, a_7\, B_6$$

$$F(6,1) = r\, h\, X^{-9}\, (315)(5 - 30\, z^2 + 33\, z^4).$$

Appendix 11

EXPRESSIONS FOR COMPONENTS OF TILT AND STRAIN FOR HALF-SPACE SOURCES

In Chapter 4 formulas are given for the surface displacement fields due to certain point sources. Expressions are given here for the surface tilt and strain fields associated with these displacement fields. The notation is the same as Chapter 4 unless noted otherwise.

For the field

$$\vec{u}(r, \theta, o) = \hat{r}\, u_r + \hat{\theta}\, u_\theta + \hat{z}\, u_z$$

the surface tilt and strain components are:

radial tilt

$$\tau_r = \frac{\partial u_z}{\partial r} \quad ,$$

theta tilt

$$\tau_\theta = \frac{1}{r} \frac{\partial u_z}{\partial \theta} \quad ,$$

radial strain

$$\varepsilon_{rr} = \frac{\partial u_r}{\partial r} \quad ,$$

theta strain

$$\varepsilon_{\theta\theta} = \frac{1}{r}\frac{\partial u_\theta}{\partial \theta} + \frac{u_r}{r} \quad ,$$

shear strain

$$\varepsilon_{r\theta} = \frac{1}{2}\left(\frac{1}{r}\frac{\partial u_r}{\partial \theta} + \frac{\partial u_\theta}{\partial r} - \frac{u_\theta}{r}\right) \quad .$$

For strike-slip motion on a vertical fault plane (the field defined by equation (4-6))

$$\tau_r = \frac{\mu_s}{2\pi} \sin 2\theta \int_0^\infty KF_P^B \left(-k^2 J_1 + \frac{2}{r} k J_2\right) dk \quad ,$$

$$\tau_\theta = \frac{\mu_s}{2\pi} \cos 2\theta \int_0^\infty KF_P^B \left(-\frac{2}{r} k J_2\right) dk \quad ,$$

$$\varepsilon_{rr} = \frac{\mu_s}{2\pi} \sin 2\theta \int_0^\infty \left\{ KF_B^B \left(-k^2 J_0 + \frac{3}{r} k J_1 - \frac{6}{r^2} J_2\right) + KF_C^C \left(-\frac{2}{r} k J_1 + \frac{6}{r^2} J_2\right)\right\} dk \quad ,$$

$$\varepsilon_{\theta\theta} = \frac{\mu_s}{2\pi} \sin 2\theta \int_o^\infty \left\{ KF_B^B \left(-\frac{1}{r} k J_1 + \frac{6}{r^2} J_2 \right) \right.$$

$$\left. + KF_C^C \left(\frac{2}{r} k J_1 - \frac{6}{r^2} J_2 \right) \right\} dk \quad ,$$

$$\varepsilon_{r\theta} = \frac{\mu_s}{2\pi} \cos 2\theta \int_o^\infty \left\{ KF_B^B \left(-\frac{2}{r} k J_1 + \frac{6}{r^2} J_2 \right) \right.$$

$$\left. + KF_C^C \left(-\frac{1}{2} k^2 J_0 + \frac{2}{r} k J_1 - \frac{6}{r^2} J_2 \right) \right\} dk \quad .$$

For a dip-slip motion on a vertical fault plane (the field defined by equations (4-7))

$$\tau_r = \frac{1}{2\pi} \sin \theta \int_o^\infty KD_P^B \left(k^2 J_0 - \frac{1}{r} k J_1 \right) dk \quad ,$$

$$\tau_\theta = \frac{1}{2\pi} \cos \theta \int_o^\infty KD_P^B \left(\frac{1}{r} k J_1 \right) dk \quad ,$$

$$\varepsilon_{rr} = \frac{1}{2\pi} \sin \theta \int_o^\infty \left\{ KD_B^B \left(-k^2 J_1 + \frac{1}{r} k J_2 \right) \right.$$

$$+ KD_C^C \left(- \frac{1}{r} k J_2 \right) \Big\} dk \quad ,$$

$$\varepsilon_{\theta\theta} = \frac{1}{2\pi} \sin\theta \int_o^\infty \left\{ KD_B^B \left(- \frac{1}{r} k J_2 \right) \right.$$

$$\left. + KD_C^C \left(\frac{1}{r} k J_2 \right) \right\} dk \quad ,$$

$$\varepsilon_{r\theta} = \frac{1}{2\pi} \cos\theta \int_o^\infty \left\{ KD_B^B \left(- \frac{1}{r} k J_2 \right) \right.$$

$$\left. + KD_C^C \left(- \frac{1}{2} k^2 J_1 + \frac{1}{r} k J_2 \right) \right\} dk \quad .$$

For the field $\vec{u}(\hat{z}, \hat{z})$ of equation (4-9)

$$\tau_r = \frac{1}{2\pi} \int_o^\infty KD_P^P \left(k^2 J_1 \right) dk \quad ,$$

$$\tau_\theta = 0 \quad ,$$

$$\varepsilon_{rr} = \frac{1}{2\pi} \int_o^\infty KD_B^P \left(k^2 J_0 - \frac{1}{r} k J_1 \right) dk \quad ,$$

$$\varepsilon_{\theta\theta} = \frac{1}{2\pi} \int_o^\infty KD_B^P \left(\frac{1}{r} k J_1 \right) dk \quad ,$$

$$\varepsilon_{r\theta} = 0 \quad .$$

For the field $\frac{\partial \vec{u}^{xF}}{\partial x} + \frac{\partial \vec{u}^{yF}}{\partial y}$ of equation (4-10)

$$\tau_r = \frac{1}{2\pi} \int_o^\infty KF_P^B \left(- k^2 J_1 \right) dk \quad ,$$

$$\tau_\theta = 0 \quad ,$$

$$\varepsilon_{rr} = \frac{1}{2\pi} \int_o^\infty KF_B^B \left(- k^2 J_0 + \frac{1}{r} k J_1 \right) dk \quad ,$$

$$\varepsilon_{\theta\theta} = \frac{1}{2\pi} \int_o^\infty KF_B^B \left(- \frac{1}{r} k J_1 \right) dk \quad ,$$

$$\varepsilon_{r\theta} = 0 \quad .$$

The above results can be used together with equations (4-8), (4-11) and (4-12) to obtain expressions for the tilts and strains associated with all the fields developed in Chapter 4.

Appendix 12

NOTATION FOR CHAPTER 6

The notations used in Chapter 6 are for the most part frequently used, but all those not defined in Chapter 6 are given here for completeness.

$^\circ$	this superscript identifies a quantity as appropriate to a spherically symmetric earth model which is considered the unperturbed earth model.
n	this subscript represents the mode type, spheroidal or torsional, and the r, θ, and ϕ mode numbers.
ρ	density
λ and μ	Lamé's constants
$\vec{g}$	gravity
$\vec{u}_n$	n'th displacement eigenfunction
ψ_n	change in the gravitational potential for the n'th eigenfunction.
σ_n	the angular frequency squared for the n'th eigenfunction
γ	the gravitational constant
r, θ, ϕ	conventional spherical coordinates
p , ℓ, m	the r, θ, and ϕ mode numbers respectively
,j	layer index; for example, the radial solution function for a spherically symmetric earth model with mode

numbers ℓ and p in the $j^{\underline{th}}$ layer is $u_{\ell p,j}$.

Appendix 13

TORSIONAL SOLUTION USED AND SENSE IN WHICH IT CAN BE EXTENDED TO THE SPHEROIDAL SOLUTION

The equations governing the radial part of the solution for a spherically symmetric earth model are given in Alterman et al (1959). For torsional motion the equations are

$$\dot{y}_1 = \frac{y_1}{r} + \frac{1}{\mu} y^2$$

$$\dot{y}_2 = \left[\mu \frac{(\ell^2 + \ell - 2)}{r^2} - \sigma\rho \right] y_1 - \frac{3}{r} y_2$$

where the notation is as in Chapter 6 except the superscript ° has been dropped for convenience; y_1 is for the displacement, y_2 is for the stress, and the dot signifies differentiation with respect to r. With the substitutions

$$R = \rho r^2$$

$$v_1 = r^{\frac{1}{2}} y_1$$

$$v_2 = r^{3/2} y_2$$

and $s = \ell n\ r$

these equations can be written

$$\begin{bmatrix} \dot{v}_1 \\ \dot{v}_2 \end{bmatrix} = \begin{bmatrix} \frac{3}{2} & \frac{1}{\mu} \\ \mu(\ell^2 + \ell - 2) - R\sigma & -\frac{3}{2} \end{bmatrix} \begin{bmatrix} v_1 \\ v_2 \end{bmatrix}$$

where v_1 and v_2 are functions of s. If μ and R are assumed constant, these equations become a first order set of simultaneous linear ordinary differential equations with constant coefficients. Such a set can be solved in closed form if the roots to the characteristic equation can be found in closed form. The procedure is well known, for example Hildebrand (1949), Chapter 1, and leads to the result given in Chapter 6.

The results necessary to use this solution in the Thomson-Haskell matrix formalism are in the notation of Chapter 3

$$\varepsilon(s) = \begin{bmatrix} 2 \cosh ks & 2 \sinh ks \\ \mu(2k \sinh ks - 3 \cosh ks) & \mu(2k \cosh ks - 3 \sinh ks) \end{bmatrix},$$

$$\varepsilon^{-1}(s) = \frac{1}{4\mu k} \begin{bmatrix} \mu(2k \cosh ks - 3 \sinh ks) & -2 \sinh ks \\ \mu(-2k \sinh ks + 3 \cosh ks) & 2 \cosh ks \end{bmatrix},$$

$$a_{11} = \cosh k\, d + \frac{3}{2k} \sinh k\, d \quad ,$$

$$a_{12} = \frac{1}{\mu k} \sinh k\, d \quad ,$$

$$a_{21} = \mu k \left(1 - \frac{9}{4k^2}\right) \sinh k\, d \quad ,$$

and

$$a_{22} = \cosh k\, d - \frac{3}{2k} \sinh k\, d$$

where for the $j^{\underline{th}}$ layer

$$d \equiv d_j = s_j - s_{j-1} = \ell n \frac{r_j}{r_{j-1}} \quad .$$

The substitution

$$K = - i\, k$$

gives the other solution form.

For the normalization used in Chapter 6 the following results are needed

$$\int_a^b u_{\ell n}^2 \rho r^2 \, dr = 2R \left\{ \left\{ \left\{ A'^2 \, a^{2k} + B'^2 \, b^{-2k} \right\} \left\{ \left(\frac{b}{a}\right)^{2k} - 1 \right\} \left\{ \frac{1}{4k} \right\} + A' \, B' \, \ell n \left(\frac{b}{a}\right) \right\} \right\} ,$$

$$A' = A + B \quad ,$$

$$B' = A - B \quad ,$$

A and B are the coefficients of equation (6-13a) ,

$$\int_a^b u_{\ell n}^2 \rho r^2 \, dr = \frac{R}{2} \left\{ \left\{ \left\{ (\alpha^2 - \beta^2) \cos x - 2\alpha\beta \sin x \right\} \left\{ \frac{\sin y}{K} \right\} + (\alpha^2 + \beta^2) \, \ell n \left(\frac{b}{a}\right) \right\} \right\} ,$$

$$x = K \ell n \left(\frac{r_{j-1}^2}{ab} \right) \quad ,$$

$$y = K \ell n \left(\frac{b}{a} \right) \quad ,$$

$$\alpha = v_1(s_{j-1}) \quad ,$$

$$\beta = \frac{3\alpha}{2K} + \frac{v_2(s_{j-1})}{\mu K} \quad ,$$

the subscript j refers to the $j^{\underline{th}}$ layer and $r_{j-1} \leqslant a \leqslant r_j$ and $r_{j-1} \leqslant b \leqslant r_j$.

It is possible to obtain a similar solution for the equations for spheroidal motion but density must be treated in a special manner. In equations (6-1a, b) let the density when it appears on the left hand side of the equals sign be called ρgravity and the density when it appears on the right hand side of the equation be called ρinertial. Make the following assumptions

$$\rho\text{inertial} = \frac{R}{r^2} \quad ,$$

$$\rho\text{gravity} = \frac{\overline{R}}{r} \quad ,$$

$$\vec{g} = g\hat{r} \quad , \quad \text{and}$$

μ, λ, g, R, and $\underline{\overline{R}}$ are constants,

then the substitutions

$$v_i = r^{n/2} y_i \quad ,$$

$$n = 1 \text{ for } i \text{ odd},$$

$$n = 3 \text{ for } i \text{ even},$$

into equations (28) through (33) in Alterman et al (1959) result in an equidimensional set of equations in the variables v_i. This set can be reduced to a set of six simultaneous linear ordinary differential equations with constant coefficients by the charge of variable $s = \ell n\ r$. It can be shown that the resulting equations have a closed form solution. The use of two different variations for density is, of course, only a mathematical artifice. This spheroidal solution was not completed since it does not appear to offer any advantages over existing numerical techniques. The existence of this solution was noted here since the author is not aware of it having been recorded previously.

Appendix 14

LIMITS AS $r \to \infty$ ($k \to 0$) OF SURFACE DISPLACEMENT FIELDS IN A LAYERED ELASTIC HALF-SPACE

The limits as $r \to \infty$ of the surface displacement fields are given for three source types to order $\frac{1}{r^3}$. The limits as $k \to 0$ to order k of each of the integral kernels in Chapter 4 are also listed. The use of the integral kernels as $k \to 0$ together with the integrals given in Appendix 10 and the formulas in Chapter 4 determine the particular point source limits given here. The limits of the surface deformational fields for any other point force or dislocation source can be derived fairly quickly since the limits as $k \to 0$ are given for all the integral kernels of Chapter 4.

Indexing of the layer parameters is given in Figure (2-2). The sth layer is the source layer. The index s' may appear in the upper or lower limit of a summation. The index s', when applied as a subscript to an elastic constant, means that elastic constant for the source layer. When s' appears as an upper limit in the summation, $\sum_{i=1}^{s}$, it means that the summation is from the surface to the source depth. For example

$$\sum_{i=1}^{s'} d_i = h \quad .$$

When s' appears as a lower index in the summation, $\sum_{s'}^{n-1}$, it means that the summation is from the source depth to the lowest layer interface. For example

$$\sum_{i=s'}^{n-1} d_i = Z_{n-1} - h \quad .$$

For clarity in this appendix only capital C is used for the parameter written as small c in Chapter 4.

$$C = 3 - 4\sigma \quad .$$

Vertical Strike-Slip Fault

$$\vec{u}(\hat{y}, -\hat{x}) = \frac{1}{8\pi}\frac{\mu_s}{\mu_n}\left[\!\!\left[\frac{1}{r^2}\left\{-2(C_n-1)\left[\hat{z}\sin 2\theta + \hat{\theta}\cos 2\theta\right] + (C_n-7)\,\hat{r}\sin 2\theta\right\}\right.\right.$$

$$+\frac{1}{r^3}\left\{-3\,L_{3z}\,\hat{z}\sin 2\theta + 4\,L_{3r\theta}\left[\hat{r}\sin 2\theta - \hat{\theta}\cos 2\theta\right]\right\}$$

$$\left.\left. + 0\left(\frac{\hat{n}}{r^4}\right)\right]\!\!\right] \quad ,$$

$$L_{3z} = (C_n+1)(Z_{n-1}-h) + (C_n-1)\sum_{i=1}^{n-1}\frac{(C_n+1)}{(C_i+1)}\left[\frac{(C_i-3)}{(C_n-1)} - 2\frac{\mu_i}{\mu_n}\right]d_i \quad ,$$

$$L_{3r\theta} = (C_n-1)(2Z_{n-1}-h) + 2\sum_{i=1}^{n-1}\frac{\mu_i}{\mu_n}\left[2 - \frac{(C_n+1)^2}{(C_i+1)}\right]d_i \quad .$$

Vertical Dip-Slip Fault

For this case there are no terms of the type $\frac{1}{r^2}$ and the z component has no terms of the type $\frac{1}{r^3}$.

$$\vec{u}(\hat{y}, -\hat{z}) = \frac{1}{2\pi} \left[\left[\frac{1}{r^3} \left\{ L_{3r}\, \hat{r} \sin\theta - 2\, L_{3\theta}\, \hat{\theta} \cos\theta \right\} + O\left(\frac{\hat{n}}{r^4}\right)\right]\right] ,$$

$$L_{3r} = \sum_{i=1}^{s'} \frac{\mu_i}{\mu_n} \left[4 \frac{(C_n+1)}{(C_i+1)} - 1 \right] d_i ,$$

$$L_{3\theta} = \sum_{i=1}^{s'} \frac{\mu_i}{\mu_n} \left[\frac{(C_n+1)}{(C_i+1)} - 1 \right] d_i .$$

For 2 layers over a half-space with the source in layer 1, the $\left(\frac{1}{r^4}\right)$ term for the z component is

$$u_z(\hat{y}, -\hat{z}) = \frac{1}{2\pi}\left[\left[\frac{1}{r^4}\left\{\left\{-3h\,\frac{\mu_i}{\mu_3}\,\frac{(C_3+1)}{(C_1+1)}\left\{(h-2Z_2)+L_{4Z1}+L_{4Z2}\right\}+0\left(\frac{1}{r^5}\right)\right]\right]\right\}\right\} \quad ,$$

$$L_{4Zi} = \left[2\,\frac{\mu_i}{\mu_3}\,\frac{(C_3-1)}{(C_i+1)} - \frac{(C_i-3)}{(C_i+1)}\right] 2d_i \quad .$$

Dilatational Source

For this case the r component contains no term of the type $\frac{1}{r^3}$ and the z component contains no term of the type $\frac{1}{r^2}$.

$$\vec{u}^{\Delta} = \frac{(C_n+1)}{4\pi} \frac{\mu_s}{\mu_n} \left[\!\!\left[\frac{1}{r^2} \hat{r} + \frac{1}{r^3} \hat{z} \left\{ (Z_{n-1}-h) + L_{3z} \right\} + 0\left(\frac{\hat{n}}{r^4}\right) \right]\!\!\right] ,$$

$$L_{3z} = \sum_{i=1}^{n-1} \left[\frac{(C_i-3)}{(C_i+1)} - 2 \frac{(C_n-1)}{(C_i+1)} \frac{\mu_i}{\mu_n} \right] d_i .$$

The limit of the integral kernels as $k \to o$ is to order k

$$KD_P^P \to 1 + 0(k^2) ,$$

$$KD_P^B \to k \left\{ \sum_{i=1}^{s'} \left[(C_i-3) - 2 \frac{\mu_i}{\mu_n} (C_n-1) \right] \frac{d_i}{(C_i+1)} \right\} ,$$

$$KD_B^P \rightarrow \quad kh \quad ,$$

$$KD_B^B \rightarrow 1 + k \left\{ - 2 \sum_{i=1}^{s'} \frac{\mu_i}{\mu_n} \frac{(C_n+1)}{(C_i+1)} d_i \right\} \quad ,$$

$$KF_P^P \rightarrow \frac{(C_n+1)}{4\mu_n} + \frac{k}{4\mu_n} \left\{ \sum_{i=s'}^{n-1} \left[4 \frac{\mu_n}{\mu_i} (C_i-1) + (C_n-1)(C_i-3) \right] \frac{d_i}{(C_i+1)} \right.$$

$$\left. - (C_n-1) \sum_{i=1}^{n-1} \left[2 \frac{\mu_i}{\mu_n} (C_n-1) - (C_i-3) \right] \frac{d_i}{(C_i+1)} \right\} \quad ,$$

$$KF_P^B \rightarrow \frac{(C_n-1)}{4\mu_n} + \frac{k}{4\mu_n} \left\{ (C_n+1)(Z_{n-1}-h) \right.$$

$$\left. + \sum_{i=1}^{n-1} \frac{(C_n+1)}{(C_i+1)} \left[(C_i-3) - 2 \frac{\mu_i}{\mu_n} (C_n-1) \right] d_i \right\} \quad ,$$

$$KF_B^P \to \frac{(C_n-1)}{4\mu_n} + \frac{k}{4\mu_n}\left\{(C_n+1)\sum_{i=s'}^{n-1}\frac{(C_i-3)}{(C_i+1)}\,d_i + (C_n+1)\,Z_{n-1} - 2(C_n-1)\sum_{i=1}^{n-1}\frac{\mu_i}{\mu_n}\frac{(C_n+1)}{(C_i+1)}\,d_i\right\} ,$$

$$KF_B^B \to \frac{(C_n+1)}{4\mu_n} + \frac{k}{4\mu_n}\left\{(C_n-1)(2Z_{n-1}-h) + 4\sum_{i=s'}^{n-1}\frac{\mu_n}{\mu_i}\,d_i - 2(C_n+1)\sum_{i=1}^{n-1}\frac{\mu_i}{\mu_n}\frac{(C_n+1)}{(C_i+1)}\,d_i\right\} ,$$

$$KD_C^C \to 1 + k\left\{-\sum_{i=1}^{s'}\frac{\mu_i}{\mu_n}\,d_i\right\} ,$$

$$KF_C^C \to \frac{1}{\mu_n} + \frac{k}{\mu_n}\left\{\sum_{i=s'}^{n-1}\frac{\mu_n}{\mu_i}\,d_i - \sum_{i=1}^{n-1}\frac{\mu_i}{\mu_n}\,d_i\right\} .$$

Appendix 15

INTEGRATION PROCEDURES FOR A LAYERED, ELASTIC HALF-SPACE

The kernels (the KD's and KF's of Chapter 4) of the Fourier-Bessel integral representations of the layered half-space were generated numerically. They are calculated by programming the matrix results given in Chapter 4. The kernel for a homogeneous half-space with the elastic properties of the source layer and with the same source type and source depth is subtracted from the kernel for the layered half-space. The kernel for the homogeneous half-space can be integrated exactly using the results given in Chapter 4 and other appendices referenced there. The remainder, that is the layered half-space kernel minus the homogeneous half-space kernel, is denoted by K(k). There are ten possible such residual kernels corresponding to the ten different KD's and KF's. Subtracting out the half-space solution can be viewed as removing the effect of the source, but in a way that fails to meet the boundary conditions exactly at the various interfaces. Integrating the K(k)'s determines how much additional solution must be added to meet the boundary conditions.

The K(k)'s are expressed in the form

$$K(k) = \sum_{\ell} A_{\ell} k^{\eta_{\ell}} e^{-\alpha_{\ell} k} + R(k) \qquad \text{(A15-1)} .$$

The terms in the summation are integrated exactly. It is attempted to choose these terms so that the term $R(k)$ does not contribute appreciably to the integral.

When plotted on a logarithmic scale in k, the functions $K(k)$ are, for the structures treated here, smooth functions with one or two maxima or minima. The difference between curves 1 and 5 in Figure 5-1 is typical of the most extreme form of $K(k)$ considered. The procedure used for approximating a $K(k)$ is as follows. The maximum value of $K(k)$, denoted $K(k_{max})$, is determined. The values of k where $K(k)$ has decreased to one-half its value at k_{max} are determined by stepping away from k_{max} toward higher and lower values of k. These values are denoted

$$K(k_{-\frac{1}{2}}) \text{ and } K(k_{+\frac{1}{2}}).$$

Let

$$F(n, A, \alpha; k) = Ak^{n} e^{-\alpha k} .$$

$F(n, A, \alpha; k)$ has a simple maximum and decreases to 0 as $k \to 0$ and as $k \to \infty$. For a specified number of values of n, A and α are determined so that

$$F(n, A, \alpha; k_{max}) = K(k_{max}).$$

The quantity

$$\left|K(k_{-\frac{1}{2}}) - F(n, A, \alpha; k_{-\frac{1}{2}})\right| + \left|K(k_{+\frac{1}{2}}) - F(n, A, \alpha; k_{+\frac{1}{2}})\right|$$

is calculated for each n. That value of n for which this quantity is a minimum is selected together with the associated A and α to determine A_1, α_1, and n_1 in equation (A15-1). The procedure is then repeated until the index ℓ or the remainder $R(k)$ have reached prespecified limits. The resulting kernel approximations are punched on cards thus constituting a permanent "structure deck" which is used in another program to evaluate the formulas for the various field components.

The quality of the approximation is judged by calculating the ratio $R(k)/KD(k)$ (or $KF(k)$) for a wide range of k's. The simple structures considered in the text have 2 layers, each from 1 to 4 units thick. For this scaling k was varied from about k = .001 to about k = 100 with equal spacing on a logarithmic scale. The ratio $R(k)/KD(k)$ was generally less than .01 and seldom exceeded .02 for the results presented in the text. When the ratio did exceed .02 it was usually associated with a zero crossing in $KD(k)$. In some of the structures tried $R(k)/KD(k)$ was not sufficiently small to justify using the approximation.

As a further check on the calculation one of the structures was approximated at two different scalings. This yields different approximations. Each structure meet the criteria given above for a satisfactory approximation. Some values of the surface displacement field in a half-space with the source layer properties, are listed in Table A15-1. The structure is a layer of unit thickness with $\mu = 1$, $\sigma = \frac{1}{4}$; overlying a layer of unit thickness with $\mu = .01$, $\sigma = \frac{1}{4}$; overlying a half-space with $\mu = 1$, $\sigma = \frac{1}{4}$. This is the largest change in rigidity which was calculated, and these are the least accurate approximations used. The source is a strike slip fault with vertical fault plane located at a depth of 0.1 of the thickness of layer 1. R is the distance from the origin measured in units of the thickness of layer 1. For UZ, the vertical displacement, the approximations agree with each other to within a few percent out to about R = 10. The only relatively large difference, about 7% is at R = 0.5. There is a zero crossing in UZH, the half-space field, at R = 0.4, and relatively small differences in the position of a nearby zero crossing in UZ account for the percentage error being greater than that for nearby values of R. At larger distances the disagreement between approximations becomes larger, but the general features shown by the two approximations are the same. A comparison of most of the other fields (displacement, tilt, or strain) from any of the sources gives results similar to those shown for UZ/UZH.

That field which showed the greatest discrepancy between the two approximations was U_θ, the displacement in the $\hat{\theta}$ direction. Some results for this case are also listed in Table 15-1. At R = 12 the two fields disagree by 30% to 40% and at R = 40 the magnitude of the field is clearly unreliable. The zero crossing between R = 20 and R = 40 occurs at substantially different distances. These discrepancies probably arise because two relatively large numbers are differenced in the calculation of U_θ. Both fields show the same trends of amplification or reduction with respect to the half-space field although the position of zero crossings and maxima or minima may occur at different values of R. Because of the general agreement of the other fields and the nature of the discrepancy for this case, the integration procedure is accepted as adequate for the purposes of this work.

The procedure described above can only give an adequate approximation to kernels for simple layered models which have the source in the uppermost layer and which have a lowermost half-space with the same properties as the uppermost layer. These two conditions insure that the subtraction of the half-space solution, as described earlier, determines the proper field for very large and very small values of r (very small and very large values of k, respectively). It may then be possible to obtain a satisfactory approximation by the simple procedure given previously, but, since the procedure is only loosely constrained, it may fail by choosing too large a value

of A_ℓ or too small a value of α_ℓ. Since the results obtained were sufficient for the points to be made here, improvement in the integration was not undertaken. It is recommended that any future applications of the theory presented in Chapter 4 use a different integration procedure. A detailed consideration of a better procedure is not attempted here, but two points are worth mentioning. The process of subtracting out the kernel for a half-space with the source layer properties is advantageous in any case. This portion is easily integrated in closed form and for shallow sources it is precisely this part of the integrand which will cause the greatest difficulty in the integration for large values of r. Numerical integration will tend to be difficult for large r because of the rapid oscillation of $J_n(kr)$. A more precise method of analytic integration than the one used here may be practicable for all values of k. In any event it should be particularly advantageous to use an analytic approximation for small values of k since this will also tend to eliminate integration problems for large r.

Appendix 16

ADDITIONAL INFORMATION ON PERMANENT TILT AND STRAIN OBSERVATIONS

As noted in Chapter 7 an attempt was made to determine the time duration during which the permanent tilt and strain offsets occurred. The records from which the offsets were determined run at 3/8 inch per hour or about 6 minutes per millimeter. The precision with which relative time can be read depends on the sharpness of the pen line, noise level, and signal level. Under the best of conditions a relative time of one minute might be achieved, but a figure of two minutes is a better estimate of the reading error for the best of the observations reported here. For some of the observations the reading error may be considerably greater due to blurring or fading of the pen line. For observations where the line was not blurred or faded the principal limitation in reading precision was the presence of large amplitude signal. The estimates of the time interval during which offset occurred for each case treated in the text are listed in Table A16-1. These are all estimates of an upper bound since all the records are consistent with the offset occurring instantaneously.

For the three earthquakes listed in Table A16-1 it is not possible to distinguish the occurrence of the offset as associated with any particular phase on the seismogram. In the case of the

Fox Island earthquake listed in Table A16-2 the occurrence of the offset recorded on the NW-SE tiltmeter is clearly associated with the time interval during which surface waves arrive. The offset takes place during a time interval of 16 ± 2 min to 22 ± 2 min after the origin time. Wideman and Major (1967) report that strain steps arrive at times characteristic of surface waves.

The offsets listed in Chapter 7 were all recorded on direct records. For the direct records the signal is amplified but not subject to any filtering. The strainmeters are also recorded at higher speed after passing through a high pass filter. By studying the filtered records it was attempted to determine the nature of the response and the sense of the input (positive or negative) for the strainmeters for the Parkfield earthquake. The filtered records for the Parkfield and Baja earthquakes were compared with the instrument response to a step function input and an impulse input. The results are tabulated in Table A16-3. The NW-SE strainmeter for the Parkfield earthquake showed a response which was reasonably clearly impulse-like, but it was not possible to clearly identify the instrument response with either a step function or impulse response in the other cases. A judgment of the nature of the response is given in Table 16-3. Both records for the Parkfield earthquake are judged more impulse like than step-like and this alone makes their use to determine the sense of a step-like offset questionable. In addition and more important the NE-SW filtered strain record for the Baja earthquake indicates extension while

the direct record shows compression. For this case the noise level on the filtered record is such that a compressive step function response could have been overridden by the noise, but this is judged unlikely. It was decided that the filtered strain record could not be used to estimate the sense of a possible offset.

Excluding the three events discussed in the main text, nineteen events were closely checked for permanent offsets on the tilt or strain records. Eleven of these were chosen from Wideman and Major's (1967) list; two were nuclear events; the rest were chosen either because of their proximity to Isabella or by scanning the records. Except for four there was no indication of a permanent offset for any of these events or for many other events which were scanned in the records. Of the four events which gave at least some indication of an offset, three showed a clear offset on at least one instrument. The three are listed in Table A16-2. As in the main text there is an estimate of the maximum possible variation after each observation.

There were records available for one or more of the two tilt and two strain components at Isabella for thirteen of the sixteen distant earthquakes for which Wideman and Major report strain steps. Of the thirteen, three showed at least one definite permanent offset, the Parkfield and Baja earthquakes treated in the main text and the Southern Nevada earthquake which is given in Table A16-2. None of the other ten earthquakes showed any definite

offsets. Considering the precision with which the instruments can be read and possible azimuthal variations in the deformational fields no definite conclusion can be reached about the consistency of Wideman and Major's data and the Isabella data. The earthquake which comes closest to being inconsistent is the Northern California (Truckee) earthquake. An estimate of the upper bound for a possible offset is given in Table A16-2. Wideman and Major report a strain step of 10^{-10} to 10^{-9} for this earthquake at a distance of 1260 km. Isabella at about 450 km from the earthquake shows that any permanent strain is less than 7×10^{-10}.

Static models were not constructed for the three earthquakes in Table A16-2 which show offsets. The theory developed is not adequate at the distance of the Fox Island earthquake. In this case however even a rough calculation shows that the observed tilt is very large. The earthquake at Isabella shows offsets on both tiltmeters and both strainmeters. It is so close to Isabella that the error in epicentral location can accommodate any azimuth from the recording site.

Appendix 17

ESTIMATE OF AVERAGE SLIP DURING THE PARKFIELD EARTHQUAKE FROM GEODIMETER DATA

Hofmann (1967) determined the relative movement between the two sides of the San Andreas fault from measurements with a geodimeter net before and after the Parkfield earthquake. The time interval between measurements was about 9 months, from October, 1966 to July, 1967. A line some 4.5 km west of the middle of the San Andreas fault zone in the Parkfield-Cholame area was assumed fixed. The relative motion of three points about 7 to 11 km east of the middle of the fault zone were determined. The relative motion was dominantly right lateral, strike-slip parallel to the average trace of the fault although there were a few centimeters of motion perpendicular to the fault trace at two of the stations. From Hofmann's data the geometry and relative motions shown in Figure A17-1 were determined. Figure A17-1 is a modification of a figure from a preprint of a publication which included the data presented by Hofmann in 1967.

Knopoff's (1957) two dimensional solution for an infinitely long, vertical strike-slip fault in a half-space was used to estimate the average slip for the Parkfield earthquake. Let r_1 be the distance along the surface of the half-space on a line

perpendicular to the fault trace to a point west of the fault trace. r_2 is similarly defined for a point on the same line east of the fault trace. "west" and "east" are used according to Figure A17-1 where r_1 and r_2 are labeled for one observation point. Let $U_z(r,o)$ be the motion parallel to the fault trace at a perpendicular distance r along the surface of the half-space. Then using Knopoff's (1957) results

$$U_z(r_1, o) - U_z(r_2, o) =$$

$$A_o \left[(r_1^2 + a^2)^{\frac{1}{2}} + (r_2^2 + a^2)^{\frac{1}{2}} - r_1 - r_2 \right] \qquad \text{(A17-1)}$$

where a is the fault depth and A_o is a constant. By assuming a value of a the constant A_o can be determined. The displacement jump across the fault plane at the surface is

$$\Delta U_z(o,o) = 2\, A_o\, a \quad .$$

The distribution of the displacement jump with depth is

$$\Delta U_z(o,x) = 2\, A_o\, (a^2 - x^2)^{\frac{1}{2}} \qquad |x| < a$$

where x is the depth beneath the surface. From this the average displacement jump is

$$\overline{\Delta U}_z = \frac{\pi}{4} U_z(o,o) \quad .$$

Using these formulas the values of $\Delta U_z(o,o)$ listed in Table 17-1 were calculated for the fault depths and other parameters shown. Since Eaton's (1967) observations show that the great majority of aftershocks occurred above 12 km depth, the values of $\Delta U_z(o,o)$ of 37 cm., 32 cm., and 30 cm. were chosen as representative. These give a $\overline{\Delta U}_z$ of about 26 cm. for a fault depth of 12 km. which are the figures used in Chapter 7. Assuming the fault length fixed, the relative source strength is determined by the product of $\overline{\Delta U}_z$ and the fault depth. Use of a 6 km fault depth would decrease the source strength by about 25%; use of a 24 km fault depth would increase the source strength by about 50%.

The above estimate assumed that all the relative displacement observed by Hofmann occurred during the earthquake. Smith and Wyss (1968) attributed about 10 cm of surface displacement to the earthquake, over 3 times less than the total figure determined above. Using Chinnery's (1961) results for a surface with depth the effect of the finite length of the fault compared with the infinite fault length used above can be estimated. Assuming a fault depth of 1 unit and a surface observation station 1 unit from the center of the fault,

then the ratio of the lateral displacement to the lateral displacement due to an infinitely long fault is about .74 for a fault length of 4 units and .42 for a fault length of 2 units. For Parkfield the ratio of fault length to fault depth is about 3 to 4, so the calculation used above should underestimate the source strength by a factor of about 1.2 to 2 if the finite length of the fault were considered. The average displacement and fault depth determined above is judged likely to be within a factor of 2 to 3.

Appendix 18

FAULT PLANE SOLUTION FOR THE BAJA EARTHQUAKE

The fault plane solution for the Baja earthquake was determined from a first motion diagram which was constructed by projecting the first motion at a station back to the lower half of the focal sphere. The lower hemisphere of the focal sphere was plotted on a Wulff stereographic projection. A surface source was assumed and the epicenter used was that reported in the California Institute of Technology, Local Bulletin of Earthquakes (Richter, 1967). The origin of the ray was determined using tables given in Ritsema (1958), except that stations at distances less than 11° were also assumed to be coming from the approximate origin of P_n on the focal sphere. The records were from the long period instruments of the World-Wide Standard Seismograph Net (Powell and Fries, 1966) with a few points from the long period instruments of the California Institute of Technology network.

Figure A18-1 shows the first motion determinations and identifies a few of the stations which are referred to later. Figure A18-2 shows amplitude data and a rough indication of the type of S-motion at some of the stations. The amplitude data are for the first peak in the record. It is on an arbitrary scale, corrected for the magnification of the instrument, but not corrected for the period of the pulse. In Figure A18-2 stations at less than

11° from the source are projected on to the portion of the focal sphere which approximates the region where P_n originates. The estimate of that portion of the focal sphere is indicated by a double headed arrow. The station JCT was excluded since it was clearly reversed and not critical in the interpretation.

The presence of a nodal line at an azimuth of about 53° is easily determined from the data. The exact position of the other nodal line is not determined very accurately. Within the error of the epicentral location (about ±.1°) the epicenter plots at the south end of the San Jacinto fault (at the north end of the Gulf of California) as given on the map in Kovach et al. (1962, p. 2846). The nodal line at an azimuth of about 53° coincides well with that expected from strike-slip motion on the San Jacinto fault and this was accepted as the fault model.

The second nodal line then essentially determines the dip of the fault plane. The position of the nodal line is not well determined by the data. This is what prompted the inclusion of amplitudes and S-wave motion at some of the stations. The California Institute of Technology stations, Riverside, Pasadena, Palomar, Barrett and San Nicolas indicate some west dip to the fault plane, but the amount of dip is poorly determined since these are P_n arrivals. The station GIE has a poorly recorded negative polarity which, if accepted, would give a nearly vertical fault plane. Sykes (1967) reports that GIE consistently shows reversed polarity compared to

other stations, and that together with the amplitudes at other South American stations led to rejection of GIE as a reliable data point. Other critical stations were either too distant or had too high a noise level to allow a very definite positioning of the nodal line. Well documented strike-slip faults on the San Andreas fault system favor a nearly vertical fault plane; however, considering all the data a nodal line which gives a dip of about 72° to the SW was chosen as the best fit. This could easily be in error by 5° and a larger error is not unlikely.

List of Tables

Table 5-1

Comparison of Results from Asymptotic Calculation and Numerical Calculation

R	Asymptotic for Large r UZ/UZH	Numerically Calculated UZ/UZH
5	1.300	.913
10	1.150	.971
20	1.075	1.045
30	1.050	1.042
40	1.038	1.034
50	1.030	1.029

ℓ	λ km	T sec Model G	T sec Model G3	Difference % b	T sec Model G4	Difference % c
2	20,000	2645.50	2645.88	.014	4755.63	79.76
5	7,280	1081.41	1081.79	.035	1797.48	66.22
10	2,670	621.77	622.32	.088	915.25	47.20
20	1,950	361.07	361.79	.20	465.26	26.36
40	988	202.14	202.90	.38	235.11	16.31
80	497	108.00	108.76	.70	118.36	9.59
160	249	56.19	57.05	1.53	59.64	6.14

Torsional Free Oscillation Periods for Three Models

Table 6-1

Table 6-2

Ratio of Perturbation Estimate of Period Change

to Actual Period Change

ℓ	Model G1	Model G2	Model G3	Model G4
2	1.0	1.0	1.1	6200
4	1.0	1.0	1.4	3600
8	1.0	1.1	1.8	1400
20	1.0	1.1	2.0	290
50	1.0	1.1	2.2	66
100	1.0		3.0	28

Weak Layer Dimension km	Total Path Length km	Model G3 ℓ=20 %	Model G3 ℓ=160 %	Model G4 ℓ=20 %	Model G4 ℓ=160 %
40,000	40,000	.20	1.5	26.	6.1
1,000	40,000	.006	.04	.83	.16
1,000	2,000	.13	.79	16.	3.2
1,000	1,000	.25	1.6	33.	6.3
500	2,000	.10	.44	13.	1.8
500	1,000	.20	.88	26.	3.5
500	500	.40	1.8	53.	7.1

Estimated Effect of a Weak Layer

on Dispersion

Table 6-3

Table 7-1

Permanent Tilts and Strains Recorded at Isabella, California,

during Parkfield, Baja, and Borrego Mountain Earthquakes

	Parkfield Earthquake	Baja Earthquake	Borrego Mountain Earthquake
Date	June 28, 1966	August 7, 1966	April 9, 1968
Origin time	04:26:13.4 GMT	17:36:26.7 GCT	02:28:58.9 GCT
Epicenter	35° 57.3' N	31° 48.0' N	33° 08.8' N
	120° 29.9' W	114° 30.0' W	116° 07.5' W
Depth	4 km	33 km?	20 km
Magnitude	5.5	6.3	6.5
Tiltmeters (radius)			
NW-SE	$+7.7 \times 10^{-8} \pm .4 \times 10^{-8}$	$+4.3 \times 10^{-8} \pm .9 \times 10^{-8}$	$< \pm .2 \times 10^{-8}$
	SE end up	SE end up	upper bound
NE-SW	$>2.1 \times 10^{-8} \pm .4 \times 10^{-8}$	$+4.4 \times 10^{-8} \pm .8 \times 10^{-8}$	$< \pm .4 \times 10^{-8}$
	NE end up-lower bound	SW end up	upper bound

Table 7-1 (continued)

	Parkfield Earthquake	Baja Earthquake	Borrego Mountain Earthquake
Strainmeters			
NW-SE	off scale	$+7.1 \times 10^{-9} \pm .6 \times 10^{-9}$ extension	$-2.9 \times 10^{-9} \pm .4 \times 10^{-9}$ compression
NE-SW	off scale	$-1.03 \times 10^{-8} \pm .03 \times 10^{-8}$ compression	$+2.5 \times 10^{-9} \pm .5 \times 10^{-9}$ extension

Table 7-2

Models for the Parkfield, Baja, and Borrego Mountain

Earthquakes Based on Field Evidence

	Parkfield	Baja	Borrego Mountain
Fault Length	38 km	100 km	50 km
Fault Depth	12 km	20 km	20 km
Average Right-Lateral Strike-slip Offset	26 cm	83 cm	38 cm
Average Dip-Slip Offset	Up to 12.7 cm SW up	Up to 11.5 cm SW up	Up to 20 cm SW up
Azimuth of Fault Plane	318° ± 6°	318° ± 6°	318° ± 9°
Dip of Fault Plane	90° 85° SW to 88° NE	72° SW 60° SW to 90°	90° 80° SW to 80° NE
Distance from Source to Isabella	175 ± 10 km	568 ± 50 km	355 ± 20 km
Azimuth from Source to Isabella	96° ± 4°	321° ± 3°	323° ± 1°

Table 7-3

Source and Structure Parameters for Some Theoretical Models of the Parkfield Earthquake

Model	Source-Station Angle	Station-Instrument Angle	Source Strength cm^3	Dip of Fault Plane	Source Depth km	Layer	Thickness km	Rigidity
A	138°	2.1°	1.14×10^{14}	90°	4	1	40	1.
						2	40	.01
B	138°	2.1°	1.14×10^{14}	90°	4	1	40	1.
						2	40	.1
C	138°	2.1°	1.14×10^{14}	90°	4	1	40	1.
						2	40	1.
D	138°	2.1°	3.00×10^{13}	90°	4	1	40	1.
						2	40	1.

Table 7-4

Source and Structure Parameters for Some Theoretical Models of the Baja Earthquake

Model	Source-Station Angle	Station-Instrument Angle	Source Strength cm^3	Dip of Fault Plane	Source Depth km	Layer	Thickness km	Rigidity
A	353°	355.6°	1.66×10^{15}	90°	75	1	100	1.
						2	100	.01
B	353°	345.6°	1.66×10^{15}	72° SW	75	1	100	1.
						2	100	.01
C	2.8°	6.7°	1.66×10^{15}	72° SW	6	1	60	1.
						2	60	.01
D	2.8°	6.7°	1.66×10^{15}	72° SW	6	1	60	1.
						2	60	1.

Table 7-5

Source and Structural Parameters for Some Theoretical

Models of the Borrego Mountain Earthquake

Model	Source-Station Angle	Station-Instrument Angle	Source Strength cm^3	Dip of Fault Plane	Source Depth km	Layer	Thickness km	Rigidity
A	356°	0.3°	3.8×10^{14}	90°	30	1	60	1.
						2	60	.01
B	5°	16.3°	3.8×10^{14}	90°	30	1	60	1.
						2	60	.01
C	356°	355.3°	3.8×10^{14}	90°	3.8	1	38	1.
						2	38	.01
D	5°	4.3°	3.8×10^{14}	90°	6	1	60	1.
						2	60	1.

Table A1-1

Observed P-ratios, S/P-ratios, and P-residuals with

"standard deviation factor" and "standard error factor"

all referenced to UBO

Station	P-ratio	"Standard Deviation Factor"	"Standard Error Factor"	Number of Observations
TFO	.6	$\times\div$ 2.5	$\times\div$ 1.1	61
WMO	.9	2.5	1.1	56
CPO	1.6	2.4	1.1	46
BMO	.6	2.2	1.1	58
	S/P-ratio			
TFO	1.2	$\times\div$ 2.6	$\times\div$ 1.2	34
WMO	2.3	3.2	1.3	24
CPO	1.8	2.0	1.2	10
BMO	4.0	4.1	1.4	21
KN	1.6	2.6	1.3	13
MN	2.0	3.2	1.5	7

Table A1-1 (continued)

Station	S/P-ratio	"Standard Deviation Factor"	"Standard Error Factor"	Number of Observations
JP	1.8	1.8	1.4	8
PG	2.7	2.4	1.2	15
	P-residual (seconds)	Standard Deviation	Standard Error	
TFO	+.4	±.8	±.1	55
WMO	-.6	1.3	.2	40
CPO	-.8	1.3	.2	37
BMO	-.7	1.0	.1	51

Table A1-2

Summary of P-ratios and S/P-ratios

Station	P-ratio P_{STA}/P_{UBO}	S/P-ratio $(S/P_{STA}/(S/P)_{UBO}$	S_{STA}/S_{UBO}*
TFO	.6	1.2	.7
WMO	.9	2.3	2.0
CPO	1.6	1.8	2.9
BMO	.6	4.0	2.4

*Derived by multiplying the S/P-ratio by the P-ratio.

Table A1-3

Calculated Q^P, Q^S, and Q^P/Q^S.						Q Values Assumed for WMO								
UBO			TFO			WMO (assumed)			CPO			BMO		
Q^P	Q^S	Q^P/Q^S	Q^P	Q^S	Q^P/Q^S	Q^P	Q^S	Q^P/Q^S	Q^P	Q^S	Q^P/Q^S	Q^P	Q^S	Q^P/Q^S
						X_1 = 100 km								
-	4.8	-	97	3.3	29	∞	∞		-	-	-	97	-	-
-	4.7	-	81	3.3	25	500	200	2.5	-	-	-	81	-	-
137	4.3	32	49	3.1	16	100	40	2.5	-	-	-	49	-	-
58	3.9	15	33	2.8	12	50	20	2.5	187	-	-	33	131	.3
10	2.2	4.7	9.1	1.8	5.0	10	4	2.5	12	6.4	1.8	9.1	4.8	1.9
						X_1 = 400 km								
-	19	-	387	13	29	∞	∞		-	-	-	387	-	-
752	18	43	218	12	18	500	200	2.5	-	-	-	218	-	-
107	13	8.3	79	9.9	8.0	100	40	2.5	158	742	.2	79	69	1.1
52	9.8	5.3	44	8.0	5.6	50	20	2.5	61	38	1.6	44	25	1.7
10	3.3	3.0	9.8	3.1	3.2	10	4	2.5	10	4.4	2.3	9.8	4.2	2.3

Table A1-4

Comparison of Station Residuals

Station	This Report	Carder, et al	Cleary and Hales	Herrin
UBO	+.4	-.3	+.0	+.10
TFO	+.7	+1.0	+.7	+.64
WMO	-.3	-.1	-.9	-.70
CPO	-.5	-.5	-1.1	-.73
BMO	-.4	-.7	-.2	-.41

Table A1-5

Calculated Q^s		Q Values Assumed for BMO		
UBO	TFO	WMO	CPO	BMO (assumed)
Q^s	Q^s	Q^s	Q^s	Q^s
	X_1 = 100 km.			
45	33	265	-	∞
41	31	173	-	500
31	25	73	187	100
24	20	42	65	50
8.2	7.7	9.6	10	10
	X_1 = 400 km			
179	130	1060	-	∞
132	103	340	1190	500
64	57	91	113	100
39	36	48	53	50
9.5	9.3	9.9	10	10

Table A 10-1

CONSTANTS IN FORMULAS FOR F(n,m)

n	d_{An}	d_{Bn}	d_{Cn}
0	1		
1	1	1	
2	1	3	3
3	3	3	15
4	3	15	15
5	15	45	315
6	45	315	315
7	315	315	945
8	315	2835	14175
9	2835	14175	155925
10	14175	155925	155925
11	155925	467775	6081075
12	467775	6081075	

Table A 10-2

Polynomials A_n for F(n,m)

n	z^0 +	z^2 −	z^4 +	z^6 −	z^8 +	z^{10} −	z^{12} +
0	1						
1	1						
2	1	3					
3	3	5					
4	3	30	35				
5	15	70	63				
6	5	105	315	231			
7	35	315	693	429			
8	35	1260	6930	12012	6435		
9	315	4620	18018	25740	12155		
10	63	3465	30030	90090	109395	46189	
11	693	15015	90090	218790	230945	88179	
12	231	18018	225225	1021020	2078505	1939938	676039

Table A 10-3

Polynomials B_n for F(n,m)

n	Z^0 +	Z^2 −	Z^4 +	Z^6 −	Z^8 +	Z^{10} −
1	1					
2	1					
3	1	5				
4	3	7				
5	1	14	21			
6	5	30	33			
7	5	135	495	429		
8	35	385	1001	715		
9	7	308	2002	4004	2431	
10	63	1092	4914	7956	4199	
11	21	1365	13650	46410	62985	29393
12	231	5775	39270	106590	124355	52003

Table A 10-4

Polynomials C_n for F(n,m)

n	Z^0 +	Z^2 -	Z^4 +	Z^6 -	Z^8 +
2	1				
3	1				
4	1	7			
5	1	3			
6	1	18	33		
7	15	110	143		
8	1	33	143	143	
9	7	91	273	221	
10	7	364	2730	6188	4199
11	21	420	2142	3876	2261

Table A15-1

Comparison of Fields from Different Approximations to the Same Structure

	Approximation 1	Approximation 2	Approximation 1	Approximation 2
R	UZ/UZH	UZ/UZH	Uθ/UθH	Uθ/UθH
.25	1.000	.986	1.020	1.019
.5	1.344	1.436	1.094	1.092
1.	2.344	2.327	1.446	1.438
4.	11.992	12.002	6.132	5.959
8.	3.947	3.932	5.046	4.174
12.	-.982	-.998	5.114	3.634
20.	.292	.285	2.665	2.402
40.	.602	.617	-.634	-.107

Table A16-1

Upper Bounds on Time Interval During Which Offset Occurred

	Offset probably occurred in min	Offset almost certainly occurred in min	Comments
Parkfield Earthquake			
NW-SW tilt	3	6	Fine line.
NE-SW tilt			Could not be estimated, but appears comparable to other tilt.
Baja Earthquake			
NW-SE tilt	12	15	Blurred line.
NE-SW tilt		15	Badly faded record.
NW-SE strain	3	6	Fine line.
NE-SW strain	9	12	Blurred line.
Borrego Mtn. Earthquake			
NW-SE strain	12	18	Some blurring.
NE-SW strain	6	12	Fine line.

Table A 16-2

Permanent Tilts and Strains Observed at Isabella

Recording Station During Four Earthquakes

	Southern Nevada Earthquake	Fox Island Earthquake	Isabella Earthquake	Northern California (Truckee) Earthquake
Date	Aug. 16, 1966	July 2, 1965	Nov. 16, 1966	Sept. 12, 1966
Origin time-GCT	18:02:36.1	20:58:40.3	23:48:30.5	16:41:01.7
Epicenter	37.4 N	53.1 N	35° 42.5' N	39.4 N
	114.2 W	167.6 W	118° 26.6' W	120.1 W
Depth	33 km	60 km	-1.4 km	8 km
Magnitude	6.1	6.7	2.9	5.4
Tiltmeter (radians)				
NW-SE	$<\pm.2 \times 10^{-8}$	1.03×10^{-7}	5.3×10^{-9}	$<\pm.6 \times 10^{-8}$
		$\pm.17 \times 10^{-7}$	$\pm 1.8 \times 10^{-9}$	
		NW end up	SE end up	

Table A 16-2 (continued)

	Southern Nevada Earthquake	Fox Island Earthquake	Isabella Earthquake	Northern California (Truckee) Earthquake
Tiltmeter (radians)				
NE-SW	No record	No record	2.37×10^{-8} $\pm.47 \times 10^{-8}$ SW end up	$<\pm.6 \times 10^{-8}$
Strain Meters				
NW-SE	$<\pm.2 \times 10^{-9}$	$<\pm.6 \times 10^{-9}$	3.7×10^{-10} $\pm 1.2 \times 10^{-10}$ extension	$<\pm.7 \times 10^{-9}$
NE-SW	1.3×10^{-9} $\pm.2 \times 10^{-9}$ compression	$<\pm.5 \times 10^{-9}$	6.6×10^{-10} $\pm2.4 \times 10^{-10}$ compression	$<\pm.6 \times 10^{-9}$

Table A 16-3

Strain Offsets from Filtered Records

	Filtered Record		Direct Record
	Response	Sense	Sense
Parkfield Earthquake			
NW-SE strain	Impulse-like	Extension	No record
NE-SW strain	Mixed-more impulse-like than step-like.	Compression	No record
Baja Earthquake			
NW-SE strain	Step-like	Extension	Extension
NE-SW strain	Step-like	Extension	Compression

Table A17-1

ESTIMATES OF SURFACE DISPLACEMENT JUMP FOR THE

PARKFIELD EARTHQUAKE

$U_z(r_1, o) - U_z(r_2, o)$ cm	r_1 km	r_2 km	Fault Depth km	Surface Displacement Jump $\Delta U_z(o,o)$
20.4	4.8	6.8	6	48
			12	32
			24	26
20.8	4.4	11.1	6	55
			12	37
			24	28
19.0	3.9	7.4	6	42
			12	30
			24	24

Figure Captions

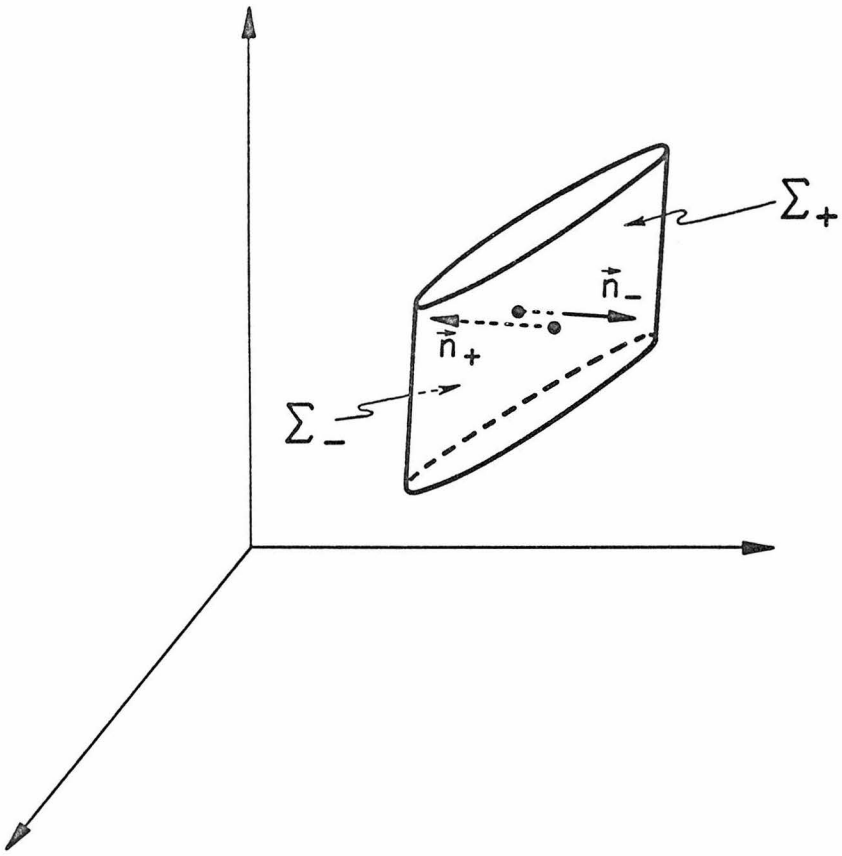

Figure 2-1

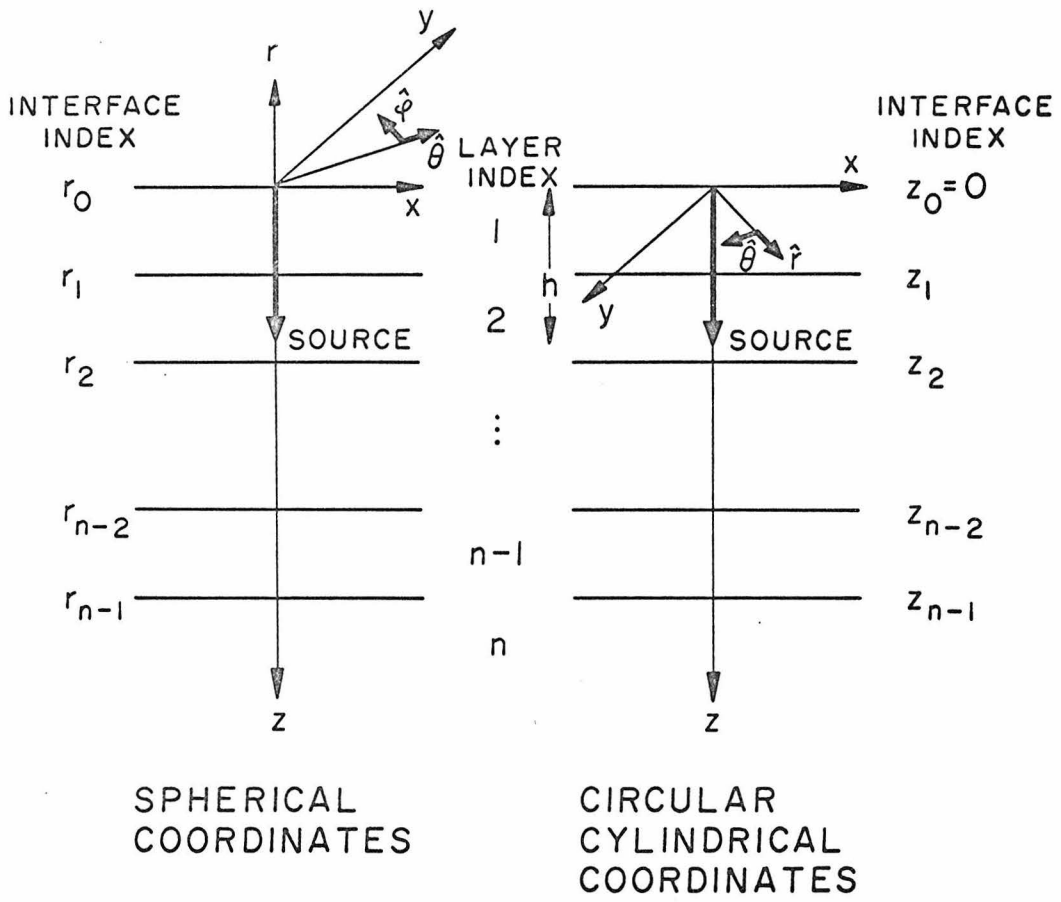
INTERFACE INDEX
LAYER INDEX
INTERFACE INDEX
r
y
x
z
SOURCE
r_0
r_1
r_2
r_{n-2}
r_{n-1}
$z_0 = 0$
z_1
z_2
z_{n-2}
z_{n-1}
1
2
n-1
n
h
$\hat{\varphi}$
$\hat{\theta}$
$\hat{r}$
SPHERICAL COORDINATES
CIRCULAR CYLINDRICAL COORDINATES

Figure 2-2

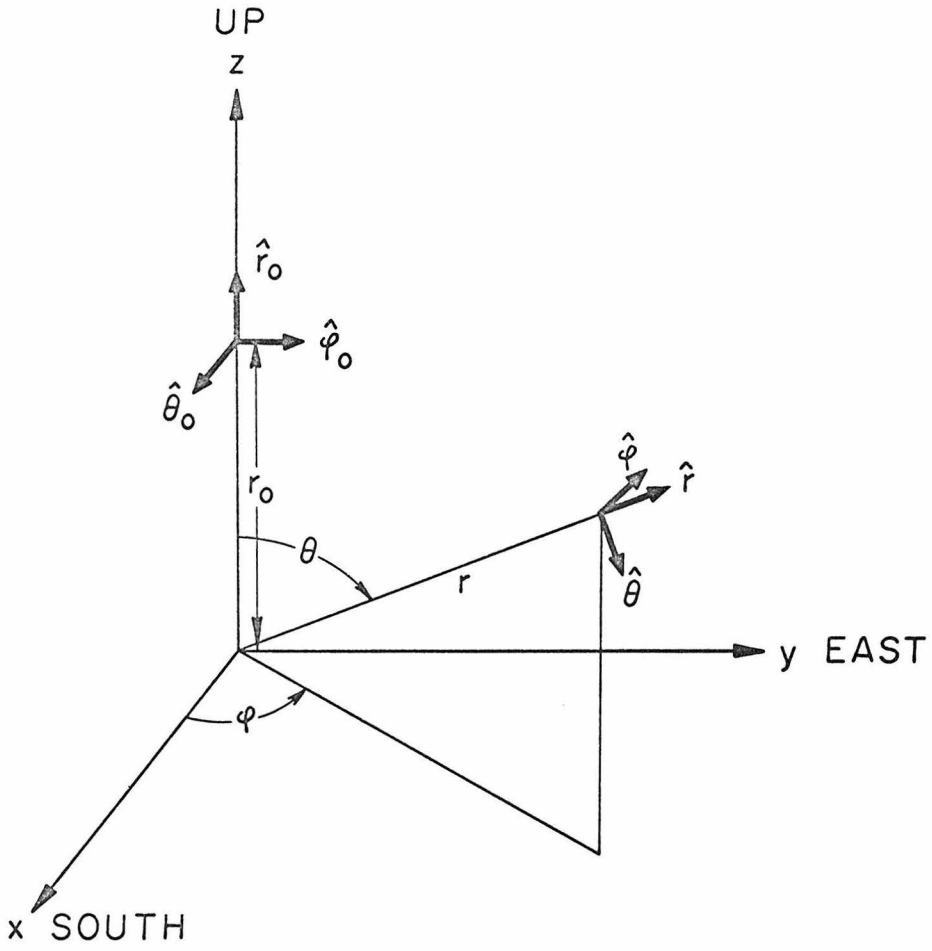
UP
z
$\hat{r}_o$
$\hat{\varphi}_o$
$\hat{\theta}_o$
r_o
θ
$\hat{\varphi}$
$\hat{r}$
r
$\hat{\theta}$
y EAST
φ
x SOUTH

Figure 3-1

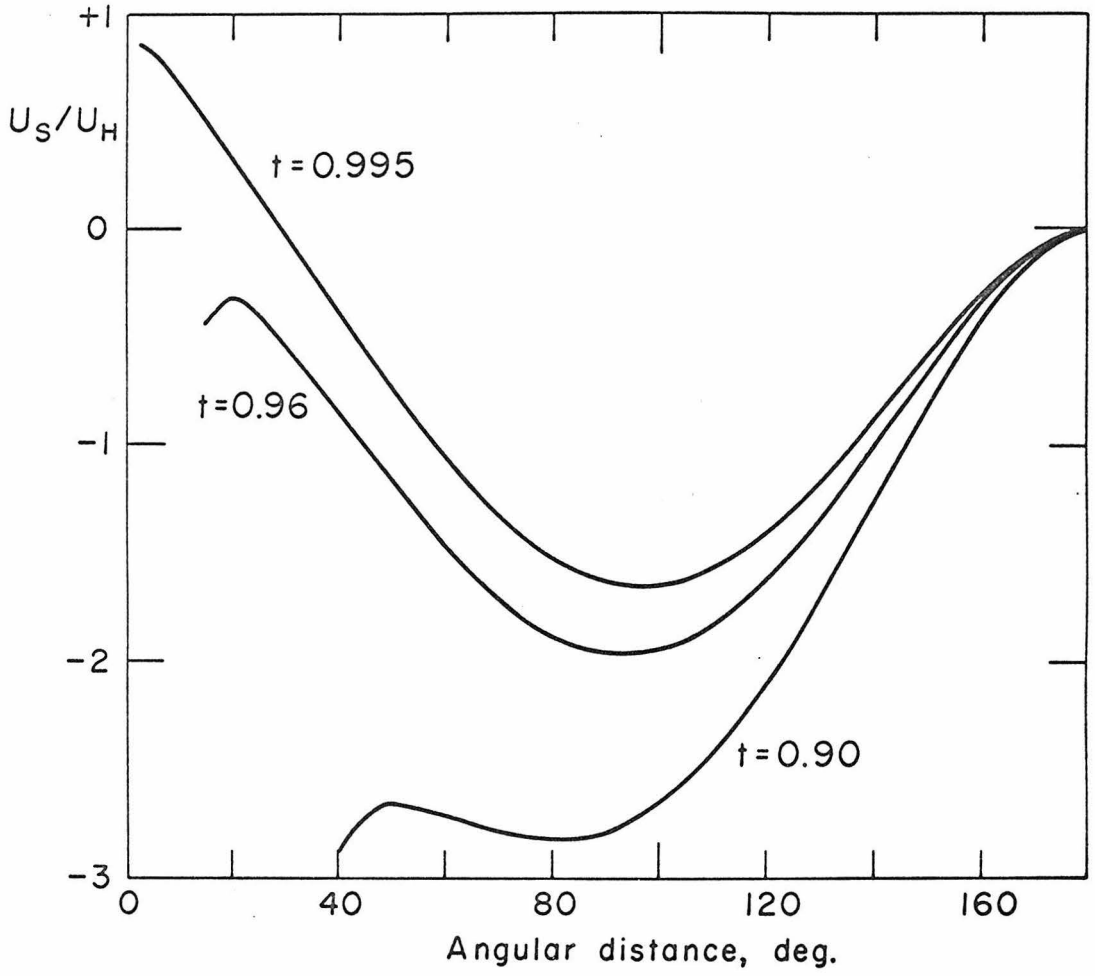
+1
U_S/U_H
0
-1
-2
-3
t = 0.995
t = 0.96
t = 0.90
0
40
80
120
160
Angular distance, deg.

Figure 3-2

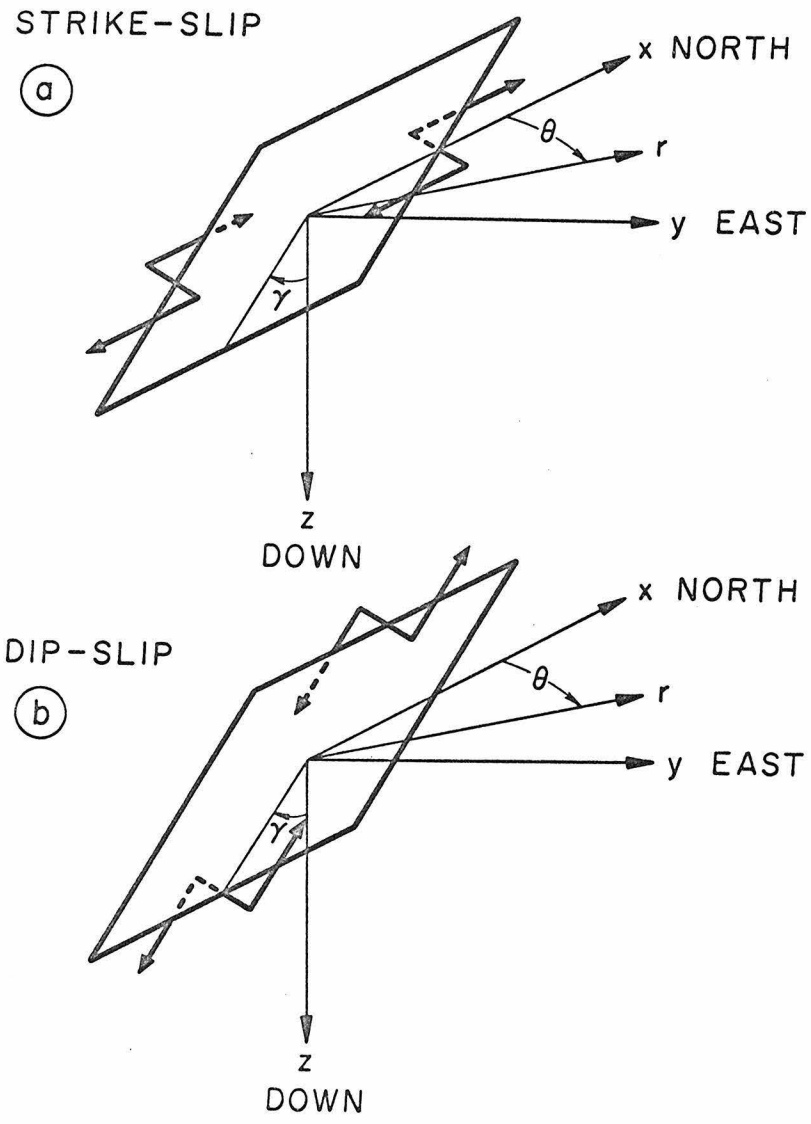
STRIKE-SLIP
a
x NORTH
θ
r
y EAST
γ
z
DOWN
DIP-SLIP
b
x NORTH
θ
r
y EAST
γ
z
DOWN

Figure 4-1

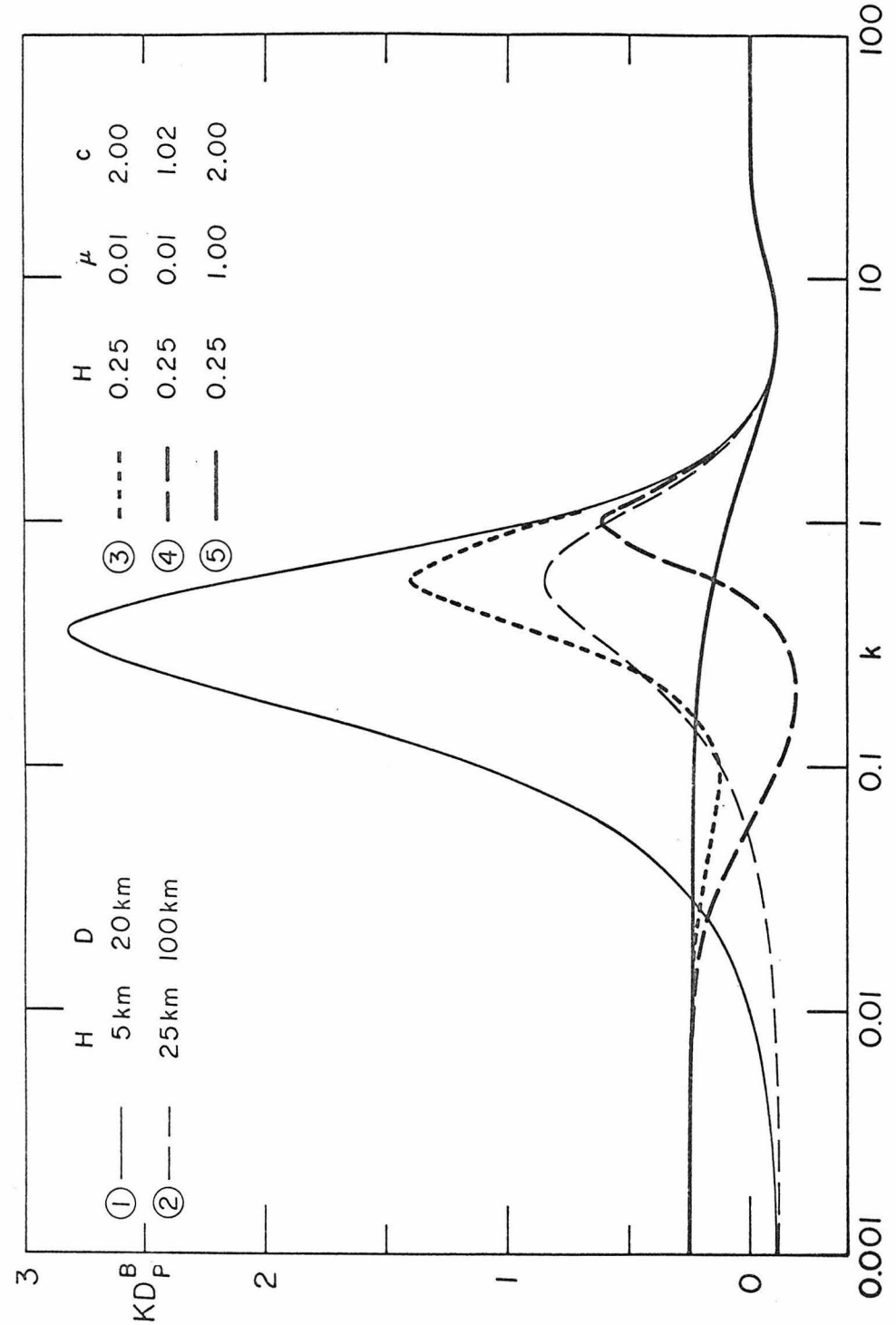
3
2
1
0
KD_P^B
0.001
0.01
0.1
1
10
100
k
H
D
① —— 5km 20km
② — — 25km 100km
H μ c
③ ---- 0.25 0.01 2.00
④ — — 0.25 0.01 1.02
⑤ —— 0.25 1.00 2.00

Figure 5-1

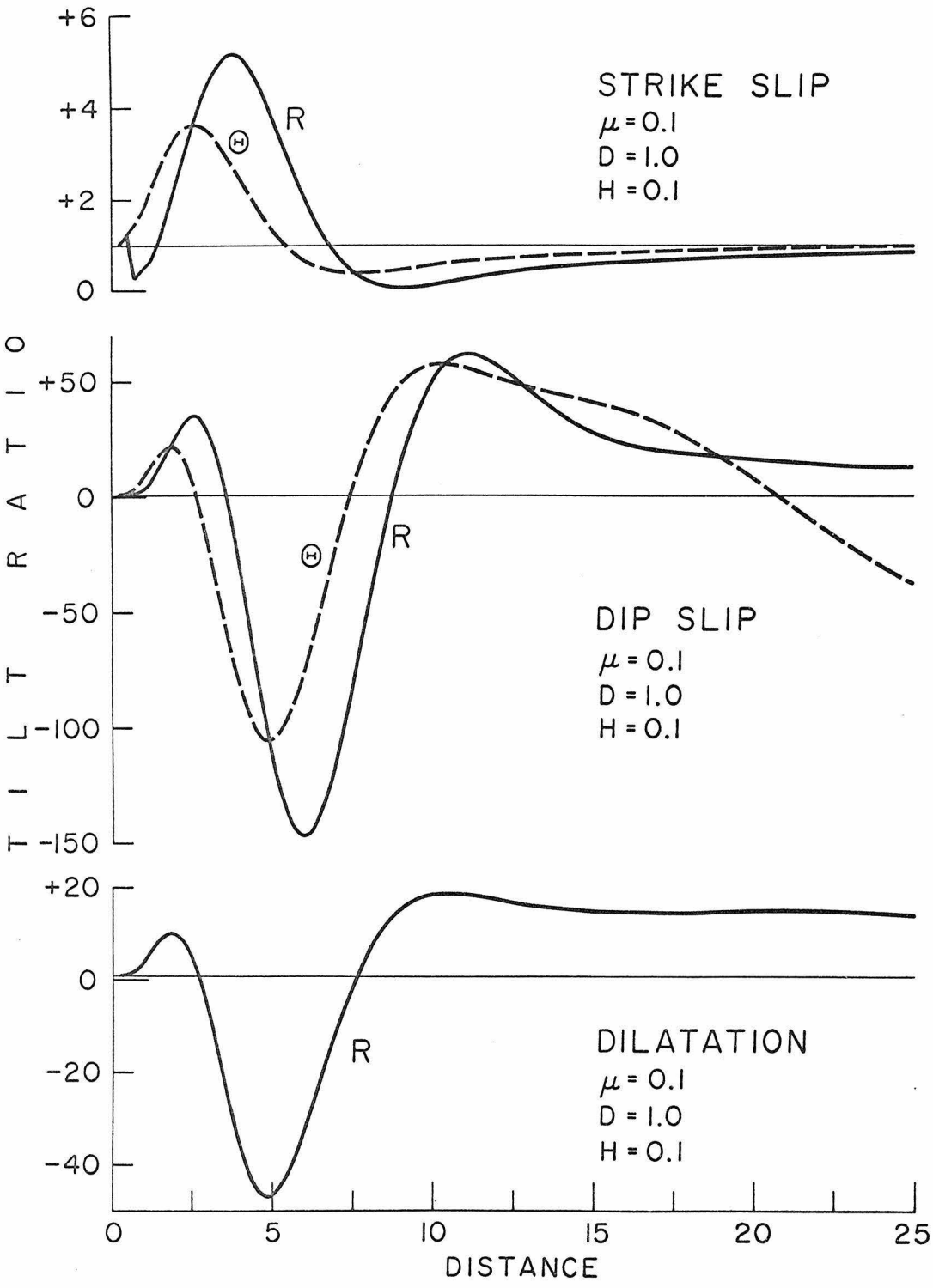
+6
+4
+2
0
R
Θ
STRIKE SLIP
μ = 0.1
D = 1.0
H = 0.1
TILT RATIO
+50
0
-50
-100
-150
Θ
R
DIP SLIP
μ = 0.1
D = 1.0
H = 0.1
+20
0
-20
-40
R
DILATATION
μ = 0.1
D = 1.0
H = 0.1
0
5
10
15
20
25
DISTANCE

Figure 5-2

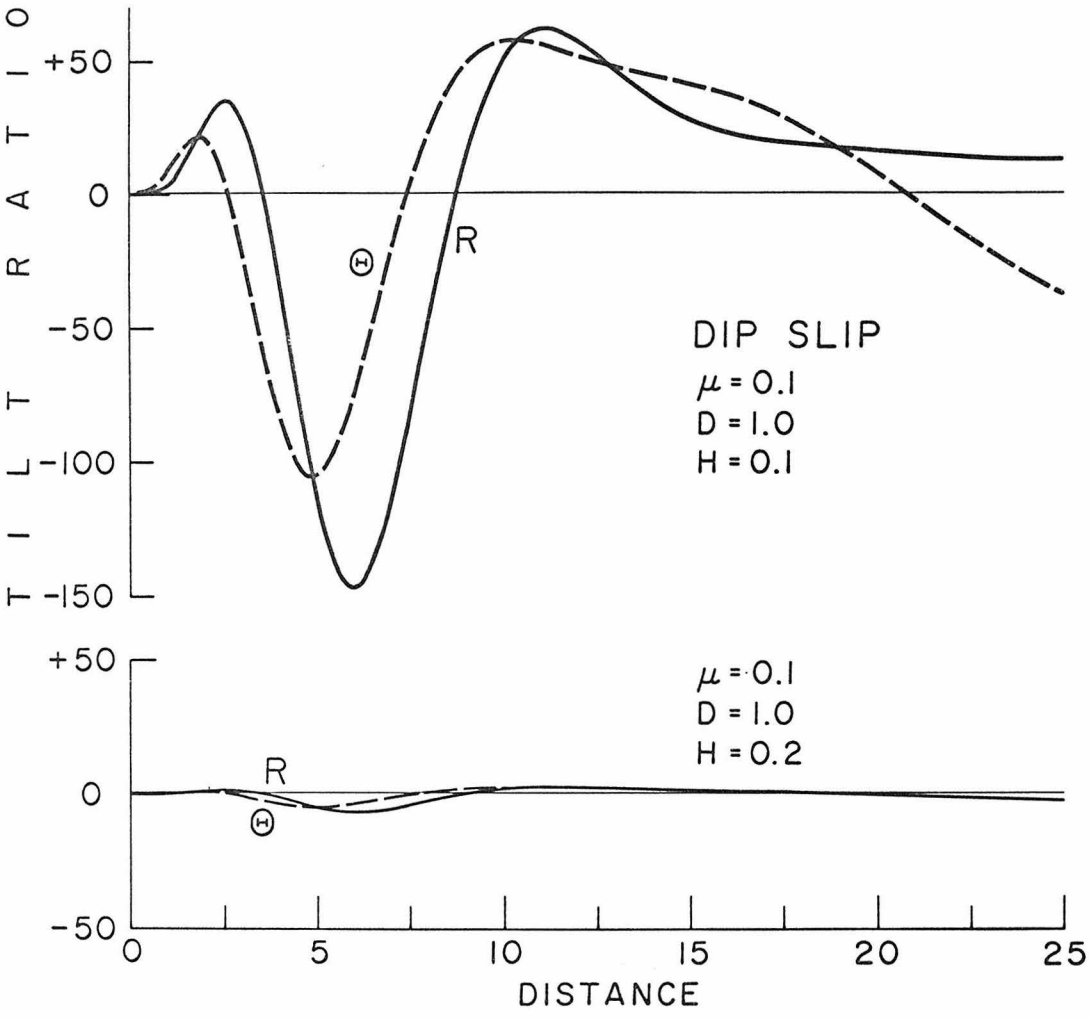
TILT RATIO
+50
0
-50
-100
-150
R
Θ
DIP SLIP
μ = 0.1
D = 1.0
H = 0.1
+50
0
-50
R
Θ
μ = 0.1
D = 1.0
H = 0.2
0
5
10
15
20
25
DISTANCE

Figure 5-3

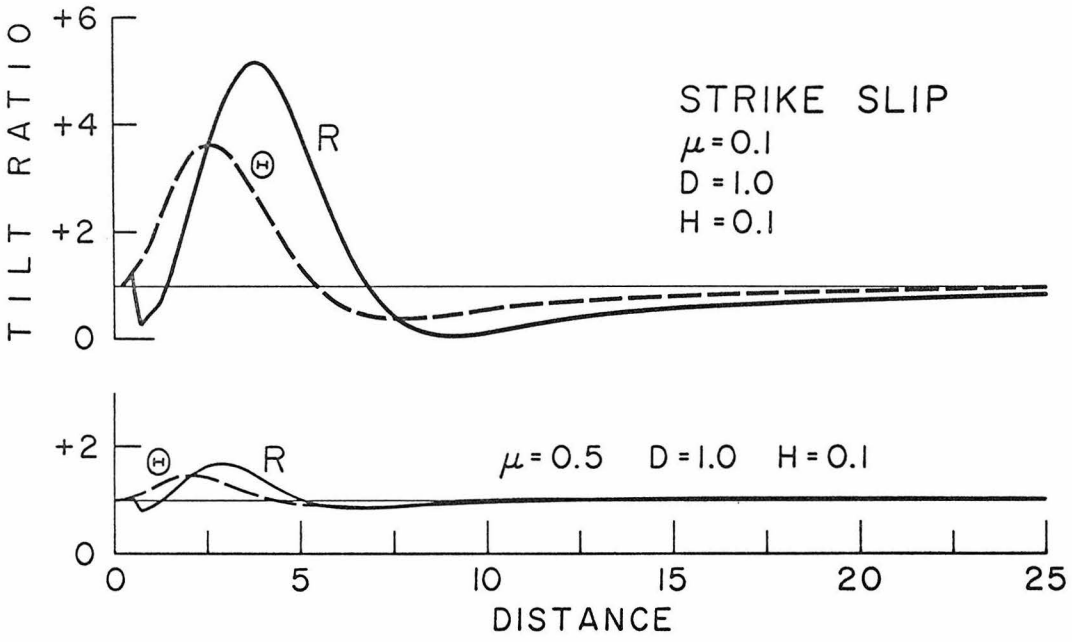
TILT RATIO
+6
+4
+2
0
R
Θ
STRIKE SLIP
μ = 0.1
D = 1.0
H = 0.1
+2
0
Θ
R
μ = 0.5 D = 1.0 H = 0.1
0
5
10
15
20
25
DISTANCE

Figure 5-4

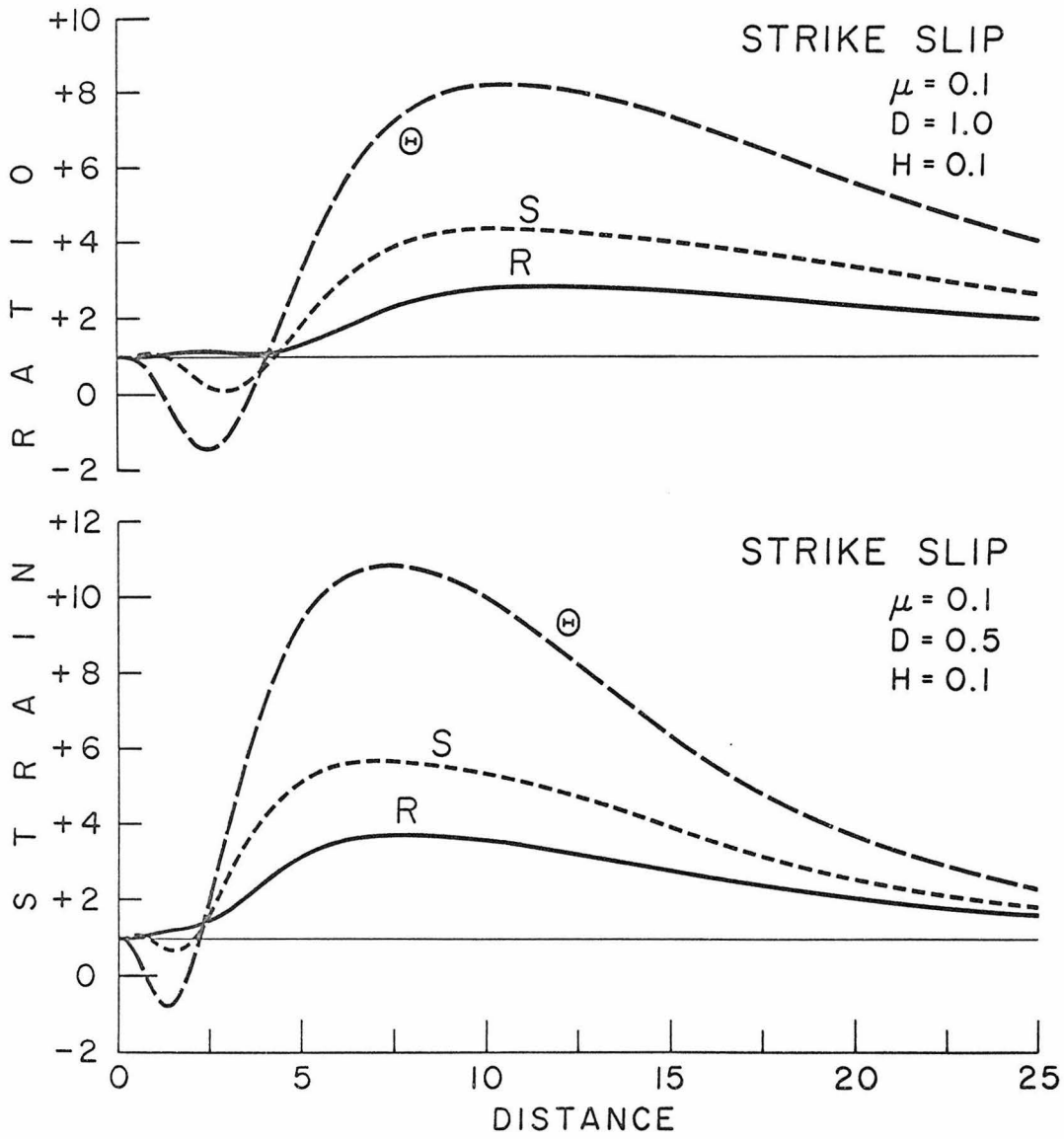
STRIKE SLIP
μ = 0.1
D = 1.0
H = 0.1
Θ
S
R
RATIO
+10
+8
+6
+4
+2
0
-2
STRIKE SLIP
μ = 0.1
D = 0.5
H = 0.1
Θ
S
R
STRAIN
+12
+10
+8
+6
+4
+2
0
-2
0
5
10
15
20
25
DISTANCE

Figure 5-5

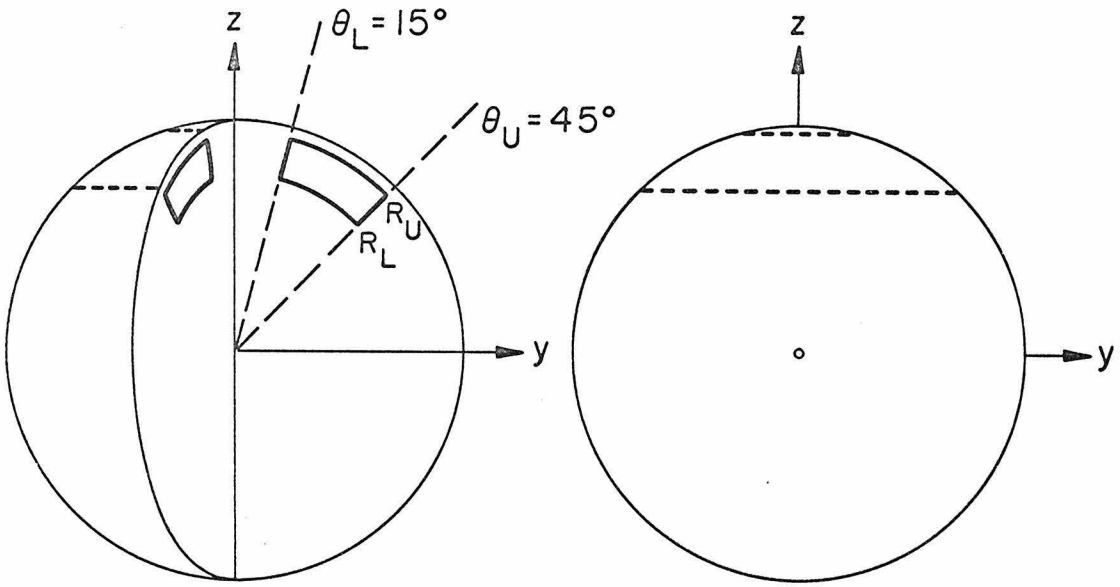

Figure 6-1

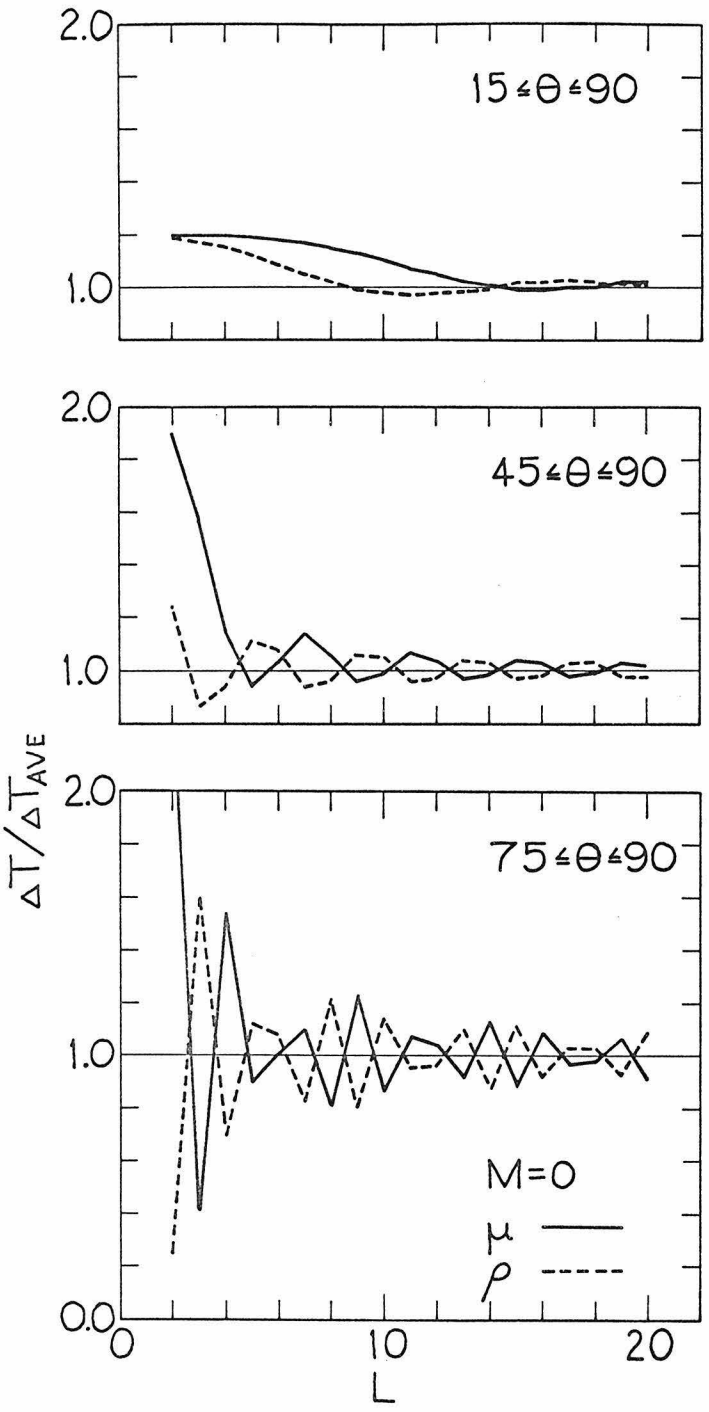

Figure 6-2

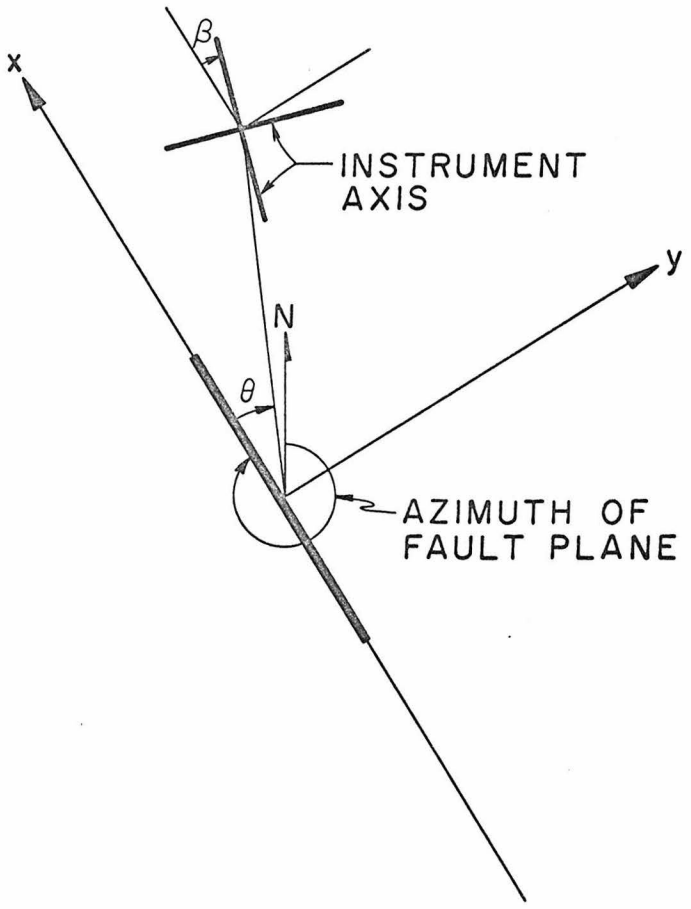

Figure 7-1

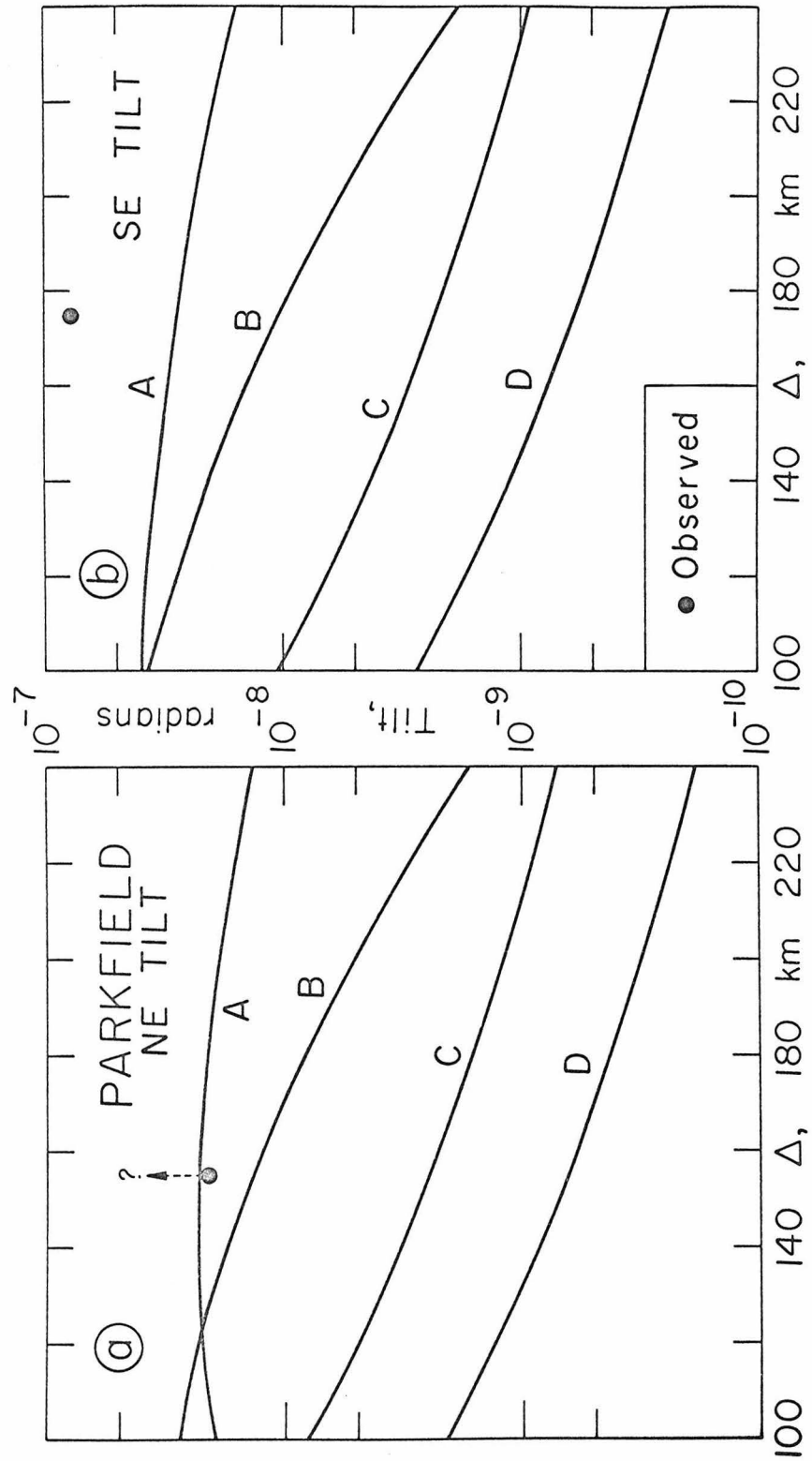
PARKFIELD
NE TILT
SE TILT
A
B
C
D
?
Observed
Tilt, radians
10^{-7}
10^{-8}
10^{-9}
10^{-10}
100
140
180
220
Δ, km

Figure 7-2

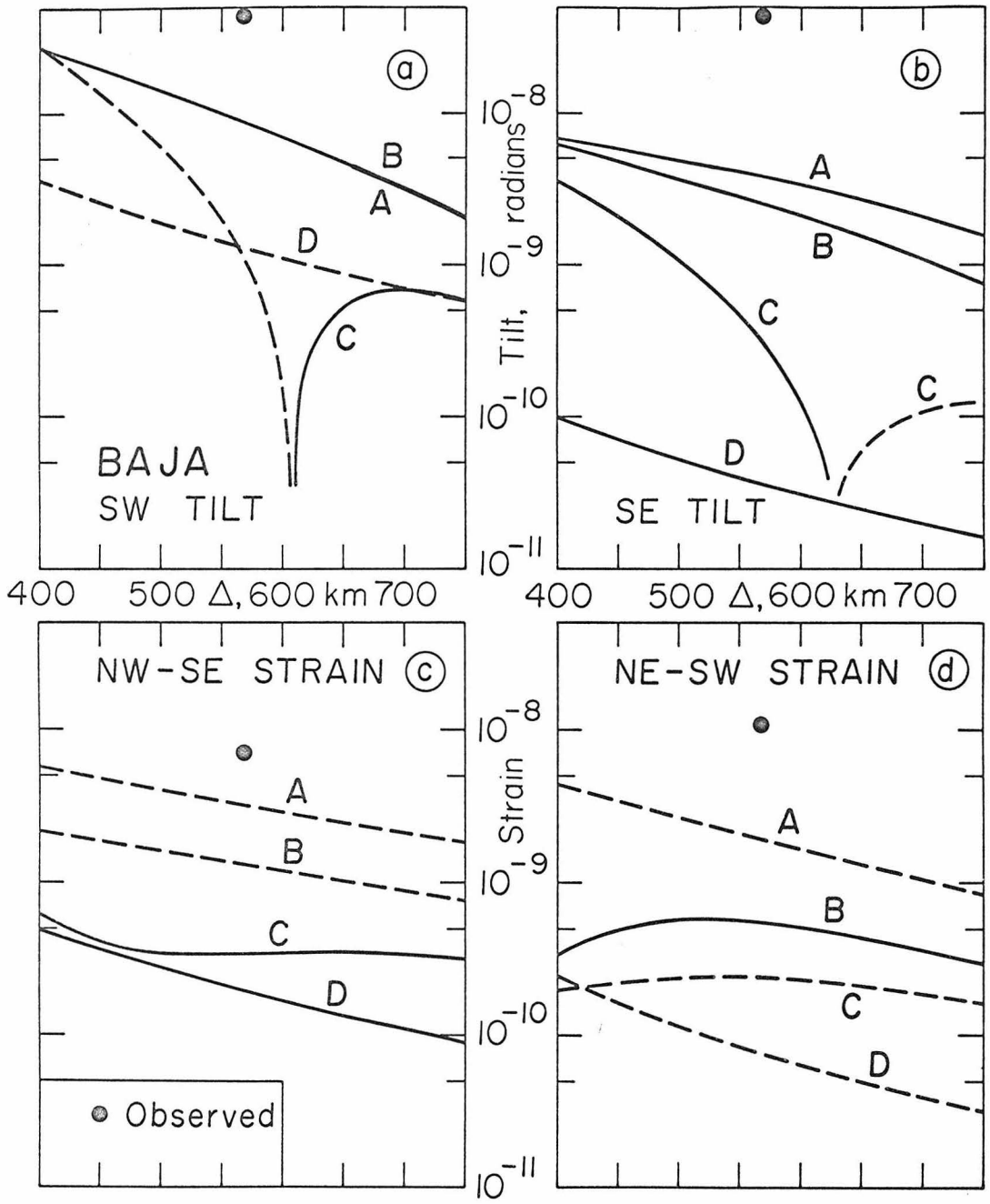
a
b
A
B
C
D
BAJA
SW TILT
SE TILT
400
500 Δ, 600 km 700
10^{-8}
10^{-9}
10^{-10}
10^{-11}
Tilt, radians
NW-SE STRAIN c
NE-SW STRAIN d
Strain
Observed

Figure 7-3

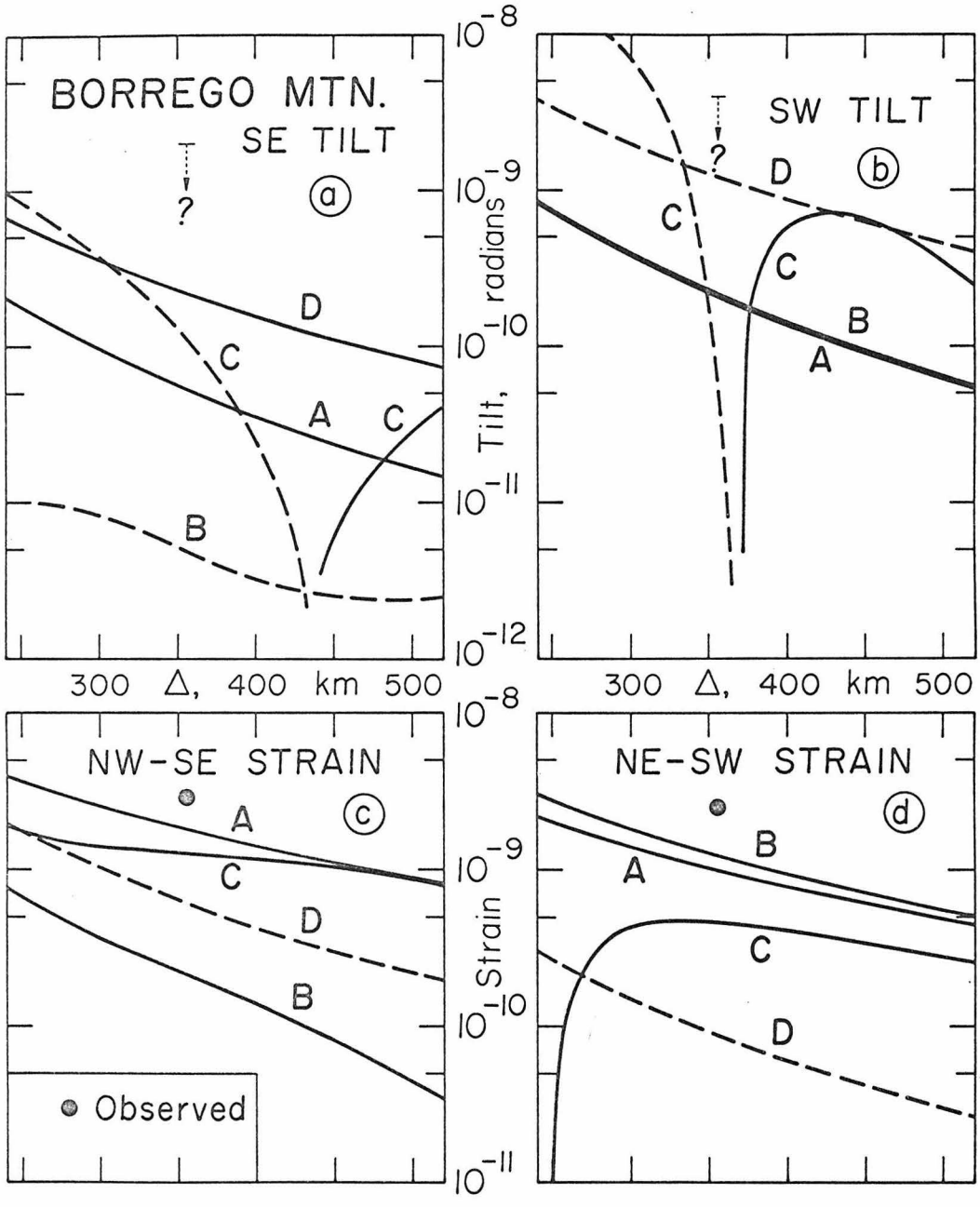
BORREGO MTN.
SE TILT
a
?
D
C
A
C
B
SW TILT
b
?
D
C
C
B
A
10^-8
10^-9
10^-10
10^-11
10^-12
Tilt, radians
300 Δ, 400 km 500
300 Δ, 400 km 500
NW-SE STRAIN
c
A
C
D
B
Observed
NE-SW STRAIN
d
B
A
C
D
Strain

Figure 7-4

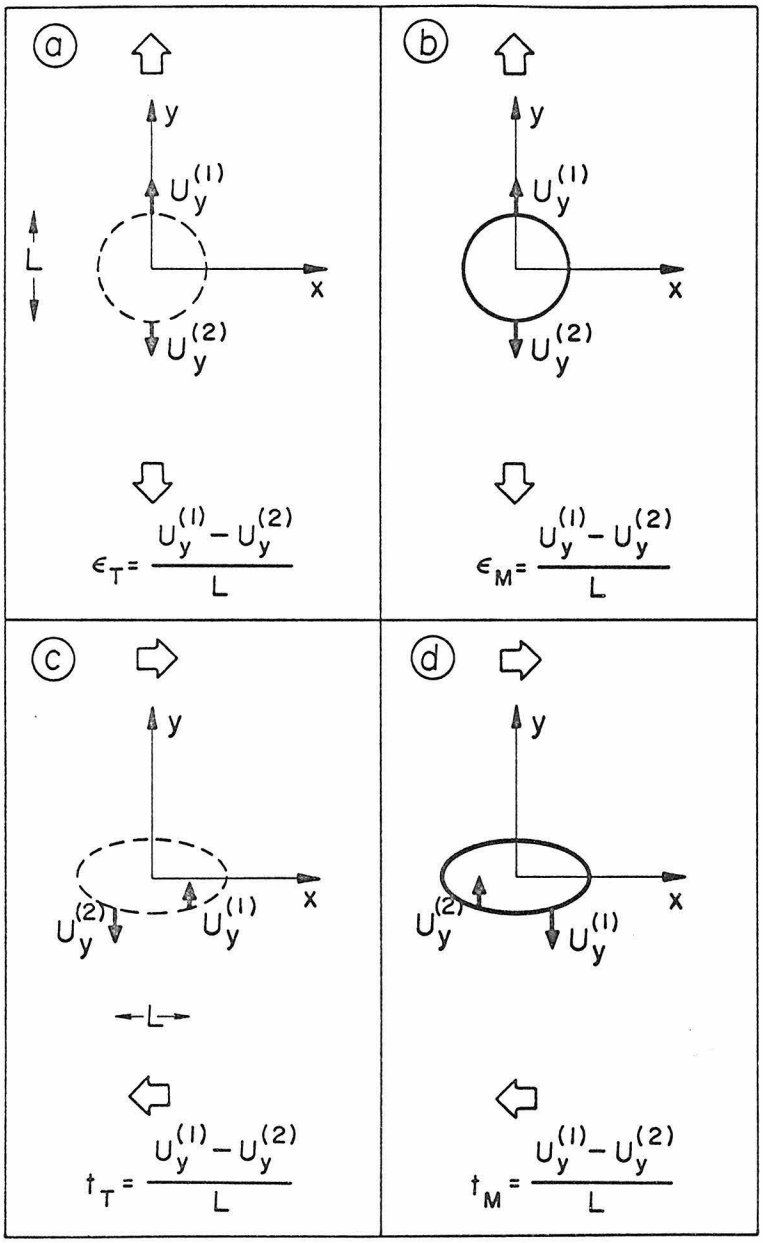
a
y
$U_y^{(1)}$
L
x
$U_y^{(2)}$
$\epsilon_T = \frac{U_y^{(1)} - U_y^{(2)}}{L}$
b
y
$U_y^{(1)}$
x
$U_y^{(2)}$
$\epsilon_M = \frac{U_y^{(1)} - U_y^{(2)}}{L}$
c
y
$U_y^{(2)}$
$U_y^{(1)}$
x
L
$t_T = \frac{U_y^{(1)} - U_y^{(2)}}{L}$
d
y
$U_y^{(2)}$
x
$U_y^{(1)}$
$t_M = \frac{U_y^{(1)} - U_y^{(2)}}{L}$

Figure 7-5

Observatory:	BMSO	CPSO	TFSO	UBSO	WMSO
Observatory identification on film seismographs	BMO	CPO	TFO	UBO	WMO
Location:	Baker, Oregon	McMinnville, Tennessee	Payson, Arizona	Vernal, Utah	Ft. Sill, Oklahoma
Geographic coordinates:	44°50' 56"N- 117°18' 20"W	35°35' 41"N- 85°34' 13"W	34°16' 04"N- 111°16' 13"W	40°19' 18"N- 109°34' 07"W	34°43' 05"N- 98°35' 21"W
Elevation (meters above mean sea level):	1189 (3900 ft)	574 (1883 ft)	1492 (4894 ft)	1600 (5248 ft)	505 (1658 ft)
Geology of bedrock:	Granite	Sandstone/ limestone	Granite	Sandstone	Granophyre (porphyritic)

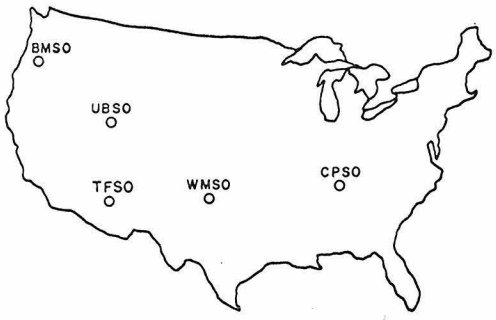

Figure A1-1

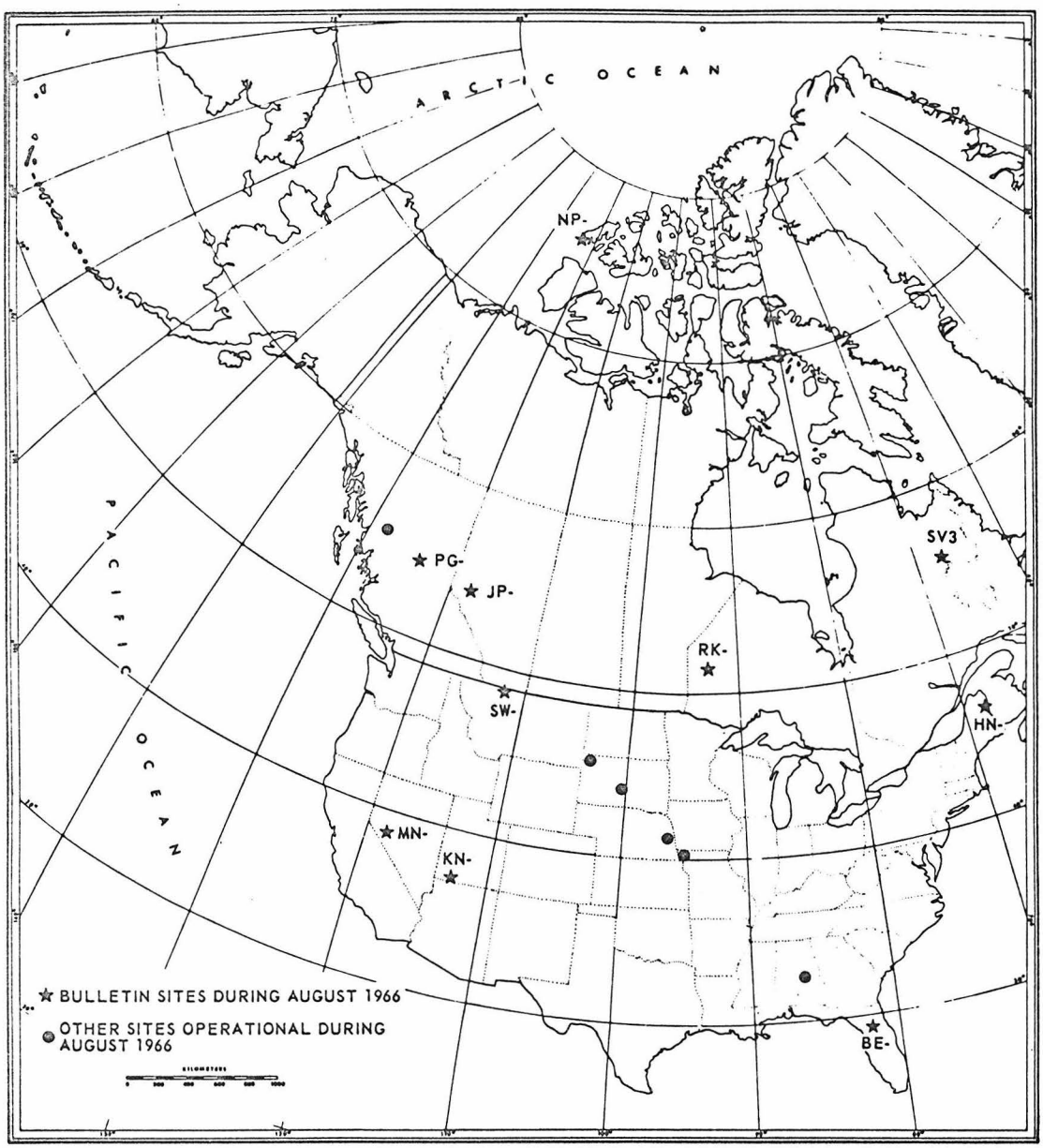
ARCTIC OCEAN
NP-
PACIFIC OCEAN
PG-
JP-
SV3
RK-
SW-
HN-
MN-
KN-
BE-
BULLETIN SITES DURING AUGUST 1966
OTHER SITES OPERATIONAL DURING AUGUST 1966

Figure A1-2

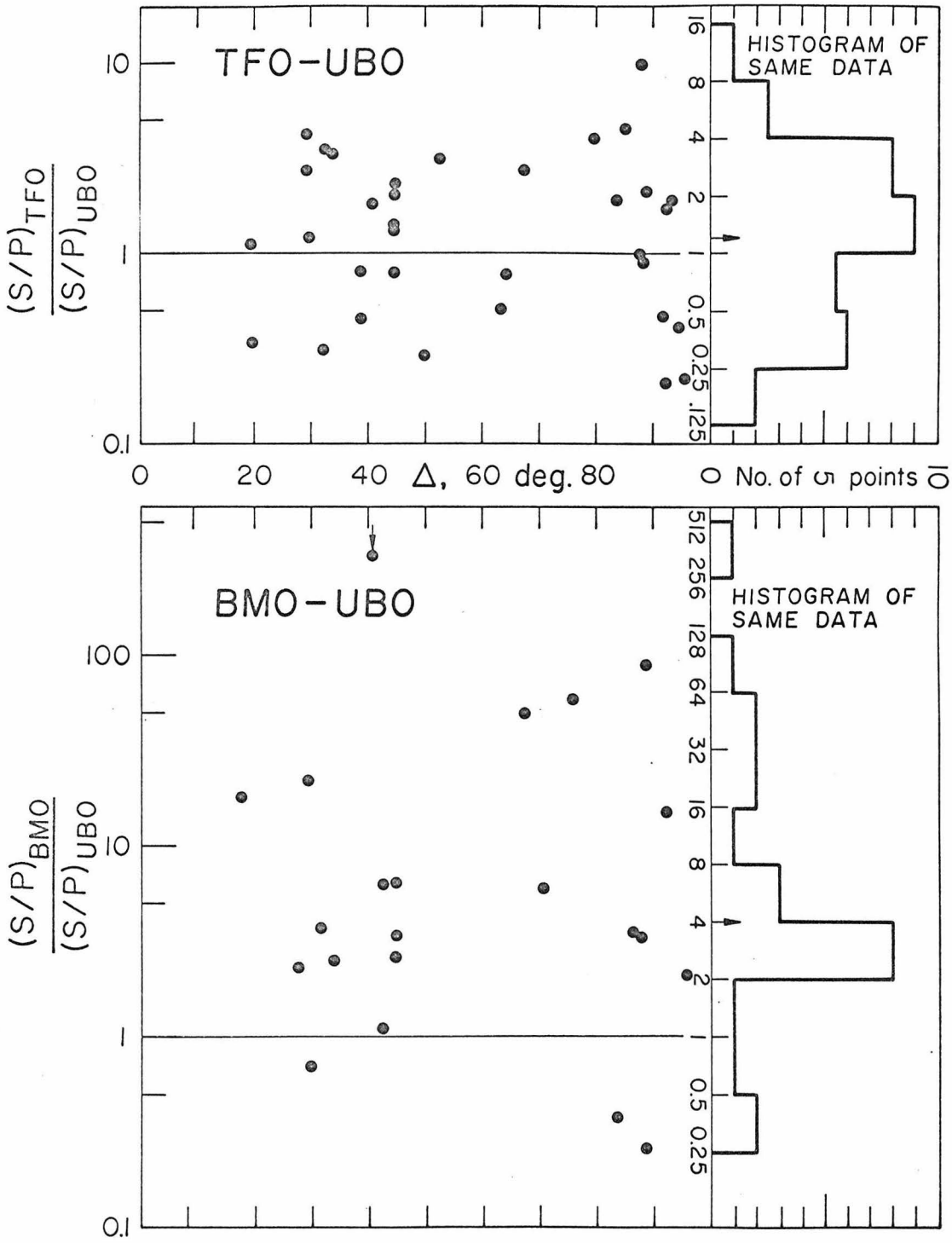
TFO-UBO
HISTOGRAM OF SAME DATA
$\frac{(S/P)_{TFO}}{(S/P)_{UBO}}$
10
1
0.1
0
20
40
Δ, 60 deg.
80
16
8
4
2
1
0.5
0.25
.125
0
No. of points
5
10
BMO-UBO
HISTOGRAM OF SAME DATA
$\frac{(S/P)_{BMO}}{(S/P)_{UBO}}$
100
10
1
0.1
512
256
128
64
32
16
8
4
2
1
0.5
0.25

Figure A1-3

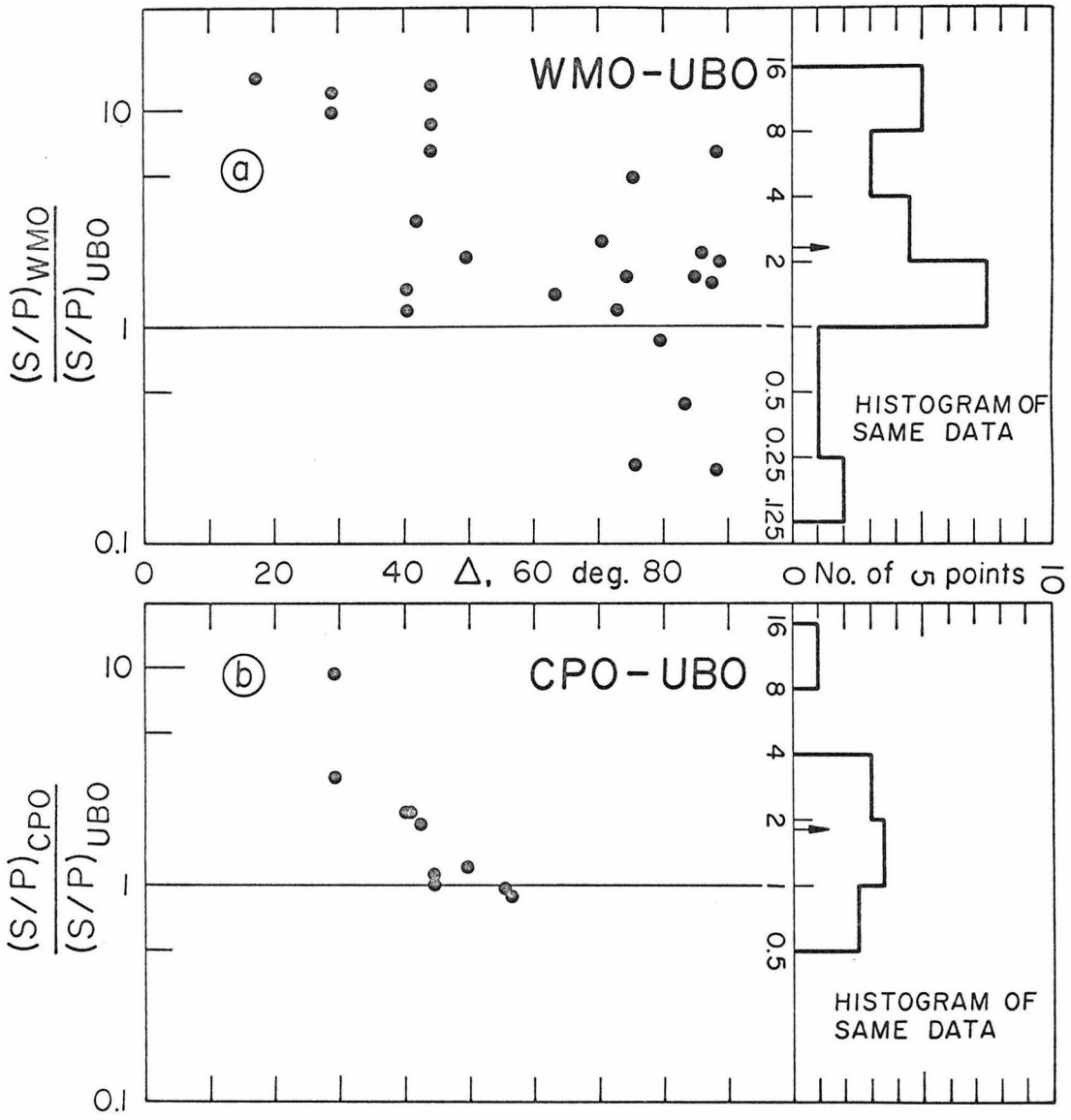
WMO-UBO
(a)
$\frac{(S/P)_{WMO}}{(S/P)_{UBO}}$
10
1
0.1
0
20
40
Δ, 60 deg. 80
16
8
4
2
1
0.5
0.25
.125
HISTOGRAM OF SAME DATA
0 No. of 5 points 10
CPO-UBO
(b)
$\frac{(S/P)_{CPO}}{(S/P)_{UBO}}$
10
1
0.1
16
8
4
2
1
0.5
HISTOGRAM OF SAME DATA

Figure A1-4

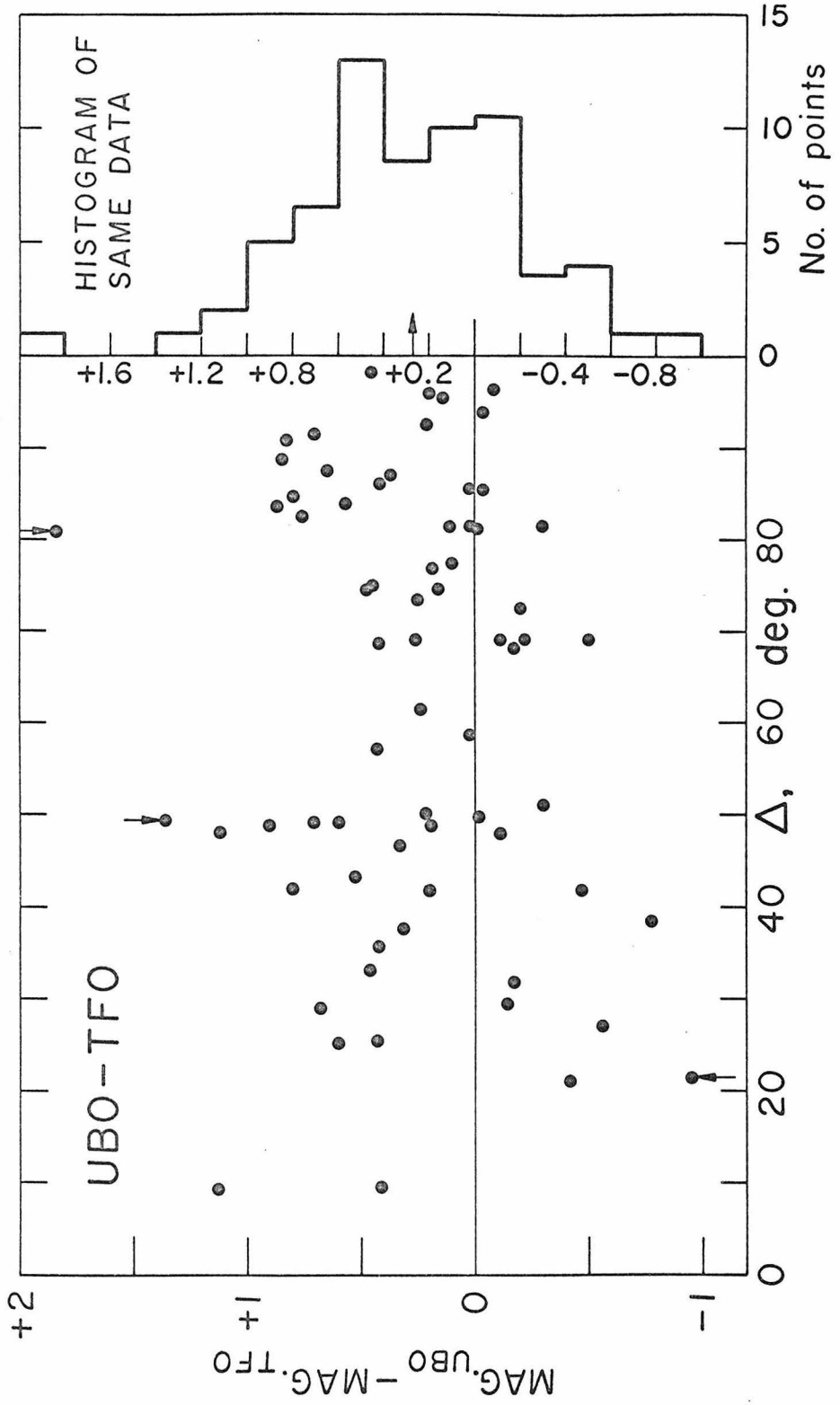
HISTOGRAM OF SAME DATA
No. of points
0
5
10
15
+1.6
+1.2
+0.8
+0.2
-0.4
-0.8
UBO-TFO
MAG.UBO − MAG.TFO
+2
+1
0
-1
0
20
40
60
80
Δ, deg.

Figure A1-5

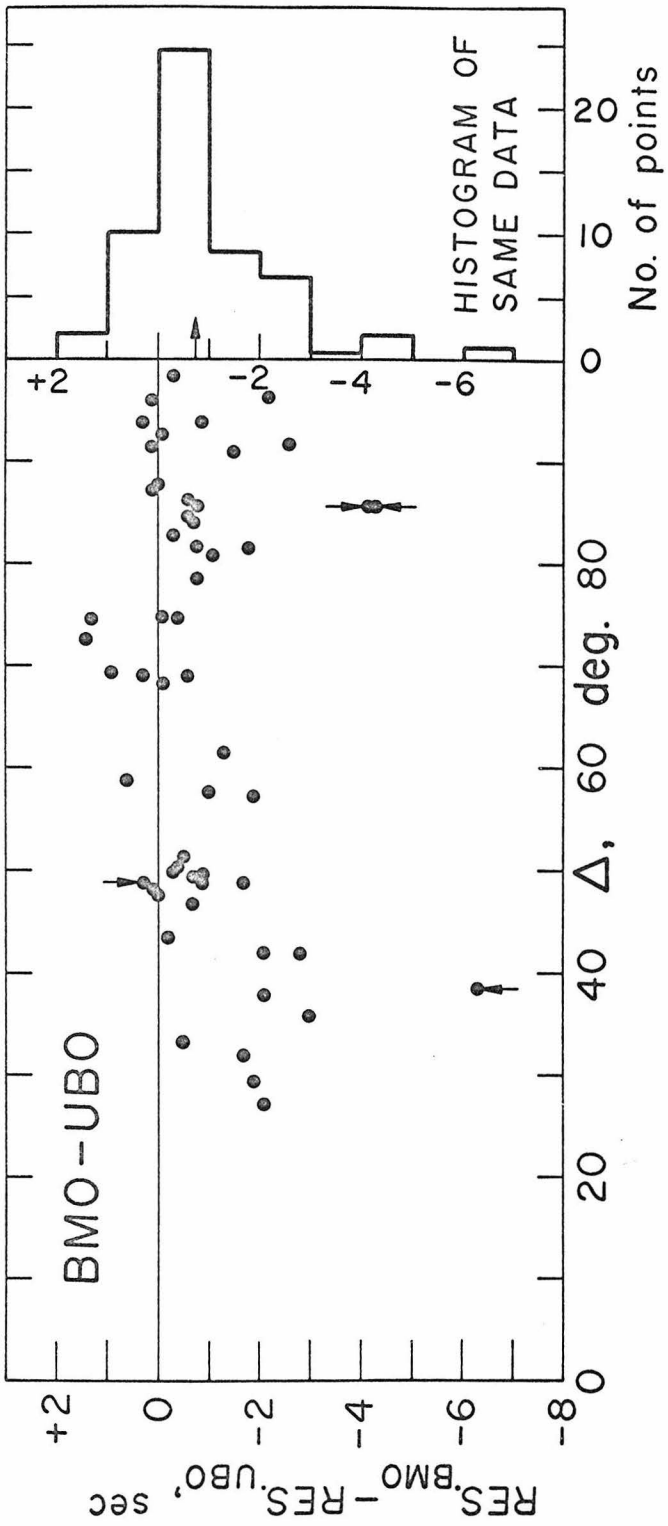
BMO-UBO
HISTOGRAM OF SAME DATA
No. of points
Δ, deg.
RES.BMO − RES.UBO, sec

Figure A1-6

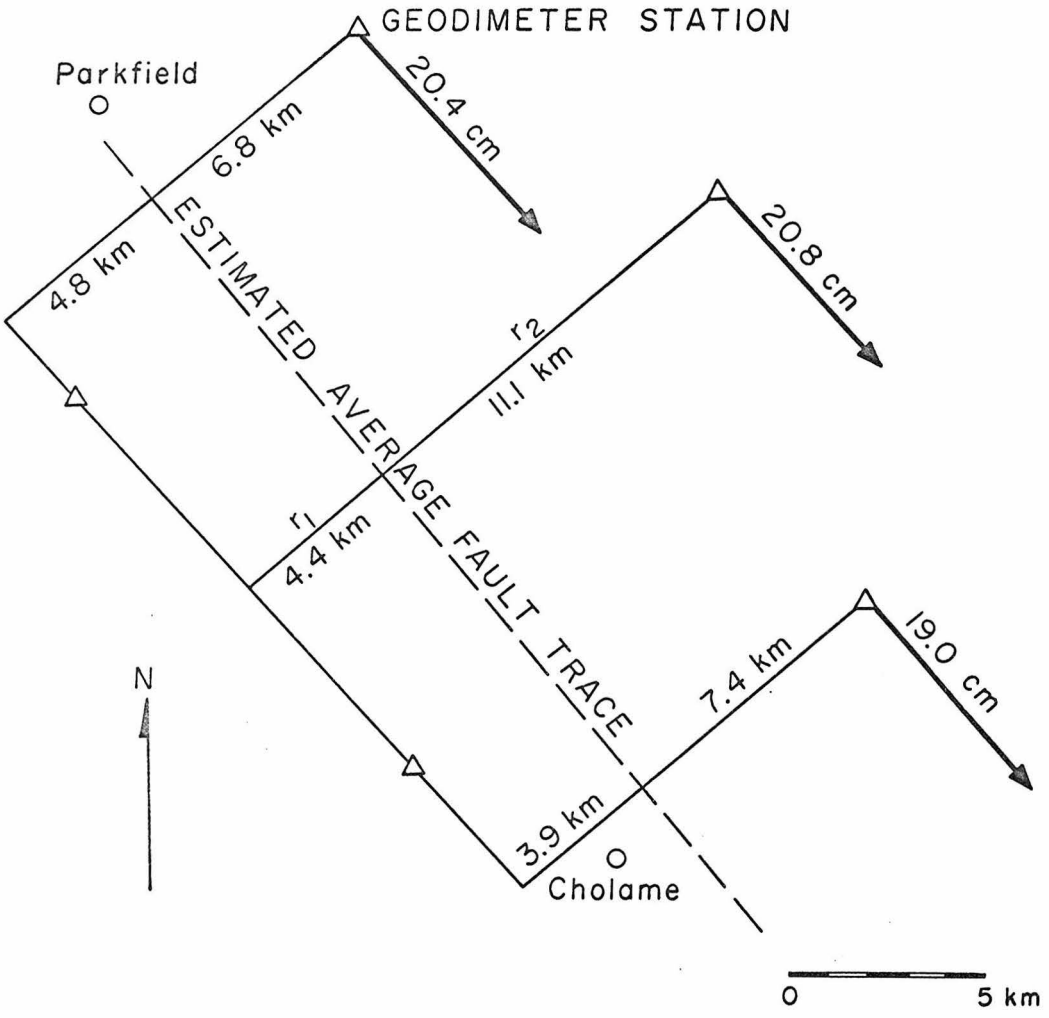
GEODIMETER STATION
Parkfield
6.8 km
20.4 cm
4.8 km
ESTIMATED AVERAGE FAULT TRACE
r2
11.1 km
20.8 cm
r1
4.4 km
7.4 km
19.0 cm
N
3.9 km
Cholame
0
5 km

Figure A17-1

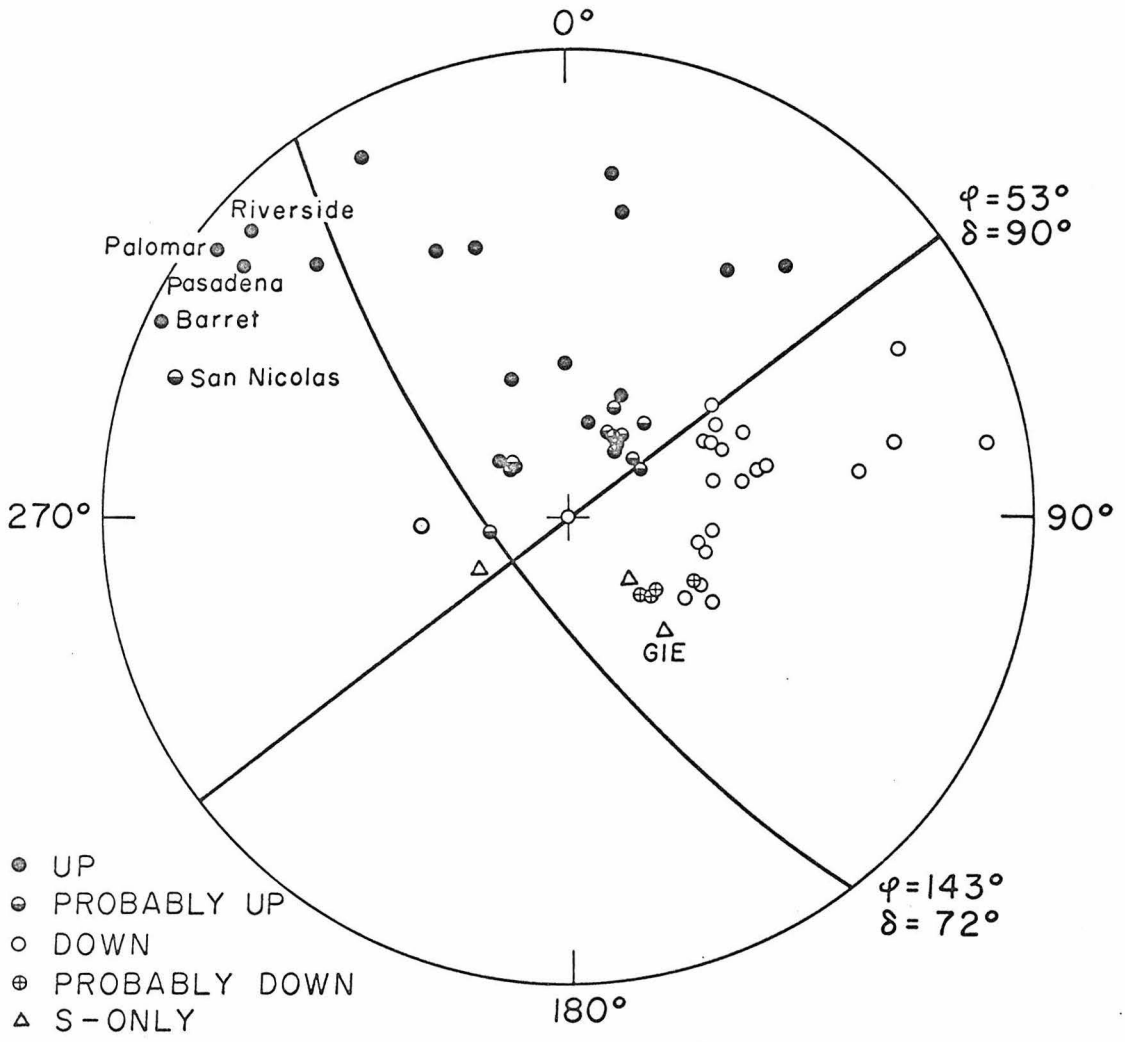
0°
φ=53°
δ=90°
Riverside
Palomar
Pasadena
Barret
San Nicolas
270°
90°
GIE
φ=143°
δ=72°
180°
UP
PROBABLY UP
DOWN
PROBABLY DOWN
S-ONLY

Figure A18-1

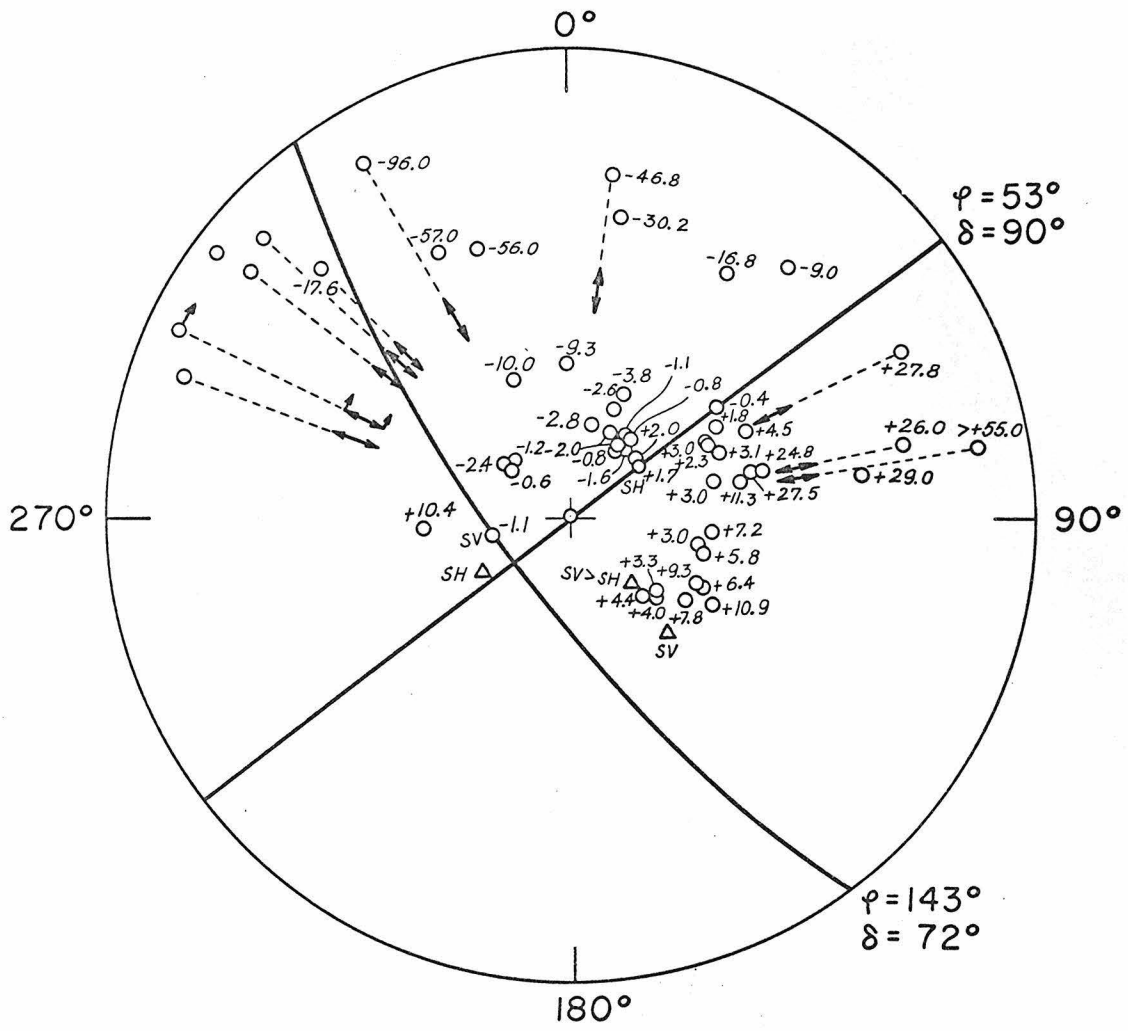
0°
φ = 53°
δ = 90°
90°
180°
φ = 143°
δ = 72°
270°
-96.0
-46.8
-30.2
-57.0
-56.0
-16.8
-9.0
-17.6
-10.0
-9.3
-3.8
-1.1
-2.6
-0.8
-0.4
+27.8
-2.8
+1.8
+4.5
+2.0
+26.0
>+55.0
-1.2
-2.0
+3.0
+3.1
+24.8
-0.8
+2.3
-2.4
-0.6
-1.6
SH
+1.7
+29.0
+3.0
+11.3
+27.5
+10.4
SV
-1.1
+3.0
+7.2
+5.8
+3.3
+9.3
SV>SH
+6.4
+4.4
+4.0
+7.8
+10.9
SV
SH

Figure A 18-2